

## Melting and Convection of Phase Change Materials in Different Shape Containers: A Review

Nabeel S. Dhaidan\* and J. M. Khodadadi\*\*

Department of Mechanical Engineering, Auburn University, 1418 Wiggins Hall

Auburn, AL 36849-5341, USA

### Abstract

A review of analytical, numerical and experimental investigations of melting and ensuing convection of phase change materials within enclosures with different shapes commonly used for thermal energy storage is presented. The common shapes of the containers being rectangular cavities, spherical capsules, tubes or cylinders (vertical and horizontal depending on orientation of gravity) and annular cavities are covered. Studies focusing on melting within rectangular cavities are categorized into two groups. The first one is melting due to isothermal heating on one or more boundaries, whereas the second is the constant heat flux-assisted melting. Moreover, constrained and unconstrained melting in both spherical and horizontal cylindrical containers were discussed. The effects of the concentric geometry and location of the heating source on melting in horizontal annular spaces are presented. The review concentrated on elucidating the heat transfer mechanisms (conduction and convection) during the multiple stages of the melting process and the effects of these mechanisms on the liquid-solid interface shape and its progress, melting rate, charging time of the storage system, etc. The strength of buoyancy driven-convection varies greatly with the dimensionless Rayleigh or Stefan numbers and depends somewhat on the location of heat source and imposed boundary condition. High dimensionless numbers and/or side position of the heat source ensure the dominant role of natural convection melting, otherwise conduction will be responsible for major melting within the container. Furthermore, the geometrical parameters such as the aspect ratio in rectangular containers and vertical cylindrical ones, diameter or radius in spherical capsules and horizontal cylindrical vessels, and eccentricity in annular cavities are reviewed. In addition, the parameters affecting the thermal behavior of the melting process in various enclosures, i.e. the Nusselt, Rayleigh, Stefan, Prandtl and Fourier numbers and are reviewed.

KEYWORDS: Annular Containers; Cylindrical Containers; Convection; Melting; Phase Change Materials; Spherical Containers; Thermal Energy Storage.

\* Department of Mechanical Engineering, Karbala University, Karbala, IRAQ.

\*\* Alumni Chair Professor; Corresponding Author, E-mail: [khodajm@auburn.edu](mailto:khodajm@auburn.edu); Tel. 1-334-844-3333; Fax: 1-334-844-3307.

## Nomenclature

$C_p$  Specific heat of the phase change material,  $\text{J kg}^{-1} \text{K}^{-1}$

$Fo$  Fourier number or dimensionless time,  $\frac{t\alpha}{H^2}$

$g$  Gravitational acceleration,  $\text{m s}^{-2}$

$H$  Characteristic length that depends on the container geometry,  $\text{m}$

$k$  Thermal conductivity of the phase change material,  $\text{W m}^{-1} \text{K}^{-1}$

$L$  Latent heat, i.e. heat of fusion,  $\text{J kg}^{-1}$

$Nu$  Local Nusselt number, defined as  $\left(\frac{H \nabla T}{T_h - T_c}\right)$  for the isothermal walls cases and  $\left(\frac{q'' H}{k(T - T_{ref})}\right)$  for the constant wall heat flux cases

$Pr$  Prandtl number,  $\frac{\nu}{\alpha}$

$q''$  Constant wall heat flux,  $\text{W m}^{-2}$

$Ra$  Rayleigh number,  $\frac{g \beta \Delta T H^3}{\alpha \nu}$

$Sc$  Subcooling parameter, defined as  $(T_m - T_{ini})$  or  $\frac{C_p (T_m - T_{ini})}{L}$

1  
2  
3  
4  
5  
6  
7  
8  
9  
10  
11  
12  
13  
14  
15  
16  
17  
18  
19  
20  
21  
22  
23  
24  
25  
26  
27  
28  
29  
30  
31  
32  
33  
34  
35  
36  
37  
38  
39  
40  
41  
42  
43  
44  
45  
46  
47  
48  
49  
50  
51  
52  
53  
54  
55  
56  
57  
58  
59  
60  
61  
62  
63  
64  
65

*Ste* Stefan number,  $\frac{C_p \Delta T}{L}$

*t* Time, s

*T* Temperature, K

*T<sub>c</sub>* Temperature of the cold wall where heat is rejected isothermally, K

*T<sub>h</sub>* Temperature of the hot wall where heat is supplied isothermally, K

*T<sub>ini</sub>* Initial temperature of the solid phase change material, K

*T<sub>m</sub>* Melting temperature of the phase change material, K

*T<sub>ref</sub>* Reference temperature, K

$\Delta T$  Temperature difference, defined as  $(T_h - T_c)$  for the isothermal walls cases and  $(q'' H/k)$  for the constant wall heat flux cases, °C

### Greek Symbols

$\alpha$  Thermal diffusivity,  $m^2 s^{-1}$

$\beta$  Thermal expansion coefficient,  $K^{-1}$

$\nu$  Kinematic viscosity,  $m^2 s^{-1}$

1  
2  
3  
4  
5  
6  
7  
8  
9  
10  
11  
12  
13  
14  
15  
16  
17  
18  
19  
20  
21  
22  
23  
24  
25  
26  
27  
28  
29  
30  
31  
32  
33  
34  
35  
36  
37  
38  
39  
40  
41  
42  
43  
44  
45  
46  
47  
48  
49  
50  
51  
52  
53  
54  
55  
56  
57  
58  
59  
60  
61  
62  
63  
64  
65

# 1. Introduction

The ongoing and rapid increase in the economic development worldwide is accompanied by a strong demand for an uninterrupted supply of energy. Conventional fossil energy sources are limited and serious uncertainties associated with their stable supply/pricing persist. Moreover, greater use of fossil fuels is linked to emission of harmful gases that in turn are responsible for climate change and environmental pollution. These serious challenges represent the main driving forces behind efforts to utilize various sources of renewable energy more effectively. Scientists and engineers all over the world are in search of new technologies that will lead to greater adoption of renewable energy sources. A very critical technology that is related to the greater adoption of renewable energies is development of energy storage systems. The varying and unpredictable gap between the supply and demand of all types of renewable energy can be eliminated through adoption of responsive, robust and effective energy storage approaches. Therefore, storage of energy and its conversion/reclamation remains a major challenge to the technologists.

Thermal energy can be stored in three ways, i.e. sensible heat, latent heat, and thermo-chemical heat storage. Among these, storage through latent heat offered by a great number of phase change materials (PCM) is considered to be a very promising option due to the high density of thermal energy storage and operation at an approximately isothermal condition. Thermal energy is stored in a material as latent heat upon melting (thawing), whereas the stored energy is utilized later when needed by freezing (solidifying) the material. PCM are also relevant to other engineering applications including electronic cooling technology, thermal comfort in dwellings, waste heat recovery, textiles and heating, ventilation and air conditioning (HVAC). For example, electronic cooling systems utilize PCM storage containers as heat sinks to control the temperature of the surface of electronic components that release instantaneous or periodic high density heat fluxes. Abhat [1] reviewed a number of desirable properties for choosing PCM such as melting/freezing temperature near the desired usage/demand temperature, high values of specific heat, latent heat of fusion and density, low vapor pressure at the operational temperature, a small variation in density between the solid and liquid phases, high thermal conductivity, insignificant supercooling, chemical stability, being non-corrosive in relation to containment materials, non-poisonous, non-flammable, non-explosive, and abundant supply at a low cost. There are a number of review articles [2-9] devoted to discussing various PCM types, specific applications, thermophysical properties, encapsulation, heat transfer enhancement and system-related issues. A serious disadvantage of PCM

1  
2  
3 is their low thermal conductivity that leads to reduced rate of heat transfer and long time for melting  
4 (charging) and freezing (discharging). Fan and Khodadadi [10] reviewed both experimental and  
5 computational studies that concerned enhancing the thermal conductivity of phase change materials  
6 through introduction of highly-conductive, meso-scale and stationary inserts, structures, fibers, etc.  
7  
8

9  
10 In addition to its inherent transient behavior, the characteristics of melting of PCM are  
11 greatly affected by the dominant heat transfer mechanisms (conduction and/or convection). From a  
12 thermal system performance point of view, evolving isotherms, velocity vectors, solid-liquid  
13 interface, in addition to the melting rate, melting time and dimensionless parameters that describe the  
14 rate of heat transfer (i.e. the Nusselt number) can be analyzed for a specific melting problem.  
15 However, these quantities are strongly influenced by the specific geometric configurations and  
16 thermal boundary conditions for a specific melting problem. The geometric configuration and  
17 orientation with respect to gravity of the containers holding PCM affect the heat transfer  
18 mechanisms which play a significant role in evolution the shape, movement and morphology of  
19 solid-liquid interface and in turn affect the thermal characteristics of the melting process of PCM.  
20 The melting rate is higher in the upper portion of all containers where natural convection dominates.  
21 Therefore, increasing the height/width ratio of the enclosure for the same volume augments the  
22 buoyancy effect and results in expediting of the melting process and decreasing of the charging time.  
23  
24  
25  
26  
27  
28  
29  
30  
31  
32  
33  
34  
35

### 36 1.1 . Common features of the PCM-container systems

37  
38 In general, melting of phase change materials in any generic container can be presented  
39 schematically, as shown in Fig. 1. An arbitrary-shaped container holds a PCM (melting temperature  
40 of  $T_m$ ) which is initially in solid phase at an initial temperature ( $T_{ini}$ ) and part of the volume of the  
41 container is a gas void. The gas within the void has a low thermal conductivity and the void has  
42 assumed its initial position and volume in relation to the gravitational field and details associated  
43 with the prior process of freezing of the container. In order to melt the PCM, the container needs to  
44 be heated and this can be accomplished through isothermal heating (establishing hot and cold  
45 temperature boundaries maintained at  $T_h$  and  $T_c$ , respectively) and/or supplying a constant wall heat  
46 flux ( $q''$ ) on the boundary of the container. Such *active* thermally boundaries are identified in Fig. 1,  
47 whereas the remaining boundaries will be thermally insulated. Upon initiation of heating, the solid  
48 phase begins to melt next to the “hot” boundary and the volume of the liquid zone increases. An  
49 evolving liquid/solid interface is formed that is at temperature  $T_m$  if the PCM is a pure material and  
50  
51  
52  
53  
54  
55  
56  
57  
58  
59  
60  
61  
62  
63  
64  
65

1  
2  
3 the distance  $H$  that is the length scale of the liquid zone in Fig. 1 will increase. The ensuing  
4 convection currents within the liquid phase depend on the spatial extent of the region occupied by  
5 the liquid phase, orientation of the gravitational field and the established temperature difference.  
6 This transient melting problem that is accompanied by buoyancy-driven convection is governed by  
7 the Rayleigh number that describes the relative importance of the buoyancy force in comparison to  
8 the diffusion force. This dimensionless grouping needs to be defined in accordance with the  
9 imposed thermal boundary condition, i.e.:

$$16 \quad Ra = \frac{g \beta \Delta T H^3}{\alpha \nu} \quad (1)$$

19 where:

$$22 \quad \Delta T = \begin{cases} T_h - T_c & \text{for isothermal heating} \\ \frac{q'' H}{k} & \text{for isoflux heating} \end{cases} \quad (2)$$

27 Note that the time-dependent Rayleigh number increases markedly due to its cubic dependence on  
28  $H$  and both laminar and turbulent regimes might be encountered. Another important dimensionless  
29 number is the Stefan number:  
30

$$33 \quad Ste = \frac{C_p \Delta T}{L} \quad (3)$$

36 with  $\Delta T$  given by equation (2).

38 The subcooling parameter also plays an important role in the melting process as it is a measure  
39 of the difference between the melting and initial temperatures. This parameter is defined as:

$$42 \quad Sc = \begin{cases} T_m - T_{ini} \\ \frac{C_p (T_m - T_{ini})}{L} \end{cases} \quad (4)$$

47 In many practical thermal energy storage systems, heat exchange is promoted through utilization of a  
48 pipe within the PCM through which a heat transfer fluid is circulated. In effect, charge/discharge of  
49 thermal energy is improved. Such a feature is not shown in Fig. 1 but has been studied by many  
50 research studies reviewed in this paper.  
51  
52  
53  
54  
55  
56  
57  
58  
59  
60  
61  
62  
63  
64  
65

1  
2  
3  
4  
5  
6  
7  
8  
9  
10  
11  
12  
13  
14  
15  
16  
17  
18  
19  
20  
21  
22  
23  
24  
25  
26  
27  
28  
29  
30  
31  
32  
33  
34  
35  
36  
37  
38  
39  
40  
41  
42  
43  
44  
45  
46  
47  
48  
49  
50  
51  
52  
53  
54  
55  
56  
57  
58  
59  
60  
61  
62  
63  
64  
65

*1.2. Scope of the present review*

In this review, melting and the ensuing natural convection within PCM that are contained in enclosures of various shapes are discussed with emphasis on the type of the geometry of the container. **These shapes include rectangular, spherical, cylindrical (both horizontal and vertical) and annular containers.** The primary aim of this review is to present a description of the analytical, numerical and experimental investigations related with the melting and ensuing convection processes of phase change materials held in various containers. Geometrical features of the containers (also called capsules, cells, enclosures, vessels, shells) such as aspect-ratio, wall curvature, eccentricity etc., in addition to the location/type of the imposed thermal conditions on the boundaries are directly linked to the variety of convection cells and liquid/solid interface patterns that are encountered in phase change systems.

**2. Melting in rectangular containers**

Melting of phase change materials in rectangular enclosures has received great attention due to its wide-ranging engineering applications in such fields as casting, metallurgy and thermal energy storage. It is appropriate that the applications associated with this type of containers are categorized according to the imposed boundary conditions as: (1) constant heat flux and (2) constant temperature problems.

*2.1. Melting due to the constant heat flux (CHF) boundary*

In this class of problems, the melting process of the phase change materials occurs primarily due to constant heat flux that is supplied on one or more sides of the container. Zhang et al. [11] presented experimental results of the melting process of n-octadecane ( $C_{18}H_{38}$ ) held in a rectangular enclosure with one wall heated by discrete sources at a constant rate and the other surfaces being adiabatic. Their study aimed to explore the possibility of using the melting process for cooling of periodically-operating electronic components. The results indicated that natural convection has a significant effect on the shape of the solid-liquid interface that becomes more pronounced with increasing of the Stefan number. Also, the effect of subcooling on the melting process was

1  
2  
3 described and an empirical correlation predicting the relationship between the liquid phase fraction  
4 and subcooling was introduced. The obtained results suggested that the cooling of heat sources  
5 using PCM melting and the ensuing natural convection leads to a drop of the mean temperatures of  
6 heat sources as much as 50% compared to natural convection cooling with air. Moreover, the  
7 highest surface temperature was recorded at the uppermost heat source.  
8  
9

10  
11  
12  
13  
14 Ho and Chu [12] simulated numerically using the finite difference method (FDM) the  
15 transient heat penetration through a vertical rectangular composite cell filled with a solid-liquid  
16 phase change material and air layer. Within the composite cell, the PCM layer was separated from  
17 the air layer by a solid partition of finite thickness as shown in Fig. 2. The numerical results for the  
18 composite cell with a thin diathermal partition demonstrated that by means of latent-heat absorption  
19 inside the PCM layer, heat penetration across the composite cell can be greatly retarded over an  
20 effective time duration until a critical instant at which the melting front of the PCM reaches the  
21 partition wall. Such an effective thermal protection duration was found to be a strong function of the  
22 modified Rayleigh number, the modified Stefan number, the subcooling factor, the relative PCM  
23 thickness ratio, and the aspect-ratio ( $AR$ ) of the composite cell ( $AR$  is defined as the ratio of the  
24 width to the height). A geometry of a shallow rectangular composite cell having a larger PCM/air  
25 thickness ratio was found to be preferable for effective thermal protection applications. In addition,  
26 the effect of a solid partition of finite thickness and conductivity on the thermal protection efficacy  
27 of the PCM/air composite cell was also examined.  
28  
29

30  
31  
32  
33  
34  
35  
36  
37  
38  
39 Jianhua et al. [13] studied experimentally the melting process of n-octadecane in a  
40 rectangular cavity with three discrete protruding heat sources on its bottom surface. The surface  
41 temperatures of the heat sources were measured by thermocouples and the solid-liquid interface  
42 motion was recorded photographically. It was observed that *fixed melting* (solid between heaters)  
43 and *contact melting* (solid above heaters) occurred simultaneously. The impacts of the Stefan  
44 number, initial subcooling and the aspect-ratio (initial PCM height/PCM width) on the melting  
45 process were reported. The experimental findings revealed that for higher values of the Stefan  
46 number and smaller aspect-ratio, melting proceeds more rapidly and contact melting occurs with  
47 greater frequency. The impact of the initial subcooling on the melting process existed only during  
48 the very early stages and disappeared after the melting process entered the contact melting stage.  
49  
50  
51  
52  
53  
54  
55  
56

57  
58  
59 The fusion mechanism of a pure substance (gallium) was examined numerically by Mbaye  
60 and Bilgen [14]. The rectangular enclosure was subjected to a constant heat flux on its left vertical  
61  
62  
63  
64  
65



1  
2  
3 wall, a constant temperature on its right wall, whereas adiabatic condition was maintained on its two  
4 horizontal walls. The enthalpy formulation with the finite difference-control volume method was  
5 developed to study phase change process where the solid-liquid change region is controlled by  
6 natural convection. It was found that an important parameter controlling the heat transfer and  
7 melting velocity was the applied heat flux, whereas heat transfer attained a maximum value at an  
8 optimal value of the aspect-ratio of about unity. Also, the melted volume was independent of the  
9 aspect-ratio in the conduction regime, but it became a decreasing function of the aspect-ratio as  
10 natural convection in the liquid develops.  
11  
12  
13  
14  
15  
16  
17

18 Pal and Joshi [15] studied computationally and experimentally (Fig. 3) the melting of an  
19 organic phase change material, i.e. n-triacontane ( $C_{30}H_{62}$ ) in a tall enclosure with an aspect-ratio of  
20 10 by supplying a constant heat flux on one side while the other sides were thermally insulated.  
21 Good agreement was obtained between experimental and computational heat transfer data and melt  
22 interface locations. They reported that natural convection played a dominant role during the initial  
23 stages of melting and at a later time, the strength of natural convection diminished as melting was  
24 completed. Correlations for variations of the heat transfer rate and melt fraction with time were  
25 obtained.  
26  
27  
28  
29  
30  
31  
32

33 An analytic study was presented by Hamdan and Al-Hinti [16] for melting process of a solid  
34 phase change material contained in a rectangular enclosure heated from a vertical side at a constant  
35 heat flux. The propagation and the inclination of the solid-liquid interface along with the time  
36 evolution of the melted fraction were studied and evaluated. It was found that the model predicted  
37 the propagation of the interface during the initial stages of the melting process very well, while it  
38 under-predicted the movement of the interface during the later stages of melting. However, accurate  
39 predictions were obtained for the variation of the melted fraction. The results relating to the position,  
40 inclination, propagation and the melted fraction were found to be in a good agreement with  
41 published experimental and numerical results.  
42  
43  
44  
45  
46  
47  
48

49 Faraji and El Qarnia [17] studied numerically the melting of n-eicosane ( $C_{20}H_{42}$ ) in a  
50 rectangular enclosure heated with three protruding heat sources with a constant and uniform  
51 volumetric heat generation on one side while the other sides were thermally insulated (Fig. 4). The  
52 power supplied to the heat sources was equal to that generated within the actual Pentium  
53 microprocessor (CPU) Centrino Duo 4 (2.8 GHz). Their model used the control volume approach  
54 and the enthalpy method for solving the momentum and energy equations. The results indicated that  
55 conduction was predominant at the bottom part of the PCM at early stage of the melting process.  
56  
57  
58  
59  
60  
61  
62  
63  
64  
65

1  
2  
3 During the second stage, natural convection developed and the streamlines became relatively packed  
4 next to the active wall and the melting front, which leads to a relatively fast-moving flow next to  
5 those boundaries. The third stage started when the location of the intersection of the melting front  
6 and non-active vertical wall moved downward. Consequently, the heat flux transmitted to the liquid-  
7 solid interface decreased with time which explains the decay of the rate of change in the liquid  
8 fraction. They found that the highest heat transfer rate was associated with the bottom heat source.  
9 Later on, El Qarnia et al. [18] investigated numerically the same model to examine the impact of  
10 several key parameters of the PCM-based heat sink on its cooling capacity. Also, correlations for  
11 the non-dimensional secure operating time (time required by the heat sink before reaching the  
12 critical temperature of  $T_{cr} = 75$  °C) and the corresponding melt fraction were derived using the  
13 asymptotic computational fluid dynamics (ACFD) technique. They found that increasing the  
14 Rayleigh number and decreasing the aspect-ratio from their reference values will result in a rise in  
15 the wall surface temperature of the heaters, reduction in operating time, and therefore, a decrease in  
16 the melted liquid fraction.  
17  
18

19  
20 Samara et al. [19] presented and compared two methods enabling the simulation of PCM  
21 melting while accounting for both conduction and natural convection. A simplified two-dimensional  
22 model was created in COMSOL Multiphysics 4.3 in order to simulate melting of PCM (type RT25)  
23 inside a rectangular container which was exposed to a constant heat flux with convection heat  
24 transfer on both vertical sides, while the top and bottom sides were adiabatic (Fig. 5). It was found  
25 that the first method, which simply used a modified viscosity, could properly simulate the phase  
26 change process only for part of the simulation, and diverged before reaching the end of the  
27 simulation. The second method (modified volume force), which was more robust and used smoother  
28 functions to account for changes in viscosity and specific heat, provided more accurate and  
29 consistent results. The mesh mode and discretization technique had a significant influence on the  
30 melting behavior, shape of the interface, and total simulated time.  
31  
32  
33  
34  
35  
36  
37  
38  
39  
40  
41  
42  
43  
44  
45  
46  
47  
48  
49  
50  
51  
52

## 53 2.2. Melting due to the constant wall temperature (CWT) boundary

54  
55  
56 Conduction and free convection-dominated melting along a heated isothermal wall in a  
57 rectangular enclosure has attracted considerable research attention due to its fundamental importance  
58  
59  
60  
61  
62  
63  
64  
65

1  
2  
3 in various technological applications. Melting is initiated when one or more walls are maintained at  
4 a temperature above the melting temperature of phase change materials.  
5  
6

7 Brent et al. [20] investigated numerically the melting of pure gallium in a rectangular cavity  
8 using the enthalpy-porosity approach for modeling combined convection-diffusion phase change.  
9 The left wall was maintained at a hot temperature of 38 °C while the right boundary was at an initial  
10 temperature of 28.3 °C, and the other walls were adiabatic. The approach was validated through the  
11 excellent agreement between the numerical predictions and experimental findings available in  
12 literature. The results indicated the features of enthalpy-porosity method such as its validity in  
13 comparison to the experimental work, applicability, convergence speed, and the ability to predict  
14 accurately both the position and morphology of the melt front at various times.  
15  
16  
17  
18  
19  
20

21 Beckermann and Viskanta [21] reported a combined experimental and numerical study of  
22 melting of a pure metal inside a vertical rectangular enclosure (Fig. 6) with natural convection in the  
23 liquid region and conduction in the shrinking solid portion. The numerical predictions were verified  
24 through a number of experiments, covering a range of the Rayleigh numbers and subcooling  
25 parameters. It was found that solid subcooling significantly reduced the melting rate when  
26 compared to melting with the solid initially at the fusion temperature. Additionally, the melting  
27 process consisted of a sequence of four regimes (an initial conduction-dominated regime, a regime  
28 characterized by developing convection in the upper portion and conduction prevalence in the lower  
29 part, a convection-dominated regime, and a regime where melting process is highly influenced by  
30 heat extraction by cold wall) and eventually approached to the steady-state condition. For small  
31 solid subcooling, the first three regimes were found to be similar to the ones observed in melting  
32 without subcooling, whereas for moderate subcooling, significant differences can be observed after  
33 the first two regimes and the steady-state interface is almost vertical and parallel to the cold wall.  
34 Large values of the subcooling parameter led to an early termination of the melting process and the  
35 last two regimes may never take place.  
36  
37  
38  
39  
40  
41  
42  
43  
44  
45  
46  
47  
48

49 Asako et al. [22] introduced a numerical study to investigate the melting of an unfixed  
50 rectangular PCM in a low-gravity environment. An enthalpy method was applied to solve the  
51 transport processes with the governing equations discretized by using a control-volume-based finite  
52 difference scheme with a new iterative method to correct the downward solid-phase velocity. The  
53 PCM, initially at its melting temperature, was placed inside a rectangular enclosure. The lower  
54 surface of the container was then exposed to a uniform temperature higher than the PCM's melting  
55 temperature. The difference in densities of the solid and liquid phases caused a force imbalance on  
56  
57  
58  
59  
60  
61  
62  
63  
64  
65

1  
2  
3 the solid in the gravitational and low-gravity environments. In the case where the density of the  
4 solid phase exceeded that of the liquid, the solid continually moved downward as melting progressed  
5 and hence generated a flow field within the liquid. The results were presented in the form of a  
6 parametric study of the effects of the Archimedes, Stefan and Prandtl numbers, and geometric  
7 parameters such as aspect ratio. The results revealed that the melt thickness increases with time and  
8 decreases with increasing Archimedes, Stefan, and Prandtl numbers, while the effect of aspect ratio  
9 on the melt thickness was small. They showed that the rate of solid volume reduction increases with  
10 increasing Archimedes and Stefan numbers, and in a low-gravity environment, the melting rate is  
11 very slow.

12  
13  
14  
15  
16  
17  
18  
19  
20 Wang et al. [23] conducted an experimental investigation (Fig. 7) to examine the thermal  
21 characteristics of the melting process in a rectangular enclosure heated from a vertical side. A flat  
22 plate heat pipe was utilized to provide a uniform wall temperature at any given time. The  
23 presentation of the results clearly captured the development of the distinct structure of the liquid-  
24 solid interface in the presence of natural convection. The temperature distributions in the PCM  
25 along the top wall, horizontal mid-plane, and the bottom wall were presented. Correlations,  
26 developed for the melted volume fraction and the time-averaged Nusselt number as a function of the  
27 parametric variables ( $Ra$ ,  $Ste$ ,  $Pr$  and  $Fo$ ), were found to yield good agreement with the experimental  
28 data. It was shown that the temporal variation of the Nusselt number distinguishes three different  
29 heat transfer regimes during the melting process (conduction-dominated regime, transition regime,  
30 and convection-dominated regime).

31  
32  
33  
34  
35  
36  
37  
38  
39  
40 Gong et al. [24] studied numerically the free convection-dominated melting of a phase  
41 change material in a rectangular cavity with an isothermally-heated vertical wall with the aid of the  
42 streamline Upwind/Petrov-Galerkin finite element technique in combination with a fixed-grid  
43 primitive variable method to solve the governing two-dimensional conservation equations. The  
44 enthalpy-porosity model was employed to account for the physics of the evolution of the flow at the  
45 solid/liquid interface leading to a good agreement with previous experimental and numerical results.  
46 The melting process was divided into two periods. The first one (isotherms not parallel with the  
47 effect of thermal stratification being low and high rate of free convection and melting) is presented  
48 in Fig. 8a, where the isotherms corresponding to Fourier ( $Fo$ ) numbers of 0.108, 0.194 and 0.302 are  
49 shown. As time progressed, the second period will appear with significant thermal stratification and  
50 low rate of convection and melting (Fig. 8a) for  $Fo = 0.432$  and  $0.562$ . The authors suggested  
51 inverting the container in the second stage (Fig. 8b) for augmenting the effect of natural convection.  
52  
53  
54  
55  
56  
57  
58  
59  
60  
61  
62  
63  
64  
65

1  
2  
3 The results indicated more than 50% increase of the energy charge rate during the melting process  
4 for some specific cases (Table 1) due to inversion of the container.  
5  
6

7 Ghasemi and Molki [25] investigated numerically isothermal melting in a rectangular cavity  
8 using the fixed-grid enthalpy formulation. The solid phase was unfixed and could move during the  
9 melting process. All walls of the cavity were maintained at a constant temperature higher than the  
10 melting temperature of the PCM. Falling of the solid in the melt and buoyancy were the main  
11 factors affecting the liquid motion and the melting process. The problem was studied numerically  
12 and the findings were validated by a comparison with the available analytical, numerical and  
13 experimental results. It was found that for low values of the Rayleigh and Archimedes numbers, the  
14 melting rate and the solid velocity were both very small, and the melting pattern was almost  
15 symmetric. Operating at higher values of the Rayleigh and Archimedes numbers, enhanced melting,  
16 faster falling velocity of the solid and distortion of the symmetry of the interface were observed.  
17  
18

19 Zivkovic and Fujii [26] presented a simple computational model for isothermal phase change  
20 of a PCM encapsulated in rectangular and cylindrical containers. The theoretical model was verified  
21 with a test problem and an experiment was performed in order to assess the validity of the  
22 assumptions of the mathematical model. Based on very good agreement between experimental and  
23 computational data, it was concluded that conduction within the PCM in the direction of heat  
24 transfer/fluid flow, thermal resistance of the container's wall, and the effects of natural convection  
25 within the melt can be ignored for the conditions investigated in the study. The computational  
26 results indicated that the rectangular container required nearly half of the melting time when  
27 compared to the cylindrical container of the same volume and heat transfer area (Fig. 9).  
28  
29

30 Lacroix [27] introduced a mathematical model for the contact melting of a subcooled PCM  
31 inside a parallelepipedic capsule where heat was supplied isothermally from the upper and lower  
32 sides, while the other sides were adiabatic. Numerical results indicated that the melted fraction from  
33 close contact melting at the bottom of the capsule was greater by an order of magnitude than that  
34 from the conduction-dominated melting near the top. Also, the melting process is positively  
35 governed by the magnitude of the Stefan number and strongly influenced by the side dimensions of  
36 the capsule, whereas the total melting time increased linearly with the degree of subcooling.  
37  
38

39 Jiji and Gaye [28] investigated analytically the problem of one-dimensional melting and  
40 solidification of a slab with uniform volumetric energy generation. Analytic solutions were obtained  
41 using a quasi-steady approximation by neglecting the transient term in the heat conduction equation  
42 under certain conditions such as the low Stefan number. This approach simplifies phase change  
43  
44  
45  
46  
47  
48  
49  
50  
51  
52  
53  
54  
55  
56  
57  
58  
59  
60  
61  
62  
63  
64  
65

1  
2  
3 problems and often eliminates the need for numerical solutions. Unlike solidification, the melting  
4 case is characterized by a pure liquid phase and a mixture of solid and liquid at the fusion  
5 temperature. The solution was governed by a single energy generation parameter. Temperature  
6 profiles, interface location and steady-state conditions were presented for both melting and  
7 solidification cases. Results were applied to two examples of solidification of a nuclear material and  
8 melting of ice.  
9

10  
11 Yanxia et al. [29] reported on an experimental study designed to investigate the thermal  
12 characteristics of the melting process of ethanolamine–water binary mixture used as PCM in a  
13 rectangular enclosure heated from a vertical side (Fig. 10a). The empirical correlations of molten  
14 fraction and time-averaged Nusselt number in convection-dominated melting were established and  
15 compared with pure conduction model. The experimental results indicated that natural convection  
16 enhanced the melting process compared with the conduction-only cases. The higher the Rayleigh  
17 number, greater differences between the molten fraction data of the natural convection-dominated  
18 and conduction-dominated cases were observed (Fig. 10b). Mechanism of pure conduction only  
19 occurred during the initial stage of melting and a conduction-convection coupled model was  
20 necessary for predicting melting process accurately at later stages.  
21  
22

23  
24 Jellouli et al. [30] reported a numerical investigation of the moving boundary problem during  
25 melting process driven by natural convection in the liquid and conduction in the solid within a  
26 rectangular cavity heated from below (Fig. 11a) by using an elliptic procedure and a control volume  
27 scheme. The agreement between numerical results and those of earlier reported studies was found to  
28 be good. During the early stage of melting, buoyancy forces cannot overcome the resistance  
29 imposed by viscous forces. The presence of convection with its temperature signature observed in  
30 the bottom panel of Fig. 11b exhibited a clear departure from the horizontal distribution of the  
31 isotherms associated with pure conduction (top panel of Fig. 11b). As the thickness of the melt layer  
32 increased with time, natural convection dominated in the liquid phase and the melting front reached  
33 a steady position (end of the melting process) when heat transfer from the liquid phase was  
34 compensated by heat transfer to the solid phase.  
35  
36

37  
38 Chen et al. [31] introduced a two-dimensional theoretical model based on the enthalpy  
39 formulation and a fully-implicit finite difference method to predict the melt fraction of PCM which  
40 were magnesium nitrate hexahydrate, stearic acid, acetamide, acetanilide and erythritol. Different  
41 materials such as glass, stainless steel, tin, aluminum alloy (called “mixed” in the paper), aluminum  
42 and copper were used as the heat exchanger’s container materials in the numerical calculations. One  
43  
44  
45  
46  
47  
48  
49  
50  
51  
52  
53  
54  
55  
56  
57  
58  
59  
60  
61  
62  
63  
64  
65

1  
2  
3 side of the cubic container was maintained at a constant temperature, whereas the other sides were  
4 adiabatic. The predicted results revealed that the selection of the thermal conductivity of the heat  
5 exchanger container material and the effective thermal conductivity of the PCM had an important  
6 influence on the melt fraction, while the thickness of the heat exchanger's container material and the  
7 initial PCM temperature did not have very significant effect on the melt fraction. Also, the  
8 temperature of the wall boundary played an important role during the melting process and has a  
9 strong impact on the observed melt fraction.  
10

11  
12  
13  
14  
15  
16 Younsi et al. [32] conducted a numerical investigation to study the thermal characteristics of  
17 the melting process of a PCM (hydrated salt) heated on a vertical wall of a rectangular enclosure.  
18 An enthalpy-based mathematical model was proposed to analyze PCM for latent storage. Solution  
19 of the governing equations was obtained by using the finite volume method (FVM). The numerical  
20 implementation was done by using a 1D FVM which was used as a comparison method for the  
21 proposed 2D FVM. The convection-dominated melting in a rectangular cavity was also investigated  
22 numerically using the commercial code FLUENT 6. The findings of the study proved that the 1D  
23 solution (pure conduction) should not be used even though the value of the aspect-ratio is very low  
24 due to the relatively large discrepancy in progress of the melting patterns predicted by the two  
25 approaches, as presented in Fig. 12. Also, both numerical methods (2D FVM and FLUENT code)  
26 provided excellent correspondence with experimental results.  
27  
28  
29  
30  
31  
32  
33  
34  
35

36  
37 Wang et al. [33] developed a comprehensive finite volume model for solving the problem of  
38 2D melting in a square cavity involving natural convection for four different cases (Fig. 13). In the  
39 model, the energy balance associated with phase change was represented by the temperature  
40 transforming model, and the velocity-pressure coupling is solved by the consistent update technique  
41 (CUT) algorithm. Furthermore, a new solid velocity correction scheme that does not employ large  
42 numbers to force the velocity in the solid phase to be negligibly small, along with an explicit update  
43 for the melting front and buoyancy force was proposed. This scheme proved to be very effective in  
44 eliminating the inconsistencies previously discussed and was able to accelerate convergence  
45 significantly. The predictions of the proposed numerical model were compared with previous  
46 theoretical, modeling and experimental results, and reasonable agreement was achieved among  
47 various approaches. It was found that melting phenomena of octadecane ( $T_m=30\text{ }^\circ\text{C}$ ) and sodium  
48 nitrate ( $T_m=306.8\text{ }^\circ\text{C}$ ), both melting in a square cavity with a Rayleigh number of  $10^8$  and a Stefan  
49 number of 0.1 were essentially identical. Such a similarity can be used as a foundation for  
50  
51  
52  
53  
54  
55  
56  
57  
58  
59  
60  
61  
62  
63  
64  
65

1  
2  
3 conducting room-temperature experiments to investigate the melting/solidification characteristics of  
4 high-temperature phase change materials.  
5

6  
7 Through comparison of reliable experimental data and numerical modeling, Joulin et al. [34]  
8 studied the energy storage and the energy recovery accommodated by using a phase change material.  
9 An experimental setup (Fig. 14a) was used to measure the temperatures and heat fluxes in order to  
10 characterize the phase change effects. A 1-D finite difference method (FDM) incorporated in an in-  
11 house FORTRAN code and the 2-D commercial CFD software FLUENT were applied for the  
12 computation of the thermal behavior of the PCM. Predictions based on both methods exhibited a  
13 very good agreement with the experimental observations for the melting process with a deviation of  
14 less than 5%, as shown in Fig. 14b. Findings of the numerical modeling suggested that the  
15 supercooling phenomenon must be taken into account correctly in order to predict the PCM thermal  
16 behavior since the numerical results of 1D and 2D simulations ignoring subcooling were very far  
17 away from the experimental ones.  
18  
19

20  
21  
22  
23  
24  
25  
26  
27 Murray and Groulx [35] performed a 2-D numerical study using the COMSOL Multiphysics  
28 package (versions 4.0a and 4.1) to simulate melting of a PCM including both conduction and  
29 convection heat transfer in a square enclosure containing octadecane as the PCM. The vertical walls  
30 were maintained at constant high and low temperatures, and the other walls were insulated. The  
31 impact of the melting temperature range ( $T_{liquidus} - T_{solidus}$ ) used in the simulation was demonstrated.  
32 Moreover, the effect of the numerical assignment of viscosity on the onset and strength of natural  
33 convection and the resulting melting interface position was discussed. The effects of viscosity and  
34 thermal conductivity of the PCM were studied as well, and changes in those material properties  
35 resulted in variations in the amount of PCM melted, as well as the shape of the melting front. The  
36 results pointed to the importance of accounting for natural convection during melting in a PCM.  
37  
38  
39

40  
41  
42  
43  
44  
45  
46 A summary of the investigations devoted to melting of phase change materials contained  
47 within rectangular vessels [11-35] are provided in Table 2. Specifically, the imposed boundary  
48 conditions (BC), PCM type, adopted methodologies/techniques, along with the highlights of the  
49 findings are summarized. It is clear from literature reviewed above that conduction heat transfer  
50 associated with high temperature gradient, high melting rate, parallel-wall isotherms and symmetric  
51 melting at upper and lower part of the containers is the characteristic of the initial period of melting  
52 for both CWT and CHF boundary conditions. Later on as buoyancy-driven convection develops, the  
53 thickness of melt liquid increases resulting in decay of temperature gradient and melting rate which  
54 is accompanied with asymmetric melting between upper and lower parts and formation of curvature  
55  
56  
57  
58  
59  
60  
61  
62  
63  
64  
65



1  
2  
3 in isotherms. Therefore, these two mechanisms of heat transfer are important in any analytical and  
4 numerical investigations. Also, the operating conditions ( $Ra$ ,  $Ste$ ,  $Sc$ ) and geometrical parameter  
5 (aspect ratio) influence the heat transfer mechanisms which in turn affects the melting behavior of  
6 PCM. Commonly, the aspect ratio is defined as the container's variable height to constant width,  
7 thus the height determines the magnitude of this ratio. Greater melted volume is achieved at higher  
8 values of  $Ra$  and  $Ste$ , and lower levels of  $Sc$  and aspect ratio. Moreover, the orientation of the heat  
9 source and specific boundary condition play a significant role on the heat transfer modes and  
10 resulting melting characteristics. Lower positioning of a heat source ensures close-contact melting at  
11 a high rate.  
12  
13  
14  
15  
16  
17  
18  
19  
20  
21  
22

### 23 3. Melting in spherical capsules

24  
25  
26 **Two-dimensional** melting in a spherical shell can be classified into two groups: constrained  
27 and unconstrained melting. Constrained melting (**also known as inward or fixed**) is unavoidable in  
28 experimental studies when thermocouples are positioned inside the spherical containers. In effect,  
29 the thermocouples hold the solid PCM in place and prevent it from sinking/rising to the bottom/top  
30 of the sphere due to gravity. For cases when there is no difference in densities between the liquid  
31 and solid phases, constrained melting will also persist. In effect, there is no direct contact melting  
32 next to the wall of the container. Unlike constrained melting, unconstrained melting (**also called**  
33 **close-contact, unfixed**) is encountered when there is no anchor inside the **capsule** for the solid PCM  
34 to cling to with the existence of difference in density between the liquid and solid phases. Therefore,  
35 the solid PCM will sink/rise to the bottom/top of the sphere and will experience thermal contact with  
36 the surface of the **cell**. Consequently, direct contact melting next to the wall of the **container** will be  
37 observed.  
38  
39  
40  
41  
42  
43  
44  
45  
46  
47

48 Saitoh and Hoshi [36] presented an approximate analytical solution for the close-contact  
49 melting heat transfer characteristics including melt flow in the liquid film subject to an inner wall  
50 temperature distribution in cylindrical or spherical capsules with neglecting the effect of natural  
51 convection in the upper liquid region. The effects of the Stefan number and variable temperature  
52 profile were clarified in detail. In addition, the effects of the variable inner wall temperature on the  
53 molten mass fraction were investigated. **The analytical results were compared with the numerical**  
54 **solutions for molten mass fraction and melt layer thickness. Agreement between the two approaches**  
55  
56  
57  
58  
59  
60  
61  
62  
63  
64  
65

1  
2  
3 was excellent. They concluded that the progress of melting is faster than the constant temperature  
4 conditions if the capsule's wall temperature distribution is exactly accounted for. Also, the same  
5 authors [37] reported details of an experimental setup (Fig. 15) used to investigate the combined  
6 close-contact and natural convection melting in both horizontal cylindrical and spherical capsules  
7 immersed in a high-temperature environment. The shape of the interface and the complete melting  
8 time under various ambient temperatures were observed. In addition, the effects of the variation of  
9 the inner wall temperature and the molten mass fraction on melting characteristics were investigated  
10 experimentally. Their findings indicated that the molten mass fraction is strongly dependent on the  
11 Stefan number. Also, the inner wall temperature varies in a complicated manner with time, and there  
12 is temperature distribution along the peripheral direction that influences the complete melting time.  
13  
14

15  
16 Fomin and Saitoh [38] researched numerically (boundary fixing method) and analytically  
17 (perturbation technique) the close-contact (unconstrained) melting process of unfixed solid in a  
18 spherical capsule. The approximate analytical solutions were found to be in good agreement with  
19 the numerical solutions of the complete mathematical model. The discrepancy in the results did not  
20 exceed 10-15% due to primarily neglecting the melting in the upper part in the analytical solution.  
21 Computed results reveal that ignoring the effect of streamwise convection in the liquid layer leads to  
22 overestimating of melting rate. Moreover, they concluded that the assumption of the constant  
23 temperature wall of the capsule can lead to the results which significantly differ from those obtained  
24 for the actual conditions of melting where the wall of the capsule is non-isothermal.  
25  
26

27  
28 Khodadadi and Zhang [39] conducted a numerical study of the effects of buoyancy-driven  
29 convection on constrained melting of phase change materials within spherical containers by using  
30 the finite volume procedure with a single-domain enthalpy formulation for simulation the phase  
31 change phenomenon. At the beginning of the melting process, the conduction mode of heat transfer  
32 is dominant, giving rise to concentric temperature contours. As buoyancy-driven convection is  
33 strengthened due to the growth of the melt zone, melting in the top region of the sphere is much  
34 faster than in the bottom region. The findings indicated that the strength of natural convection  
35 during the melting process is clearly dependent on the Rayleigh number when compared to the  
36 Stefan number. In addition, the Prandtl number plays an important role in the melting process. A  
37 melting experiment was also conducted to support the validity of the computational findings through  
38 comparison of the instantaneous melting patterns.  
39  
40

41  
42 Assis et al. [40] explored experimentally and numerically the process of unfixed melting of a  
43 phase change material in a spherical vessel. The numerical simulations followed the melting process  
44  
45  
46  
47  
48  
49  
50  
51  
52  
53  
54  
55  
56  
57  
58  
59  
60  
61  
62  
63  
64  
65

1  
2  
3 from the beginning to the end and incorporated such phenomena as convection in the liquid phase,  
4 volumetric expansion due to melting, sinking of the solid in the liquid, and close contact melting.  
5 The experimental findings included visualization of melting that compared favorably with the  
6 numerical results and thus served to validate the numerical approach. The computational results  
7 showed how the transient phase change process depended on the thermal and geometrical parameters  
8 of the system, including the temperature difference between the wall and the mean melting  
9 temperature (impact of the Stefan number), and the diameter of the sphere. They reported that the  
10 melting time was slightly shorter in the results of simulation due to an additional thermal resistance  
11 of the glass container, albeit small, in the experiments. Dimensional analysis of the results was  
12 performed and presented as variations of the mean Nusselt numbers and PCM melt fractions  
13 depending on an appropriate combination of the Fourier, Stefan and Grashof numbers. This analysis  
14 led to generalizations that encompassed the cases of melting in spherical capsules.

15  
16  
17  
18  
19  
20  
21  
22  
23  
24  
25  
26  
27  
28  
29  
30  
31  
32  
33  
34  
35  
36  
37  
38  
39  
40  
41  
42  
43  
44  
45  
46  
47  
48  
49  
50  
51  
52  
53  
54  
55  
56  
57  
58  
59  
60  
61  
62  
63  
64  
65

Tan [41] investigated experimentally the constrained and unconstrained melting (Fig. 16a) of phase change materials inside a sphere using n-octadecane for multiple wall temperatures and subcooling ranges. He reported that in unconstrained melting, the melting of PCM at the beginning is dominated by heat conduction across the wall. As the PCM melts, it sinks to the bottom of the sphere due to the density difference of the two phases. Thus, melting at the bottom half is much faster due to heat conduction at the inner wall (close-contact melting), while the buoyancy effect is responsible for melting in upper half. In constrained melting, heat conduction only exists at the beginning of the melting process; therefore melting is mainly through natural convection in the liquid at the top and bottom halves of the liquid part of the PCM. This effect causes the melting PCM to melt almost concentrically inward. An oval shape of the solid PCM is formed within the top half of the sphere due to natural convection heat transfer in the liquid PCM. The top half of the sphere melted at a faster rate than the bottom half. Natural convection cells were also formed in the bottom half, thus causing the wavy profile on the bottom of the solid phase, as shown in Fig. 16b. Thereafter, Tan et al. [42] studied numerically and experimentally the constrained melting of n-octadecane inside a spherical capsule. The computations were based on an iterative, finite-volume numerical procedure that incorporated a single-domain enthalpy formulation for simulation of the phase change phenomenon. The results revealed that conductive heat transfer dominates during the early period, as evident by the near-spherical shape of the PCM. As buoyancy-driven convection was strengthened due to the growth of the melt zone, it was observed that melting in the top region of the sphere is much faster than in the bottom region of the sphere. Waviness of the bottom surface

1  
2  
3 of the PCM was also observed due to unstable fluid layer that supports chaotic fluctuations and high  
4 discrepancy between numerical and experimental readings of temperatures, while this discrepancy in  
5 relatively low in the stable molten liquid layer in the top half of the sphere (Fig. 17). Thermal  
6 stratification within the constant temperature bath that encloses the capsule may play a role in the  
7 experiments. They reasoned that the underestimated experimental observations of waviness and  
8 excessive melting of the bottom region of PCM due to existence a support structure that held the  
9 sphere could have also inhibited heat from reaching the bottom of the sphere.

10  
11 Veerappan et al. [43] presented an analytical model based on quasi-steady approximations  
12 for solidification and melting of PCM in a spherical container under isothermal boundary conditions  
13 on the external surface of the spherical shell. The study involved five kinds of PCM which were 65  
14 mol% capric acid and 35 mol% lauric acid, calcium chloride hexahydrate, n-octadecane, n-  
15 hexadecane, and n-eicosane. The problem of melting inside a PCM can be treated as a problem of  
16 natural convection inside concentric spheres. Movement of the solid phase due to density difference  
17 was neglected. The problem was solved by defining conduction as the dominant mode of heat  
18 transfer and merging the convective effects in the thermal conductivity of the liquid. The results of  
19 the analytical models were validated against the previous experimental results and the deviations  
20 were found to be within 15% for solidification and 20% for melting. The transient interface  
21 positions and complete charging time predicted by the model that included conduction, natural  
22 convection, and heat generation effects matched with the experimental measurements as shown in  
23 Fig. 18. Initially, the experimental data closely matched the results of the pure-conduction model  
24 which is the dominant mode of heat transfer. After that, melting is greatly influenced by natural  
25 convection phenomena. The pure-conduction model overpredicts the complete melting time. The  
26 influence of the size of encapsulation, initial temperature of the PCM, the external fluid temperature  
27 on the solidified and molten mass fraction and the total phase change time were also investigated.  
28 According to the melting and solidification characteristics of PCM, the results revealed that the 65  
29 mol% capric acid with 35 mol% lauric acid and calcium chloride hexahydrate were better options for  
30 melting and solidification, respectively.

31  
32  
33  
34  
35  
36  
37  
38  
39  
40  
41  
42  
43  
44  
45  
46  
47  
48  
49  
50  
51  
52  
53  
54  
55  
56  
57  
58  
59  
60  
61  
62  
63  
64  
65  
66  
67  
68  
69  
70  
71  
72  
73  
74  
75  
76  
77  
78  
79  
80  
81  
82  
83  
84  
85  
86  
87  
88  
89  
90  
91  
92  
93  
94  
95  
96  
97  
98  
99  
100  
101  
102  
103  
104  
105  
106  
107  
108  
109  
110  
111  
112  
113  
114  
115  
116  
117  
118  
119  
120  
121  
122  
123  
124  
125  
126  
127  
128  
129  
130  
131  
132  
133  
134  
135  
136  
137  
138  
139  
140  
141  
142  
143  
144  
145  
146  
147  
148  
149  
150  
151  
152  
153  
154  
155  
156  
157  
158  
159  
160  
161  
162  
163  
164  
165  
166  
167  
168  
169  
170  
171  
172  
173  
174  
175  
176  
177  
178  
179  
180  
181  
182  
183  
184  
185  
186  
187  
188  
189  
190  
191  
192  
193  
194  
195  
196  
197  
198  
199  
200  
201  
202  
203  
204  
205  
206  
207  
208  
209  
210  
211  
212  
213  
214  
215  
216  
217  
218  
219  
220  
221  
222  
223  
224  
225  
226  
227  
228  
229  
230  
231  
232  
233  
234  
235  
236  
237  
238  
239  
240  
241  
242  
243  
244  
245  
246  
247  
248  
249  
250  
251  
252  
253  
254  
255  
256  
257  
258  
259  
260  
261  
262  
263  
264  
265  
266  
267  
268  
269  
270  
271  
272  
273  
274  
275  
276  
277  
278  
279  
280  
281  
282  
283  
284  
285  
286  
287  
288  
289  
290  
291  
292  
293  
294  
295  
296  
297  
298  
299  
300  
301  
302  
303  
304  
305  
306  
307  
308  
309  
310  
311  
312  
313  
314  
315  
316  
317  
318  
319  
320  
321  
322  
323  
324  
325  
326  
327  
328  
329  
330  
331  
332  
333  
334  
335  
336  
337  
338  
339  
340  
341  
342  
343  
344  
345  
346  
347  
348  
349  
350  
351  
352  
353  
354  
355  
356  
357  
358  
359  
360  
361  
362  
363  
364  
365  
366  
367  
368  
369  
370  
371  
372  
373  
374  
375  
376  
377  
378  
379  
380  
381  
382  
383  
384  
385  
386  
387  
388  
389  
390  
391  
392  
393  
394  
395  
396  
397  
398  
399  
400  
401  
402  
403  
404  
405  
406  
407  
408  
409  
410  
411  
412  
413  
414  
415  
416  
417  
418  
419  
420  
421  
422  
423  
424  
425  
426  
427  
428  
429  
430  
431  
432  
433  
434  
435  
436  
437  
438  
439  
440  
441  
442  
443  
444  
445  
446  
447  
448  
449  
450  
451  
452  
453  
454  
455  
456  
457  
458  
459  
460  
461  
462  
463  
464  
465  
466  
467  
468  
469  
470  
471  
472  
473  
474  
475  
476  
477  
478  
479  
480  
481  
482  
483  
484  
485  
486  
487  
488  
489  
490  
491  
492  
493  
494  
495  
496  
497  
498  
499  
500  
501  
502  
503  
504  
505  
506  
507  
508  
509  
510  
511  
512  
513  
514  
515  
516  
517  
518  
519  
520  
521  
522  
523  
524  
525  
526  
527  
528  
529  
530  
531  
532  
533  
534  
535  
536  
537  
538  
539  
540  
541  
542  
543  
544  
545  
546  
547  
548  
549  
550  
551  
552  
553  
554  
555  
556  
557  
558  
559  
560  
561  
562  
563  
564  
565  
566  
567  
568  
569  
570  
571  
572  
573  
574  
575  
576  
577  
578  
579  
580  
581  
582  
583  
584  
585  
586  
587  
588  
589  
590  
591  
592  
593  
594  
595  
596  
597  
598  
599  
600  
601  
602  
603  
604  
605  
606  
607  
608  
609  
610  
611  
612  
613  
614  
615  
616  
617  
618  
619  
620  
621  
622  
623  
624  
625  
626  
627  
628  
629  
630  
631  
632  
633  
634  
635  
636  
637  
638  
639  
640  
641  
642  
643  
644  
645  
646  
647  
648  
649  
650  
651  
652  
653  
654  
655  
656  
657  
658  
659  
660  
661  
662  
663  
664  
665  
666  
667  
668  
669  
670  
671  
672  
673  
674  
675  
676  
677  
678  
679  
680  
681  
682  
683  
684  
685  
686  
687  
688  
689  
690  
691  
692  
693  
694  
695  
696  
697  
698  
699  
700  
701  
702  
703  
704  
705  
706  
707  
708  
709  
710  
711  
712  
713  
714  
715  
716  
717  
718  
719  
720  
721  
722  
723  
724  
725  
726  
727  
728  
729  
730  
731  
732  
733  
734  
735  
736  
737  
738  
739  
740  
741  
742  
743  
744  
745  
746  
747  
748  
749  
750  
751  
752  
753  
754  
755  
756  
757  
758  
759  
760  
761  
762  
763  
764  
765  
766  
767  
768  
769  
770  
771  
772  
773  
774  
775  
776  
777  
778  
779  
780  
781  
782  
783  
784  
785  
786  
787  
788  
789  
790  
791  
792  
793  
794  
795  
796  
797  
798  
799  
800  
801  
802  
803  
804  
805  
806  
807  
808  
809  
810  
811  
812  
813  
814  
815  
816  
817  
818  
819  
820  
821  
822  
823  
824  
825  
826  
827  
828  
829  
830  
831  
832  
833  
834  
835  
836  
837  
838  
839  
840  
841  
842  
843  
844  
845  
846  
847  
848  
849  
850  
851  
852  
853  
854  
855  
856  
857  
858  
859  
860  
861  
862  
863  
864  
865  
866  
867  
868  
869  
870  
871  
872  
873  
874  
875  
876  
877  
878  
879  
880  
881  
882  
883  
884  
885  
886  
887  
888  
889  
890  
891  
892  
893  
894  
895  
896  
897  
898  
899  
900  
901  
902  
903  
904  
905  
906  
907  
908  
909  
910  
911  
912  
913  
914  
915  
916  
917  
918  
919  
920  
921  
922  
923  
924  
925  
926  
927  
928  
929  
930  
931  
932  
933  
934  
935  
936  
937  
938  
939  
940  
941  
942  
943  
944  
945  
946  
947  
948  
949  
950  
951  
952  
953  
954  
955  
956  
957  
958  
959  
960  
961  
962  
963  
964  
965  
966  
967  
968  
969  
970  
971  
972  
973  
974  
975  
976  
977  
978  
979  
980  
981  
982  
983  
984  
985  
986  
987  
988  
989  
990  
991  
992  
993  
994  
995  
996  
997  
998  
999  
1000

1  
2  
3 thin layer of melted PCM was observed between the hot container's wall and the solid PCM. The  
4 solid PCM sinks and the liquid rises up to the top half of the sphere. Then, natural convection  
5 becomes dominant at the top half of sphere where the melting rate is lower than the bottom half  
6 causing a reduction of the heat transfer and melting rate, in general. Although the Stefan number is  
7 an important parameter in the melting process, the simulation results indicate that the geometrical  
8 parameter such as the diameter of the sphere has more influence on the melting rate and heat release  
9 compared to the operating condition.  
10

11 Rizan et al. [45] studied experimentally the melting of n-octadecane in a spherical flask  
12 under the constant heat flux condition. The flask was immersed in a water tank and subjected to  
13 690, 850 and 950 W power-rated heater, respectively, until full melting was obtained as shown in  
14 Fig. 19. The melt-fraction versus time results indicated that melting was primarily dependent on the  
15 temperature level to which the PCM is subjected to and the area of the contact plane surface.  
16 Conduction heat transfer from the flask walls dominates the initial melting condition with increasing  
17 liquid boundary layer shifting dominant heat transfer mode to internal convection. Furthermore, it  
18 was found that the surface area in contact with the liquid front plays a major role as a larger surface  
19 area of the same volume will yield a higher melting rate due to internal convection.  
20

21 Outline of studies [36-45] associated with melting inside spherical capsules are listed in  
22 Table 3 and include information on the melting type (constrained and unconstrained), the imposed  
23 boundary conditions, PCM type, adopted methodologies/techniques, along with the highlights of the  
24 reported findings. The studies report on two melting modes which are constrained and  
25 unconstrained. Conduction heat transfer with concentric isotherms identifies the initial stages of  
26 PCM melting for both modes. After time progresses, buoyancy-driven convection will develop and  
27 dominate in constrained melting causing faster melting rate in the upper region of spherical capsule  
28 compared to the lower zone. In contrast, conduction and high rate of melting are registered at the  
29 lower part of the vessel where close-contact between solid PCM and wall dominates in  
30 unconstrained melting, while natural convection and low melting rate are dominant within the upper  
31 region. Furthermore, thermally stable melt layer of PCM in the upper half of sphere and unstable  
32 melt liquid with waviness in lower half are recorded in inward melting. The melting behavior is  
33 affected by operating parameters ( $Ra$ ,  $Ste$ ) and geometrical factor (diameter and thickness of the  
34 spherical capsule), Moreover, variation of prescribed constant wall temperature boundary condition  
35 due to free natural currents through outside medium has some effect on the melting rate.  
36  
37  
38  
39  
40  
41  
42  
43  
44  
45  
46  
47  
48  
49  
50  
51  
52  
53  
54  
55  
56  
57  
58  
59  
60  
61  
62  
63  
64  
65

#### 4. Melting in cylindrical vessels

Melting in cylindrical containers (having circular cross sections) is affected by the orientation of the symmetry axis of the cylindrical vessel with the gravity vector, i.e. vertically-oriented containers correspond to colinearity of the two vectors (section 4.1), whereas these two vectors are normal to each other for horizontally-oriented containers (section 4.2). Moreover, melting is categorized as constrained or unconstrained similar to the two-dimensional melting in a spherical shell discussed in section 3. It will be observed that melting in a horizontal cylinder or tube is similar to spherical containers due to the curvature effects common to both shapes.

##### 4.1. Vertical cylindrical containers

Melting of phase change materials in a vertical tube or vertical cylinder somewhat resembles the developing patterns associated with the two phases in tall rectangular enclosures. For these configurations, the cylinder is heated from the side and/or base or both.

Sparrow and Broadbent [46] conducted experimental study for melting of phase change material (n-eicosane) in a vertical tube heated isothermally from its side, insulated thermally from the bottom, while an air space was presented above the PCM for accommodating the volume change during melting. Numerical solutions based on pure conduction analytical model were also performed for comparison purposes. It is found that the melting process is significantly affected by fluid motions in liquid melt induced by the volume change and natural convection. Experimental findings indicated that the melting process with no subcooling displayed melting-related energy transfers and melting fraction were about 50% greater than that predicted by a model based on pure conduction. This deviation reflects the enhancing effects of fluid motions and natural convection in the liquid melt. In addition, they correlated the experimental results by using the Fourier, Stefan, and Grashof number. Initial subcooling substantially decreases the melting rate, the energy transfer for melting, and sensible heat storage.

Wenzhen et al. [47] studied analytically close-contact melting of phase change materials contained inside a vertical cylinder capsule which is isothermally-heated at bottom and its side (Fig. 20). They applied the liquid film theory to analyze heat transfer in the contact liquid layer and assumed that melting is dominated by heat transfer in the close-contact layer film at the bottom and by heat conduction through the stable liquid at the side with the top wall kept adiabatic. The results revealed that the effect of heat conduction through the liquid phase on the total melted mass fraction

1  
2  
3 is not significant. The theoretical formulas of the melting rate and thickness of the liquid layer  
4 during the heat transfer process were obtained through the analysis, which were convenient for  
5 engineering predictions. Also, the effects of the Stefan number and the aspect-ratio were reported.  
6  
7 The analytical findings indicated that increasing the Stefan number and/or reducing the aspect-ratio  
8 were advantageous to increasing the melting rate and lowering the total charging time.  
9

10  
11  
12 Wu and Lacroix [48] carried out a numerical study of natural convection that controlled  
13 melting of a phase change material within an isothermal vertical cylinder heated from its top, bottom  
14 and side walls (Fig. 21a). The governing conservation equations were formulated in terms of the  
15 stream function, vorticity and temperature. Body-fitted coordinates with finite difference method  
16 were employed for tracking the irregular shape of the time-wise changing solid–liquid phase front.  
17 Results showed that heat transfer for the case of top-heated surface is dominated by conduction.  
18 Also, the Nusselt number on the top surface decreases monotonically to zero as melting progressed,  
19 showing that no heat is transferred across the top layer once natural convection is fully developed in  
20 the melt (Fig. 21b). The highest heat transfer rates were observed on the bottom surface where the  
21 Benard convective cells developed. The convective flow patterns and time evolution of the phase  
22 front, resulting from simultaneous heating from the bottom, side, and top surfaces were far more  
23 complicated than those for the melting from a single isothermal boundary. Due to the convective  
24 motion of the melt along the vertical heated wall, the onset of the Benard convection occurred at a  
25 much earlier time than that for the case of melting within a cylinder heated from below.  
26  
27  
28  
29  
30  
31  
32  
33  
34  
35  
36  
37

38 Jones et al. [49] conducted an experimental (Fig. 22a) study of the melting of subcooled n-  
39 eicosane in a vertical cylindrical enclosure, complemented by a numerical investigation of the  
40 melting process where the enclosure was heated isothermally from the sides, maintained at a  
41 constant temperature at the bottom, and insulated at the top. The numerical simulations employing  
42 the enthalpy method adopted the finite volume method. Experimental results included temperature  
43 measurements, solid/liquid interface locations and volumetric liquid fractions. A semi-automated  
44 approach for extracting the solid/liquid interface locations using digital image processing techniques  
45 was developed. Comparisons between experimental measurements and numerical predictions for  
46 both melt front locations and temperature data revealed good general agreements for the Stefan  
47 numbers up to 0.1807. It has been shown from experimental findings that four distinct regimes  
48 occurred during the melting process which are: a) pure conduction, b) mixed convection/conduction,  
49 c) convection dominant, and d) “shrinking solid”, as shown in the Fig. 22b.  
50  
51  
52  
53  
54  
55  
56  
57  
58  
59  
60  
61  
62  
63  
64  
65

1  
2  
3  
4 Shmueli et al. [50] performed a numerical investigation of melting of PCM in vertical  
5 circular tubes insulated from bottom and isothermally heated at sides, while the upper part was  
6 exposed to air. The numerical analysis used an enthalpy–porosity formulation and was accompanied  
7 by image processing of the experimental results from the previous studies, yielding quantitative  
8 information about the local melt fractions and heat transfer rates. The model analyzed the effects of  
9 the mushy zone constant, pressure-velocity coupling and pressure discretization schemes on the  
10 thermal behavior of the melting process and quantitative agreement was obtained between the  
11 simulations and experiments. It was demonstrated that at the beginning of the process, heat transfer  
12 is governed by conduction from the tube wall to the solid phase through a relatively thin layer of  
13 already-molten liquid. As melting progresses, natural convection in the liquid dominates, changing  
14 the solid shape to conical and making it shrink from top to bottom (Fig. 23).

15  
16 Wang et al. [51] developed a finite-volume model for analyzing inward (external heat source)  
17 and outward (internal heat source) melting with natural convection in vertical cylindrical enclosures.  
18 The model was verified through detailed comparison with previous experimental and numerical  
19 results. Although there is general agreement between the numerical predictions and the experimental  
20 measurements for inward melting, there exists a quantitative mismatch due to the effects of the heat  
21 loss through the top wall and the air pockets formed in the solid PCM. For outward melting, the  
22 simulated melting front locations and the Nusselt number agree quite well with previous predictions  
23 for the low Rayleigh number cases. As for the high Rayleigh number cases, the differences between  
24 the two findings are substantial. Based on the modeling results of outward melting around  
25 isothermal vertical cylinders, consistent correlations for the Nusselt number as well as total and  
26 latent energy storage, all as functions of  $Ste Fo Ra^{1/2}$  were derived. These correlations provide  
27 convenient tools for engineering design purposes.

#### 28 29 30 31 32 33 34 35 36 37 38 39 40 41 42 43 44 45 46 47 48 49 *4.2. Horizontal cylindrical vessels*

50  
51  
52 A two-dimensional melting configuration of phase change materials in a horizontal tube or  
53 horizontal cylinder is similar to that encountered in spherical vessels where constrained or  
54 unconstrained melting are considered.

55  
56  
57  
58  
59  
60  
61  
62  
63  
64  
65  
Nicholas and Bayaziloglu [52] developed a mathematical model to examine the effect of  
unequal densities (unconstrained melting) on the shape and location of the solid-liquid interface for a



1  
2  
3 horizontal cylindrical enclosure that was heated by a constant heat flux. The numerical solutions  
4 were obtained by applying the implicit alternating direction method for the finite difference scheme.  
5  
6 For small values of the Stefan number, closest agreement was obtained between analytical results  
7 and numerical ones. As the Stefan number increases, the deviation between two results became  
8 more pronounced. The results showed that the wall temperature increases at the top due to the  
9 presence of a thick melt layer causing prevalent convection heat transfer, while the minimum wall  
10 temperature was registered at the bottom where close-contact melting due to heat conduction was  
11 occurring.  
12  
13  
14  
15  
16  
17

18 Ho and Viskanta [53] studied experimentally and numerically the inward constrained melting  
19 of n-octadecane in a horizontal cylindrical capsule heated isothermally. The experimental results  
20 emphasized the dominated-natural convection effect in the melt during inward melting. In addition  
21 to this effect in the liquid, a secondary vortex circulation initiated at the bottom part of the melt  
22 region which significantly affects the melting pattern as well as the heat transfer characteristics on  
23 the heated tube wall. As the thickness of the melt layer grows, the intensity of this vortex motion  
24 tends to decrease and eventually merges with the major convective recirculating flow. The initial  
25 subcooling affects diversely on both the melting rate and the intensity of the natural convection  
26 recirculation. Reasonable agreement was achieved between numerical predictions and experimental  
27 findings.  
28  
29  
30  
31  
32  
33  
34  
35

36 Bareiss and Beer [54] introduced an analytical and experimental study of close-contact  
37 melting of phase change material (n-octadecane and p-xylene) in a horizontal, isothermal-wall tube.  
38 The solid-liquid interface shape, melting rate, and heat flux intensity were evaluated experimentally.  
39 The analytical solutions of the melting rate and heat transfer coefficient agreed very well with the  
40 experimentally-evaluated quantities. The results revealed that the Nusselt number is a maximum at  
41 the beginning and decreases monotonically to zero at the end of the melting process. This behavior  
42 is due to the decreasing contact-heat transfer-area of the molten solid bulk.  
43  
44  
45  
46  
47  
48

49 Sparrow and Geiger [55] studied experimentally and numerically melting of n-eicosane  
50 encapsulated in a horizontal tube. Two types of melting were involved, namely constrained  
51 (centered mode) and unconstrained (free or wall-adjacent mode). The results illustrated that the  
52 quantity of mass melted in the unconstrained mode exceed that of the constrained mode by about 50-  
53 100% depending on the operating conditions. In addition, numerical solutions showed that  
54 approximately 90% of melting in the wall-adjacent mode occurred at the lower portion of the solid  
55 where conduction dominated heat transfer. The experimental findings demonstrated that the melting  
56  
57  
58  
59  
60  
61  
62  
63  
64  
65

1  
2  
3 process in constrained pattern is basically 3-D, while the unconstrained melting can be considered as  
4 2-D problem through neglecting the end effect.  
5  
6

7 Prasad and Sengupta [56] studied numerically the unconstrained melting of a PCM inside a  
8 horizontal tube subjected to a constant wall temperature. The model evaluated the irregular,  
9 temporal shape of the solid-liquid interface, the downward-motion of unmelt PCM due to density  
10 difference, and natural convection currents in the liquid phase. The effects of the Rayleigh, Stefan,  
11 and Prandtl numbers on the Nusselt number were also investigated within the range of interest in  
12 solar storage devices. The findings showed that the Nusselt number increases as the Rayleigh  
13 number increases. This is due to the fact that the higher Rayleigh number is associated with strong  
14 natural convection velocities resulting in higher heat transfer rates at the upper wall. The computed  
15 results explained that both the Stefan and Prandtl numbers has a significant influence on the melting  
16 rate. Conversely, the melting rate varies unimportantly with the Rayleigh number (controls the heat  
17 flux at the upper wall and the interfaces). Also, useful correlations for melt time and the Nusselt  
18 number were obtained.  
19  
20  
21  
22  
23  
24  
25  
26  
27  
28

29 Hirata and Nishida [57] presented an analytical and experimental investigation of constrained  
30 melting of n-octadecane inside an isothermally heated horizontal cylinder. The analysis utilized the  
31 equivalent thermal conductivity of the liquid phase which is estimated from the results for natural  
32 convection heat transfer between concentric cylinders (solid PCM phase and heated cylinder);  
33 therefore, the melting was analyzed as pure conduction problem. Analytical results showed a good  
34 agreement with experimental data for wide range of the Rayleigh numbers. Also, the influence of  
35 buoyancy-driven convection was insignificant when  $Ra < 10^5$ .  
36  
37  
38  
39  
40  
41

42 An experimental study of unfixed melting inside a horizontal tube subjected to an external  
43 forced convective heating condition is presented by Maldonado et al. [58]. The experiments were  
44 conducted for a wide range of the Stefan (0.026-0.053) and Archimedes numbers ( $8.76 \times 10^6$ -  
45  $3.34 \times 10^8$ ). In about half the tests, the melt rate was indicated to be approximately identical to that  
46 for constant-wall heated capsule. Generally, the melt rate appeared to be highly affected by the  
47 dynamics of the melting process. The experimental findings revealed that in most cases, the melt  
48 rate during the initial stages of melting was significantly lower than expected. An analysis of  
49 experimental results suggested this was due to asymmetric melting during this period. Whereas, the  
50 two remaining tests registered higher melt rates than expected.  
51  
52  
53  
54  
55  
56  
57

58 Park et al. [59] investigated numerically the constrained melting of phase change material  
59 inside a horizontal cylindrical capsule that is heated isothermally. They simulated the problem by  
60  
61  
62  
63  
64  
65

1  
2  
3 utilizing the pseudo-compressibility method based on finite volume approach with the enthalpy  
4 formulation utilized in the energy equation. Initial disturbance was assumed for the sake of  
5 examining its effect on the solution for two values of the Rayleigh number. The results exposed that  
6 at  $Ra=1 \times 10^6$  natural convection flow pattern was unicellular in the symmetric half domain  
7 throughout the melting process for all the types of perturbations. In contrast, when the Rayleigh  
8 number was increased to  $8 \times 10^6$ , two branching solutions (bi-cellular and tri-cellular flow) were  
9 obtained according to the type of the initial disturbances, where secondary vortex circulation was  
10 shown at the lower part of the melt region due to thermal instabilities. Also, the results revealed that  
11 initial small perturbations of very minor difference can induce different melting patterns.

12  
13  
14  
15  
16  
17  
18  
19  
20 Saitho and Kato [60] studied experimentally and numerically the close-contact melting  
21 behavior accompanying with natural convection of n-octadecane in the melt liquid region inside  
22 horizontal cylindrical capsule subjected to either constant temperature-bath or constant wall  
23 temperature. The experimental results were compared with the numerical ones in which both heat  
24 transfer mechanisms are included. The experimental and numerical findings revealed that small  
25 Stefan number confirms that the close-contact melting is the dominant mode of heat transfer with  
26 10-15% being the contribution of natural convection to the melting rate. As the Stefan number  
27 increases, the role of natural convection becomes significant.

28  
29  
30  
31  
32  
33  
34  
35  
36  
37  
38  
39  
40  
41  
42  
43  
44  
45  
46  
47  
48  
49  
50  
51  
52  
53  
54  
55  
56  
57  
58  
59  
60  
61  
62  
63  
64  
65  
66  
67  
68  
69  
70  
71  
72  
73  
74  
75  
76  
77  
78  
79  
80  
81  
82  
83  
84  
85  
86  
87  
88  
89  
90  
91  
92  
93  
94  
95  
96  
97  
98  
99  
100  
101  
102  
103  
104  
105  
106  
107  
108  
109  
110  
111  
112  
113  
114  
115  
116  
117  
118  
119  
120  
121  
122  
123  
124  
125  
126  
127  
128  
129  
130  
131  
132  
133  
134  
135  
136  
137  
138  
139  
140  
141  
142  
143  
144  
145  
146  
147  
148  
149  
150  
151  
152  
153  
154  
155  
156  
157  
158  
159  
160  
161  
162  
163  
164  
165  
166  
167  
168  
169  
170  
171  
172  
173  
174  
175  
176  
177  
178  
179  
180  
181  
182  
183  
184  
185  
186  
187  
188  
189  
190  
191  
192  
193  
194  
195  
196  
197  
198  
199  
200  
201  
202  
203  
204  
205  
206  
207  
208  
209  
210  
211  
212  
213  
214  
215  
216  
217  
218  
219  
220  
221  
222  
223  
224  
225  
226  
227  
228  
229  
230  
231  
232  
233  
234  
235  
236  
237  
238  
239  
240  
241  
242  
243  
244  
245  
246  
247  
248  
249  
250  
251  
252  
253  
254  
255  
256  
257  
258  
259  
260  
261  
262  
263  
264  
265  
266  
267  
268  
269  
270  
271  
272  
273  
274  
275  
276  
277  
278  
279  
280  
281  
282  
283  
284  
285  
286  
287  
288  
289  
290  
291  
292  
293  
294  
295  
296  
297  
298  
299  
300  
301  
302  
303  
304  
305  
306  
307  
308  
309  
310  
311  
312  
313  
314  
315  
316  
317  
318  
319  
320  
321  
322  
323  
324  
325  
326  
327  
328  
329  
330  
331  
332  
333  
334  
335  
336  
337  
338  
339  
340  
341  
342  
343  
344  
345  
346  
347  
348  
349  
350  
351  
352  
353  
354  
355  
356  
357  
358  
359  
360  
361  
362  
363  
364  
365  
366  
367  
368  
369  
370  
371  
372  
373  
374  
375  
376  
377  
378  
379  
380  
381  
382  
383  
384  
385  
386  
387  
388  
389  
390  
391  
392  
393  
394  
395  
396  
397  
398  
399  
400  
401  
402  
403  
404  
405  
406  
407  
408  
409  
410  
411  
412  
413  
414  
415  
416  
417  
418  
419  
420  
421  
422  
423  
424  
425  
426  
427  
428  
429  
430  
431  
432  
433  
434  
435  
436  
437  
438  
439  
440  
441  
442  
443  
444  
445  
446  
447  
448  
449  
450  
451  
452  
453  
454  
455  
456  
457  
458  
459  
460  
461  
462  
463  
464  
465  
466  
467  
468  
469  
470  
471  
472  
473  
474  
475  
476  
477  
478  
479  
480  
481  
482  
483  
484  
485  
486  
487  
488  
489  
490  
491  
492  
493  
494  
495  
496  
497  
498  
499  
500  
501  
502  
503  
504  
505  
506  
507  
508  
509  
510  
511  
512  
513  
514  
515  
516  
517  
518  
519  
520  
521  
522  
523  
524  
525  
526  
527  
528  
529  
530  
531  
532  
533  
534  
535  
536  
537  
538  
539  
540  
541  
542  
543  
544  
545  
546  
547  
548  
549  
550  
551  
552  
553  
554  
555  
556  
557  
558  
559  
560  
561  
562  
563  
564  
565  
566  
567  
568  
569  
570  
571  
572  
573  
574  
575  
576  
577  
578  
579  
580  
581  
582  
583  
584  
585  
586  
587  
588  
589  
590  
591  
592  
593  
594  
595  
596  
597  
598  
599  
600  
601  
602  
603  
604  
605  
606  
607  
608  
609  
610  
611  
612  
613  
614  
615  
616  
617  
618  
619  
620  
621  
622  
623  
624  
625  
626  
627  
628  
629  
630  
631  
632  
633  
634  
635  
636  
637  
638  
639  
640  
641  
642  
643  
644  
645  
646  
647  
648  
649  
650  
651  
652  
653  
654  
655  
656  
657  
658  
659  
660  
661  
662  
663  
664  
665  
666  
667  
668  
669  
670  
671  
672  
673  
674  
675  
676  
677  
678  
679  
680  
681  
682  
683  
684  
685  
686  
687  
688  
689  
690  
691  
692  
693  
694  
695  
696  
697  
698  
699  
700  
701  
702  
703  
704  
705  
706  
707  
708  
709  
710  
711  
712  
713  
714  
715  
716  
717  
718  
719  
720  
721  
722  
723  
724  
725  
726  
727  
728  
729  
730  
731  
732  
733  
734  
735  
736  
737  
738  
739  
740  
741  
742  
743  
744  
745  
746  
747  
748  
749  
750  
751  
752  
753  
754  
755  
756  
757  
758  
759  
760  
761  
762  
763  
764  
765  
766  
767  
768  
769  
770  
771  
772  
773  
774  
775  
776  
777  
778  
779  
780  
781  
782  
783  
784  
785  
786  
787  
788  
789  
790  
791  
792  
793  
794  
795  
796  
797  
798  
799  
800  
801  
802  
803  
804  
805  
806  
807  
808  
809  
810  
811  
812  
813  
814  
815  
816  
817  
818  
819  
820  
821  
822  
823  
824  
825  
826  
827  
828  
829  
830  
831  
832  
833  
834  
835  
836  
837  
838  
839  
840  
841  
842  
843  
844  
845  
846  
847  
848  
849  
850  
851  
852  
853  
854  
855  
856  
857  
858  
859  
860  
861  
862  
863  
864  
865  
866  
867  
868  
869  
870  
871  
872  
873  
874  
875  
876  
877  
878  
879  
880  
881  
882  
883  
884  
885  
886  
887  
888  
889  
890  
891  
892  
893  
894  
895  
896  
897  
898  
899  
900  
901  
902  
903  
904  
905  
906  
907  
908  
909  
910  
911  
912  
913  
914  
915  
916  
917  
918  
919  
920  
921  
922  
923  
924  
925  
926  
927  
928  
929  
930  
931  
932  
933  
934  
935  
936  
937  
938  
939  
940  
941  
942  
943  
944  
945  
946  
947  
948  
949  
950  
951  
952  
953  
954  
955  
956  
957  
958  
959  
960  
961  
962  
963  
964  
965  
966  
967  
968  
969  
970  
971  
972  
973  
974  
975  
976  
977  
978  
979  
980  
981  
982  
983  
984  
985  
986  
987  
988  
989  
990  
991  
992  
993  
994  
995  
996  
997  
998  
999  
1000

Costa et al. [61] studied numerically the inherent three-dimensional behavior that takes place  
in the center-mode melting process inside a horizontal isothermal cylinder enclosure and how it  
affects the main design parameters. The numerical results have been compared with a two-  
dimensional numerical prediction and with some experimental data. The differences encountered  
between the three- and two-dimensional simulations had been studied in two different cases of  
imposed wall temperatures and the corresponding Rayleigh and Stefan numbers. In case A  
( $Ra=3.68 \times 10^5$  and  $Ste=0.04$ ) the component of the velocities in the axial direction is small in  
comparison with the other components. However, the flow pattern developed is completely different  
from that predicted by a two-dimensional simulation, and consequently, a different melting front is  
developed. Case B ( $Ra=1.22 \times 10^6$  and  $Ste=0.133$ ) exhibits a distinct three-dimensional flow pattern  
with a marked wavy shape of the melting front at the bottom in the axial direction. Although the  
computational results showed that the effect of the three-dimensionality on both the melted mass  
fraction and the overall Nusselt number seems to be unimportant (Fig. 24), the mean Nusselt number  
along the axis varies significantly according to the flow pattern.

1  
2  
3  
4 Chung et al. [62] analyzed numerically by using the enthalpy method the multi-cell structure  
5 and the thermal instability at the early stage of the inward melting process in a horizontal cylinder  
6 heated isothermally for a relatively wide range of the Rayleigh numbers. The results exhibited that  
7 at the low Rayleigh number, the flow in the liquid gap is in the stable state as the viscous force is  
8 dominant. For the intermediate Rayleigh number, the thermal buoyancy and viscous forces were  
9 balanced in a neutrally stable state. Thus, the flow is prone to transit to different patterns by  
10 infinitesimal experimental or numerical disturbances. At the high Rayleigh number, the Benard  
11 convection shows an orderly behavior without being affected by the base flow.  
12  
13  
14  
15  
16  
17

18 Kawanami et al. [63] performed an experimental study to evaluate the close-contact melting  
19 characteristics of slush ice (mixture of fine ice particles and ethylene glycol aqueous solution) in a  
20 horizontal cylindrical capsule which was heated by a constant heat flux. Initially, conduction heat  
21 transfer dominates and buoyancy force draws the slush ice to the top of the heated capsule where  
22 close-contact melting occurs. As time progresses, natural convection developed causing formation  
23 of a number of stratified layers in the melt. The results revealed that the local heat transfer  
24 coefficient is greatest at the top of the vessel and tends to decrease along the wall and this coefficient  
25 is proportional to the heat flux and the initial solution concentration. Also, the melting rate varied  
26 monotonically with the melting time, irrespective of the heat flux and initial solution concentration.  
27  
28  
29  
30  
31  
32  
33

34 Hirose et al. [64] studied experimentally and numerically the combined natural convection  
35 heat transfer of water around tubes with the constrained melting of ice inside horizontal elliptical  
36 tubes. The numerical solution of the governing equations depended on the boundary fixing method  
37 to obtain the transient melting front contours and the body-fitted coordinate system to solve  
38 convection heat transfer around horizontal elliptical tubes. The results were presented in terms of  
39 the melting front contours of the phase change material, wall temperature distributions, isotherms,  
40 flow patterns and melting fraction. Also, good agreement of the melting fraction was achieved  
41 between analysis and experiment.  
42  
43  
44  
45  
46  
47  
48

49 The constrained melting characteristics of paraffin wax encapsulated in a cylindrical  
50 capsule used in a latent heat solar thermal energy storage system were investigated numerically and  
51 experimentally by Regin et al. [65]. The melting occurred due to heat transfer isothermally from the  
52 surrounding hot water. The numerical analysis was performed by adopting the enthalpy method and  
53 the results were verified with the experimental findings. The results revealed that the Stefan  
54 number,  $Ste$ , phase change temperature range and the capsule radius were the main parameters that  
55 govern the melting process. Also, the agreement between analytical and experimental results was  
56  
57  
58  
59  
60  
61  
62  
63  
64  
65

1  
2  
3 significantly improved when the results were obtained considering phase change temperature range  
4 and the natural convection in the liquid phase instead of considering the process to be dominated by  
5 conduction only.  
6  
7

8  
9 A summary of the studies focusing on melting of phase change materials contained within  
10 cylindrical vessels [46-65] are provided in Table 4. Specifically, cylindrical vessels' orientations,  
11 the imposed boundary conditions, PCM type, adopted methodologies/techniques, along with the  
12 highlights of the findings are summarized. The location of the heat source or boundary condition  
13 (BC), density variation of the two phases and existence of an anchor or thermocouples determine the  
14 melting mode (unfixed or fixed) inside vertical cylinders, whereas the BC does not determine the  
15 melting mode inside horizontal vessels which are heated peripherally. For both orientations, the  
16 operating conditions ( $Ste$ ,  $Ra$ ,  $Sc$  and somewhat  $Pr$ ) and geometrical parameter (AR in vertical  
17 cylinder and radius in horizontal tube) have various effects on the melting rate and resulting  
18 charging time.  
19  
20

21  
22 For melting inside vertical cylinders, the heat transfer mechanisms depend on both the  
23 location of heat source and time period of melting process. The close-contact heat transfer is  
24 responsible for the majority of unfixed melting where the heat source is applied at the bottom  
25 surface, while the small fraction of PCM is melted due to conduction heat transfer through the stable  
26 liquid phase at the side. On the other hand, the lateral location of the heat source insures fixed  
27 melting and both conduction and buoyancy-driven convection play successive roles at different  
28 times with associated effects on the characteristics of the melting process. Initially, viscous effect  
29 acts significantly and later, melting process will be under dominance of the buoyancy force. Also, in  
30 fixed melting, the temporal evolution of the solid-liquid interface and developed flow pattern  
31 generated from the simultaneous heating from the bottom, side and top walls are more complicated  
32 than those found for the melting resulting from heating at a single boundary.  
33  
34

35  
36 Constrained and unconstrained melting is considered in the horizontal tubes like that  
37 observed in spherical capsules. Constrained melting emphasizes the dominant natural convection  
38 effect in the melt where circulating secondary vortices lead to formation of surface waviness on the  
39 bottom of the solid PCM, whereas conduction appears only during the initial period of melting. In  
40 contrast, close-contact heat transfer forms the important contribution in unconstrained melting with  
41 small fraction of melting resulted from the buoyancy effect. For the same operational and  
42 geometrical parameters, unconstrained melting exhibits higher melting rate than that associated with  
43 constrained melting.  
44  
45  
46  
47  
48  
49  
50  
51  
52  
53  
54  
55  
56  
57  
58  
59  
60  
61

## 5. Melting in annular cavities

The applications of this type of containers are related to the shell and tube heat exchangers where the phase change material exists in the annular space. Melting of the PCM occurs when there is heat exchange between the PCM and the hot fluid/ambient. On the other hand, 2D analysis of melting process in vertically-oriented annular spaces is similar to that in rectangular and vertically-oriented cylindrical cavities.

Khillarkar et al. [66] presented a streamline Upwind/Petrov Galerkin finite element computational study of the free convection-dominated melting of a pure phase change material contained in the concentric horizontal annuli of the two configurations shown in Fig. 25. Simulations were carried out for melting of a pure phase change material (n-octadecane) in a cylindrical-horizontal annular space heated isothermally from inside, outside or both walls. For both horizontal annuli arrangements, it was observed that the effect of heating both walls is the same as heating the inside wall and the outside wall separately until there is interaction between the two melt zones. However, during the late stages melting appears to occur at a faster rate due to good mixing between the melt zones formed by heating both the inside and outside walls. This suppressed thermal stratification, which occurred in both configurations for heating from the inside wall. Effect of the Rayleigh number on the two flow patterns within the melt and the local heat transfer rate on the inner wall were also examined. High Rayleigh number results in an earlier onset of convection, expediting the melting process for both heating cases and higher degree of thermal stratification was shown for the case of inside wall heating.

Dutta et al. [67] studied experimentally (Fig. 26) and numerically heat transfer and phase change within a PCM (paraffin wax) encapsulated in the horizontal annulus of two coaxial circular cylinders with isothermal and adiabatic conditions on the inner and the outer cylinders, respectively. The two-dimensional unsteady Navier–Stokes and energy (enthalpy formulation) equations were solved using the finite volume method (FVM) using the SIMPLE scheme to track the temperature at different points and the moving solid–liquid interface numerically. The predicted results exhibited good agreement with the experimental findings. The computational results revealed that both the eccentricity and the variation in the angle of inclination of the eccentricity played an important role for the net circulation of the molten phase as well as the thermal flux on the inner surface of the annulus, where the maximum heat flux value increased monotonically both with angle of inclination

1  
2  
3 and eccentricity. For certain values of eccentricity, the maximum heat flux occurs at the bottom  
4 (inclination angle=0°) and decreases to a minimum value at the top point, that is almost at 180°.   
5  
6 Furthermore, the maximum value of the heat flux was attained for the highest eccentricity of 0.5 for  
7  
8 a fixed angle of inclination. Also, the results exhibited the enhancement in the convective heat  
9  
10 transfer with the increase of the Rayleigh number.

11  
12 Akgun et al. [68] performed an experimental investigation directed at studying melting and  
13  
14 solidification characteristics of three different types of paraffin as phase change materials. A shell-  
15  
16 in-tube thermal energy storage unit was considered. The PCM was placed in a vertically-oriented  
17  
18 annular space between a shell and a tube in which the heat transfer fluid (water) was flowing (Fig.  
19  
20 27). The results showed two regions coexisted during the charging process which are the melted  
21  
22 liquid and the non-melted PCM region in the solid phase. Heat conduction is responsible for the heat  
23  
24 transfer process inside the solid PCM and this region receives heat from the melted part by  
25  
26 convection. It was observed that the PCM in the lower outer region of the annulus took much longer  
27  
28 time than the other regions to melt. Therefore, the total melting time of the whole PCM was  
29  
30 prolonged. In order to improve heat transfer during the melting and solidification, the surface of the  
31  
32 shell (the outer surface of the PCM storage container) was inclined with an inclination angle of 5  
33  
34 degrees (Fig. 27). In addition, the effects of the Reynolds number of the heat exchange fluid in the  
35  
36 tube and the Stefan number on the melting and solidification behavior were determined.

37  
38 Sugawara et al. [69] investigated numerically freezing/melting of water/ice around a  
39  
40 horizontal cylinder placed in a square cavity of the inner side length  $H$  as shown in the Fig. 28a,  
41  
42 where heat was rejected or supplied isothermally. The governing equations were solved numerically  
43  
44 adopting a continuum model for phase change in porous media. The computed results indicated that  
45  
46 the degree of subcooling affected melting considerably during the early phase of the process,  
47  
48 however, its effect became gradually small with advancing time. In addition, melting decreased  
49  
50 considerably with increasing the distance  $h$  from the center of the cylinder to the bottom of the  
51  
52 container, as shown in Fig. 28b.

53  
54 Wei et al. [70] studied numerically the melting process of a phase change material held in the  
55  
56 concentric horizontal annuli of a square external adiabatic shell with a circular tube inside that was  
57  
58 heated isothermally. The simulation model adopted the enthalpy-porosity method and finite-volume  
59  
60 numerical procedure to solve the simultaneous governing equations. The results exhibited that  
61  
62 melting in the top part of shell is under convection-dominated mode and conduction-dominated  
63  
64 mode takes place in the bottom of the shell. In effect, the top portion melted far faster than the  
65

1  
2  
3 bottom (Fig. 29) suggesting that the heat surface should be placed lower in order to enhance melting  
4 and reduce the total melting time. The middle zone was dominated by both convection and  
5 conduction. Also, the melt fraction grows with time and the heat flux on the tube wall decreases  
6 sharply initially, then increases slowly and drops sharply after the solid PCM melts completely.  
7  
8

9  
10 Darzi et al. [71] presented a numerical study of melting of PCM contained between two  
11 horizontally-oriented cylinders for concentric and eccentric arrangements to investigate the effect of  
12 the position of the inner cylindrical tube on phase change. The inner cylindrical tube was heated  
13 isothermally, while the outer tube was insulated. The governing partial differential equations were  
14 solved using the enthalpy-porosity method which utilizes the finite volume method to obtain the  
15 computational findings. Predicted results showed that heat conduction to the PCM is dominant at  
16 the beginning of melting for all zones through contact melting. After a few minutes, natural  
17 convection becomes dominant at the top half of the hot cylinder while heat conduction remains  
18 dominant in the bottom of the hot cylinder. Thus, melting rate in the top half became faster than the  
19 bottom half of the horizontal annulus. It is interesting to note that when the inner cylinder tube is  
20 moved downward, the melting rate increases sharply due to the dominance of natural convection  
21 heat transfer in most areas of PCM which reflects the effect of eccentricity.  
22  
23

24  
25 Hosseini et al. [72] undertook an experimental (Fig. 30a) and numerical study to evaluate the  
26 role of buoyancy-driven convection during constrained melting of phase change material inside a  
27 shell and tube heat exchanger. The commercial paraffin RT50 (Rubitherm GmbH) was used as a  
28 latent heat energy storage material that melted due to heat transfer from hot water in the tube. The  
29 computational investigation relied on an iterative, finite-volume numerical procedure that  
30 incorporated a single-domain enthalpy formulation for simulation of the phase change phenomenon.  
31 Experimental results showed that the sharp rise in temperatures takes place at the uppermost section  
32 of the store because of the buoyancy effects. The computational results indicated the strong thermal  
33 stratification of the molten liquid in the upper half of the heat exchanger (Fig. 30b). Also, upon  
34 increasing the inlet temperature of water, the total melting time was decreased.  
35  
36

37  
38 Outline of studies [66-72] associated with melting inside annular cavities are listed in Table 5  
39 with relevant details on the melting type (constrained and unconstrained), the imposed boundary  
40 conditions, PCM type, adopted methodologies/techniques along with the highlights of the reported  
41 findings. Two melting configurations are presented in the above literature. The first is due to  
42 heating from the inside tube that causes the melt front to progress outward away from the tube  
43 toward the shell. High degree of thermal stratification and low melting rate are associated with this  
44  
45  
46  
47  
48  
49  
50  
51  
52  
53  
54  
55  
56  
57  
58  
59  
60  
61  
62  
63  
64  
65



1  
2  
3 configuration as the supplied energy is used mainly in overheating the liquid PCM in the upper  
4 region of annulus instead of melting the solid PCM contained in the lower zone of the annulus.  
5  
6 Heating from outside (also called shell heating) where the melting interface moves circumferentially  
7 inward away from the shell form the second melting mode in annular containers. In this  
8 configuration, lower degree of thermal stratification and higher melting rate are observed in  
9 comparison with first mode under the same geometrical and operating conditions. Effects of the  
10 operating parameters and interchanging roles between conduction and convection with accompanied  
11 melting characteristics are same as that discussed for other container shapes. Furthermore, the  
12 vertical positioning of the tube relative to the shell leads to eccentricity which has positive effects of  
13 enhancement of the melting rate and decreasing the related charging time.  
14  
15  
16  
17  
18  
19  
20  
21  
22

## 23 6. Conclusions

24  
25 Melting of phase change materials and the ensuing natural convection within containers  
26 of different shapes is reviewed. In the absence of the close-contact melting effect, it is noticed in all  
27 containers that there are two heat transfer mechanisms that control the melting process, namely heat  
28 conduction and natural convection. Heat conduction plays a significant role during the early stage  
29 accompanied with high heat transfer rate, temperature contours fully orthogonal to the applied  
30 temperature gradient and the solid-liquid interface, high Nusselt numbers and temperature gradient,  
31 and significant melting rate. As time progressed, the volume of the melted liquid layer increases and  
32 convection-dominated melting will develop causing curvature of the melting interface and the  
33 isotherms, lowering of the heat transfer rate, and decrease in melting rate or increase of charging  
34 time. Buoyancy-driven flow depends on the thermophysical properties of the PCM, heat supplied or  
35 operating condition ( $Ra$ ,  $Ste$ ) and the geometry configuration of the enclosure. Thus, the shape and  
36 extent of the enclosure containing the PCM have an important effect on the dynamic behavior of the  
37 melting process and on the temperature of the cooled wall. The location of heat source and density  
38 difference between the solid and liquid phases determines the melting mode (constrained (fixed) or  
39 unconstrained (close-contact)). Close-contact melting where the solid PCM is continuously touching  
40 the container wall is accompanied with high heat transfer rate and leads to high melting rate. Also,  
41 geometrical orientations and parameters have a great influence on the heat transfer mechanisms-  
42 melting characteristics such as the aspect ratio in rectangular containers and vertical cylindrical  
43 vessels, radius in spherical capsules and eccentricity in annular cavities. Furthermore, to improve  
44 the melting rate, research should concentrate on upgrading the effective thermal conductivity of  
45  
46  
47  
48  
49  
50  
51  
52  
53  
54  
55  
56  
57  
58  
59  
60  
61  
62  
63  
64  
65

1  
2  
3 phase change materials through using thermal conductivity enhancers such as fixed promoters such  
4 as fins or using dispersions of high-conductivity nanostructures in the phase change materials.  
5  
6  
7

## 8 **Acknowledgement**

9  
10  
11 The first author (NSD), at that time a Ph.D.-candidate in Mechanical Engineering at the  
12 Baghdad University, acknowledges the support of the Ministry of Higher Education and Scientific  
13 Research (MOHESR) in Iraq through availability of a short-term scholarship to conduct research at  
14 Auburn University. He also acknowledges the Mechanical Engineering Department of the Samuel  
15 Ginn College of Engineering at Auburn University for providing laboratory space, machine shop  
16 support and assistance during his stay.  
17  
18

19  
20  
21  
22 The second author acknowledges support by the US Department of Energy under Award  
23 Number DE-SC0002470 (<http://www.eng.auburn.edu/nepcm>). This report was prepared as an  
24 account of work sponsored by an agency of the United States Government. Neither the United States  
25 Government nor any agency thereof, nor any of their employees, makes any warranty, express or  
26 implied, or assumes any legal liability or responsibility for the accuracy, completeness, or usefulness  
27 of any information, apparatus, product, or process disclosed, or represents that its use would not  
28 infringe privately owned rights. References herein to any specific commercial product, process, or  
29 service by trade name, trademark, manufacturer, or otherwise do not necessarily constitute or imply  
30 its endorsement, recommendation, or favoring by the United States Government or any agency  
31 thereof. The views and opinions of authors expressed herein do not necessarily state or reflect those  
32 of the United States Government or any agency thereof.  
33  
34  
35  
36  
37  
38  
39  
40  
41  
42  
43

## 44 **References**

- 45  
46  
47 [1] Abhat A. Low temperature latent heat thermal energy storage-heat storage Materials. Sol Energy  
48 1983; 30: 313–32.  
49  
50 [2] Kamimoto M. Thermal energy storage technology, Int J Sol Energy 1987; 5: 21–33.  
51  
52 [3] Hasnain SM. Review on sustainable thermal energy storage technologies, Part I: Heat storage  
53 materials and techniques. Energy Convers Manage 1998; 39: 1127–38.  
54  
55 [4] Zalba B, Marin JM, Cabeza LF, Mehling H. Review on thermal energy storage with phase  
56 change: materials, heat transfer analysis and applications. Appl Therm Eng 2003; 23: 251–83.  
57  
58  
59  
60  
61  
62  
63  
64  
65

- 1  
2  
3 [5] Farid MM, Khudhair AM, Razack SAK, Al-Hallaj S. A review on phase change energy storage:  
4 materials and applications. *Energy Convers Manage* 2004; 45: 1597–615.  
5  
6 [6] Sharma SD, Sagara K. Latent heat storage materials and systems: a review. *Int J Green Energy*  
7 2005; 2: 1–56.  
8  
9 [7] Kenisarin M, Mahkamov K. Solar energy storage using phase change materials. *Renew Sust*  
10 *Energy Rev* 2007; 11: 1913–65.  
11  
12 [8] Regin AF, Solanki SC, Saini JS. Heat transfer characteristics of thermal energy storage system  
13 using PCM capsules: a review. *Renew Sust Energy Rev* 2008; 12: 2438–58.  
14  
15 [9] Agyenim F, Hewitt N, Eames P, Smyth M. A review of materials, heat transfer and phase change  
16 problem formulation for latent heat thermal energy storage systems (LHTESS). *Renew Sust*  
17 *Energy Rev* 2010; 14: 615–28.  
18  
19 [10] Fan L, Khodadadi JM. Thermal conductivity enhancement of phase change materials for  
20 thermal energy storage: a review. *Renew Sust Energy Rev* 2011; 15: 24–46.  
21  
22 [11] Zhang Y, Chen Z, Wang Q, Wu Q. Melting in an enclosure with discrete heating at a constant  
23 rate. *Exp Fluid Therm Sci* 1993; 6: 196–201.  
24  
25 [12] Ho CJ, Chu CH. Numerical simulation of heat penetration through a vertical rectangular phase  
26 change material/air composite cell. *Int J Heat Mass Transfer* 1996; 39: 1785–95.  
27  
28 [13] Jianhua Z, Zhongqi C, Dengying L, Ji L. Experimental study on melting in a rectangular  
29 enclosure heated below with discrete heat sources. *Int J Therm Sci* 2001; 10: 254–9.  
30  
31 [14] Mbaye M, Bilgen E. Phase change process by natural convection-diffusion in rectangular  
32 enclosures. *Int J Heat Mass Transfer* 2001; 37: 35–42.  
33  
34 [15] Pal D, Joshi YK. Melting in a side heated tall enclosure by a uniformly dissipating heat source.  
35 *Int J Heat Mass Transfer* 2001; 44: 375–87.  
36  
37 [16] Hamdan MA, Al-Hinti I. Analysis of heat transfer during the melting of a phase-change  
38 material. *App Therm Eng* 2004; 24: 1935–44.  
39  
40 [17] Faraji M, El Qarnia H. Numerical study of melting in an enclosure with discrete protruding heat  
41 sources. *App Math Model* 2010; 34: 1258–75.  
42  
43 [18] El Qarnia H, Draoui A, Lakhel EK. Computation of melting with natural convection inside a  
44 rectangular enclosure heated by discrete protruding heat sources. *App Math Model* 2013; 37:  
45 3968–81.  
46  
47  
48  
49  
50  
51  
52  
53  
54  
55  
56  
57  
58  
59  
60  
61  
62  
63  
64  
65

- 1  
2  
3  
4 [19] Samara F, Groulx D, Biwole PH. Natural convection driven melting of phase change material:  
5 comparison of two methods. Excerpt from the proceeding of the COMSOL conference, 2012,  
6 Boston, USA.  
7  
8  
9 [20] Brent AD, Voller VR, Reid KJ. Enthalpy–porosity technique for modeling convection–diffusion  
10 phase change: application to the melting of a pure metal. *Numer Heat Transfer* 1988; 13: 297–  
11 318.  
12  
13  
14 [21] Beckermann C, Viskanta R. Effect of solid subcooling on natural convection melting of a pure  
15 metal. *ASME J Heat Transfer* 1989; 111: 416-24.  
16  
17 [22] Asako Y, Faghri M, Charmchi M, Bahrami PA. Numerical solution for melting of unfixed  
18 rectangular phase-change material under low-gravity environment. *Numer Heat Transfer, Part A*  
19 1994; 25: 191–208.  
20  
21  
22 [23] Wang S, Faghri A, Bergman TL. An experimental investigation of the melting process in a  
23 rectangular enclosure. *Int J Heat Mass Transfer* 1999; 42: 3659–72.  
24  
25  
26 [24] Gong ZX, Devahastin S, Mujumdar AS. Enhanced heat transfer in free convection-dominated  
27 melting in a rectangular cavity with an isothermal vertical wall. *App Therm Eng* 1999; 19:  
28 1237-51.  
29  
30  
31 [25] Ghasemi B, Molki M. Melting of unfixed solids in square cavities. *Int J Heat Fluid Flow* 1999;  
32 20: 446–52.  
33  
34  
35 [26] Zivkovic B., Fujii I. An analysis of isothermal phase change materials within rectangular and  
36 cylindrical containers. *Sol Energy* 2001; 70: 51–61.  
37  
38  
39 [27] Lacroix M. Contact melting of a phase change material inside a heated parallelepipedic capsule.  
40 *Energy Convers Manage* 2001; 42: 35–47.  
41  
42  
43 [28] Jiji LM, Gaye S. Analysis of solidification and melting of PCM with energy generation. *Appl*  
44 *Therm Eng* 2006; 26: 568–75  
45  
46  
47 [29] Yanxia D, Yanping Y, Daiyong J, Baoyi C, Jinfeng M. Experimental investigation on melting  
48 characteristics of ethanolamine–water binary mixture used as PCM. *Int Commun Heat Mass*  
49 2007; 34: 1056–1063.  
50  
51  
52 [30] Jellouli Y, Chouikh R, Guizani A, Belghith A. Numerical study of the moving boundary  
53 problem during melting process in a rectangular cavity heated from below. *Am J Appl Sci* 2007;  
54 4: 251–6.  
55  
56  
57 [31] Chen CR, Sharma A, Tyagi SK, Buddhi D. Numerical heat transfer studies of PCMs used in a  
58 box-type solar cooker. *Renew Energy* 2008; 33: 1121–9.  
59  
60  
61  
62  
63  
64  
65

- 1  
2  
3  
4 [32] Younsi Z, Joulin A, Zalewski L, Lassue S, Rousse DR. Phase change materials: a numerical  
5 method for the behavior predictions. Proceedings of the Fourth International Conference on  
6 Thermal Engineering: Theory and Applications, January 2009, Abu Dhabi, UAE.  
7  
8  
9 [33] Wang S, Faghri A, Bergman TL. A comprehensive numerical model for melting with natural  
10 convection. *Int J Heat Mass Transfer* 2010; 53: 1986–2000.  
11  
12 [34] Joulin A, Younsi Z, Zalewski L, Lassue S, Rousse DR, Cavrot JP. Experimental and numerical  
13 investigation of a phase change material: Thermal-energy storage and release. *Appl Energy*  
14 2011; 88: 2454–62.  
15  
16  
17 [35] Murray RE, Groulx D. Modeling convection during melting of a phase change material.  
18 Abstract from the proceedings of the COMSOL conference, 2011, Boston, USA.  
19  
20 [36] Saitoh TS, Hoshi A. Analysis of close-contact melting with inner wall temperature variation in  
21 a horizontal cylindrical capsule. *IEEE Energy Conversion Engineering Conference 4(1997)*.  
22 *IECEC-97, Proceedings of the 32nd Intersociety: 1641–45*.  
23  
24 [37] Saitoh TS, Hoshi A. Experimental investigation on combined close-contact and natural  
25 convection in horizontal cylindrical and spherical capsules. *IEEE Energy Conversion*  
26 *Engineering Conference 3(1996), IECEC-96, Proceedings of the 31st Intersociety: 2090-4*.  
27  
28 [38] Fomin SA, Saitoh TS. Melting inside a spherical capsule with nonisothermal wall. *Int J Heat*  
29 *Mass Transfer* 1999; 42: 4197–205.  
30  
31 [39] Khodadadi JM, Zhang Y. Effects of buoyancy-driven convection on melting within spherical  
32 containers. *Int J Heat Mass Transfer* 2001; 44: 1605-18.  
33  
34 [40] Assis E, Katsman L, Ziskind G, Letan R. Numerical and experimental study of melting in a  
35 spherical shell. *Int J Heat Mass Transfer* 2007; 50: 1790–804.  
36  
37 [41] Tan FL. Constrained and unconstrained melting inside a sphere. *Int Commun Heat Mass*  
38 *Transfer* 2008; 35: 466-75.  
39  
40 [42] Tan FL, Hosseinizadeh SF, Khodadadi JM, Fan L. Experimental and computational study of  
41 constrained melting of phase change materials (PCM) inside a spherical capsule. *Int J Heat*  
42 *Mass Transfer* 2009; 52: 3464-72.  
43  
44 [43] Veerappan M, Kalaiselvam S, Iniyam S, Goic R. Phase change characteristic study of spherical  
45 PCMs in solar energy storage. *Sol Energy* 2009; 83: 1245–52.  
46  
47 [44] Hosseinizadeh SF, Darzi AR, Tan FL, Khodadadi JM. Unconstrained melting inside a sphere.  
48 *Int J Therm Sci* 2013; 63: 55-64.  
49  
50  
51  
52  
53  
54  
55  
56  
57  
58  
59  
60  
61  
62  
63  
64  
65

- 1  
2  
3  
4 [45] Rizan MM, Tan FL, Tso CP. An experimental study of n-octadecane melting inside a sphere  
5 subjected to constant heat rate at surface. *Int Commun Heat Mass Transfer* 2012; 39: 1624–30.  
6  
7 [46] Sparrow EM, Broadbent JA. Inward melting in a vertical tube which allows free expansion of  
8 the phase-change medium. *ASME J Heat Transfer* 1982; 104: 309–15.  
9  
10 [47] Wenzhen C, Shangmo C, Zhen L, Wangmin G. Study of contact melting inside isothermally  
11 heated vertical cylindrical capsules. *J Therm Sci* 1993; 2: 190–5.  
12  
13 [48] Wu Y, M. Lacroix, Melting of a PCM inside a vertical cylindrical capsule. *Int J Numer Meth*  
14 *Fluids* 1995; 20: 559–72.  
15  
16 [49] Jones BJ, Sun D, Krishnan S, Garimella SV. Experimental and numerical study of melting in a  
17 cylinder. *Int J Heat Mass Transfer* 2006; 49: 2724–38.  
18  
19 [50] Shmueli H, Ziskind G, Letan R. Melting in a vertical cylindrical tube: Numerical investigation  
20 and comparison with experiments. *Int J Heat Mass Transfer* 2010; 53: 4082–91.  
21  
22 [51] Wang Y, Amiri A, Vafai K. Melting in Cylindrical Enclosures: Numerical Modeling and Heat  
23 Transfer Correlations. *Numer Heat Transfer, Part A-Applications* 2012; 61: 837–59.  
24  
25 [52] Nicholas D, Bayazitoglu Y. Heat transfer and melting front within a horizontal cylinder. *ASME*  
26 *J Sol Energy* 1980; 102: 229–32.  
27  
28 [53] Ho CJ, Viskanta R. Heat transfer during inward melting in a horizontal tube. *Int J Heat Mass*  
29 *Transfer* 1984; 27(5): 705–16.  
30  
31 [54] Bareiss M, Beer H. An analytical solution of the heat transfer process during melting of an  
32 unfixed solid phase change material inside a horizontal tube. *Int J Heat Mass Transfer* 1984;  
33 27(5): 739–46.  
34  
35 [55] Sparrow EM, Geiger GT. Melting in a horizontal tube with the solid either constrained or free  
36 to fall under gravity. *Int J Heat Mass Transfer* 1986; 29(7): 1007–16.  
37  
38 [56] Prasad A, Sengupta S. Nusselt number and melt time correlations for melting inside a horizontal  
39 cylinder subjected to an isothermal wall temperature condition. *ASME J Heat Transfer* 1988;  
40 110: 340–5.  
41  
42 [57] Hirata T, Nishida K. An analysis of heat transfer using equivalent thermal conductivity of liquid  
43 phase during melting inside an isothermally heated horizontal cylinder. *Int J Heat Mass Transfer*  
44 1989; 32(9): 1663–70.  
45  
46 [58] Maldonado JJ, Sengupta S, Roy SK. Gravity-assisted melting in horizontal cylinder heated by  
47 external forced convection. *Int Commun Heat Mass Transfer* 1990; 17: 637–45.  
48  
49  
50  
51  
52  
53  
54  
55  
56  
57  
58  
59  
60  
61  
62  
63  
64  
65

- 1  
2  
3  
4 [59] Park CE, Kim SS, Chang KS. Branching solutions to inward melting problem in a horizontal  
5 tube. *Int Commun Heat Mass Transfer* 1991; 18: 343-50.  
6  
7 [60] Saitoh T, Kato K. Experiments on melting in heat storage capsule with close contact and natural  
8 convection. *Exp Therm Fluid Sci* 1993; 6: 273-81.  
9  
10 [61] Costa M, Oliva A, Pérez-Segarra CD. Three-Dimensional numerical study of melting inside an  
11 isothermal horizontal cylinder, *Numer Heat Transfer, Part A-Applications* 1997; 32: 531–53.  
12  
13 [62] Chung JD, Lee JS, Yoo H. Thermal instability during the melting process in an isothermally  
14 heated horizontal cylinder. *Int J Heat Mass Transfer* 1997; 40(16): 3899–907.  
15  
16 [63] Kawanami T, Fukusako S, Yamada M, Itoh K. Experimental on melting of slush ice in a  
17 horizontal cylindrical capsule. *Int J Heat Mass Transfer* 1999; 42: 2981–90.  
18  
19 [64] Hirose K, Yoshii T, Watanabe H. Melting heat transfer of phase change material in elliptical  
20 tubes immersed in working fluid. *Nippon Dennetsu Shinpojiumu Koen Ronbunshu* 2003; 40(3):  
21 671-2.  
22  
23 [65] Regin AF, Solanki SC, Saini JS. Latent heat thermal energy storage using cylindrical capsule:  
24 numerical and experimental investigations. *Renew Energy* 2006; 31: 2025–41.  
25  
26 [66] Khillarkar DB, Gong ZX, Mujumdar AS. Melting of a phase change material in concentric  
27 horizontal annuli of arbitrary cross-section. *Appl Therm Eng* 2000; 20: 893–912.  
28  
29 [67] Dutta R, Atta A, Dutta TK. Experimental and numerical study of heat transfer in horizontal  
30 concentric annulus containing phase change material. *Can J Chem Eng* 2008; 86: 700–10.  
31  
32 [68] Akgun M, Aydin O, Kaygusuz K. Thermal energy storage performance of paraffin in a novel  
33 tube-in-shell system. *Appl Therm Eng* 2008; 28: 405–13.  
34  
35 [69] Sugawara M, Komatsu Y, Beer H. Melting and freezing around a horizontal cylinder placed in a  
36 square cavity. *Int J Heat Mass Transfer* 2008; 45: 83–92.  
37  
38 [70] Wei L, Xinguo L, Jun Z. Numerical study of melting in a square annulus. *IEEE, International*  
39 *conference on Mechanic Automation and Control Engineering (MACE)*, 2010.  
40  
41 [71] Darzi AR, Farhadi M, Sedighi K. Numerical study of melting inside concentric and eccentric  
42 horizontal annulus. *Appl Math Model* 2012; 36: 4080–6.  
43  
44 [72] Hosseini MJ, Ranjbar AA, Sedighi K, Rahimi M. A combined experimental and computational  
45 study on the melting behavior of a medium temperature phase change storage material inside  
46 shell and tube heat exchanger. *Int Commun Heat Mass Transfer* 2012; 39: 1416–24.  
47  
48  
49  
50  
51  
52  
53  
54  
55  
56  
57  
58  
59  
60  
61  
62  
63  
64  
65

1  
2  
3  
4  
5  
6  
7  
8  
9  
10  
11  
12  
13  
14  
15  
16  
17  
18  
19  
20  
21  
22  
23  
24  
25  
26  
27  
28  
29  
30  
31  
32  
33  
34  
35  
36  
37  
38  
39  
40  
41  
42  
43  
44  
45  
46  
47  
48  
49  
50  
51  
52  
53  
54  
55  
56  
57  
58  
59  
60  
61  
62  
63  
64  
65

**List of Tables**

Table 1. Effects of the Rayleigh number on energy charge rate (Gong et al. [24]).

Table 2. Summary of studies on PCM melting inside rectangular containers.

Table 3. Outline of studies on PCM melting inside spherical containers.

Table 4. Summary of studies on PCM melting inside cylindrical containers.

Table 5. Outline of studies on PCM melting inside annular cavities.



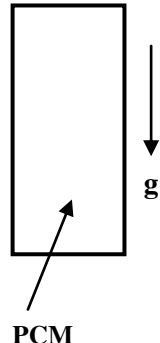
1  
2  
3  
4  
5  
6  
7  
8  
9  
10  
11  
12  
13  
14  
15  
16  
17  
18  
19  
20  
21  
22  
23  
24  
25  
26  
27  
28  
29  
30  
31  
32  
33  
34  
35  
36  
37  
38  
39  
40  
41  
42  
43  
44  
45  
46  
47  
48  
49  
50  
51  
52  
53  
54  
55  
56  
57  
58  
59  
60  
61  
62  
63  
64  
65

Table 1. Effects of the Rayleigh number on energy charge rate (Gong et al. [24]).

<i>Ra</i>	First period		Second period, $(\Delta Q/Q_M)/\Delta Fo$		
	$\Delta Q/Q_M$	<i>Fo</i>	No inverting	Inverting	Enhancement
$7.11 \times 10^5$	0.582	0.302	0.687	1.047	52.4%
$2.844 \times 10^6$	0.532	0.467	0.961	1.504	56.5%
$5.688 \times 10^6$	0.515	0.251	1.099	1.766	60.1%

$Q_M$  = the maximum amount of energy which can be charged during the melting process.

Table 2. Summary of studies on PCM melting inside rectangular containers.

Container Shape	Constant Heat Flux (CHF) Boundary Condition (BC)				
	Authors (Year)	Location of BC	PCM	Type of Study	Highlighted Results/Findings
Rectangular 	Zhang et al. [11] (1993)	Vertical side (discrete heaters)	Octadecane	E (TCs, 3 heaters, camera, etc.)	Interface is highly affected by NC especially at higher $Ste$ and lower $Sc$ . Electronic cooling by PCM is more effective than that by forced air flow. The highest surface temperature was recorded at the uppermost heat source.
	Ho and Chu [12] (1996)	Vertical side (PCM/Air composite)	Octadecane	C (FDM)	Effective thermal protection duration was found to be a strong function of $Ra$ , $Ste$ , $Sc$ , PCM thickness, and $AR$ . Shallow geometry is preferable for thermal protection.
	Jianhua et al. [13] (2000)	Bottom side (discrete heaters)	Octadecane	E (TCs, 3 heaters, camera, etc.)	Fixed melting (solid between heaters) and contact melting (solid above heaters) occurred simultaneously. Higher $Ste$ and smaller $AR$ have a positive effect on melting, while $Sc$ is only important during early stages.
	Mbaye and Bilgen [14] (2001)	One side at CHF and the other at CWT	Gallium	C (EPM with CVA-based FDM)	Melted volume is independent for $AR$ at CON regime, but it becomes a decreasing function of $AR$ as NC in the liquid develops. Applied heat flux is an important parameter, and optimum $AR$ is unity.
	Pal and Joshi [15] (2001)	Vertical side	Triacontane	E (TCs, heater, camera, etc.) and C (EPM with CVA)	Comparisons between experimental and computational heat transfer data and melt interface locations were good. For tall enclosures, NC plays an important role in the beginning and then diminishes as melting is completed.
	Hamdan and Al-Hinti [16] (2004)	Vertical side	Octadecane	A (Interface is smooth and planar)	During the initial stages, the model predicted the propagation of the interface very well, but later the interface was under-predicted. The analysis model can be used with good accuracy for investigating melting of PCM.
	Faraji and El Qarnia [17] (2010)	Vertical side (3 discrete heaters)	Eicosane	C (EPM with CVA)	Heat flux transmitted to interface and resulting melting rate decreased with time. Lower heater transmits high rate of heat

1  
2  
3  
4  
5  
6  
7  
8  
9  
10  
11  
12  
13  
14  
15  
16  
17  
18  
19  
20  
21  
22  
23  
24  
25  
26  
27  
28  
29  
30  
31  
32  
33  
34  
35  
36  
37  
38  
39  
40  
41  
42  
43  
44  
45  
46  
47  
48  
49

El Qarnia et al. [18] (2013)	Vertical side (3 discrete heaters)	Eicosane	C (EPM with CVA)	transfer. Raising $Ra$ and lowering $AR$ lead to increasing wall surface temperature and reducing operating time of electronic device.
Samara et al. [19] (2012)	One side at CHF with convection BC on two vertical sides	Paraffin RT25	C (FEM with modified viscosity and volume force techniques)	Modified volume force method is robust/stable with improved convergence in melting problem. The simulated melting behavior was significantly influenced by mesh mode and discretization technique.
<b>Constant Wall Temperature (CWT) Boundary Condition (BC)</b>				
Brent et al. [20] (1988)	Two vertical sides are at two different $T_w$	Gallium	C (EPM with CVA-based FDM)	Excellent agreement between the numerical predictions and experimental findings available in literature. Capability of EPM for predicting accurately position/morphology of the melting interface.
Beckermann and Viskanta [21] (1989)	Two vertical sides are at two different $T_w$	Gallium	E (TCs, two constant-temperature baths, etc.) and C (CVA)	Classified melting process to 4 regimes according heat transfer mechanisms. High $Sc$ reduces the melting rate.
Asako et al. [22] (1994)	Bottom side (unfixed solid) in low- $g$ environment	Depending on the $Pr$	C (EPM with CVA-based FDM)	Melting rate increases with the Archimedes and $Ste$ numbers and it is very slow in low- $g$ environment. Melt thickness increases with time and decreases with increasing Archimedes, $Ste$ , and $Pr$ numbers, while the effect of $AR$ on the melt thickness was small.
Wang et al. [23] (1999)	Two vertical sides are at two different $T_w$	Hydrated salt	E (TCs, constant-temp. heat exchanger, etc.)	Good agreement between correlated melted volume fraction and $Nu$ with the experimental data. Transient $Nu$ distinguishes 3 regimes during the melting which are (CON-dominated, transition, and NC-dominated).
Gong et al. [24] (1999)	Vertical side	Octadecane	C (EPM with FEM)	The first melting period is characterized with low thermal stratification effect and high rate of NC and melting. As time progressed, the second period will appear with significant thermal stratification and low rate of NC and melting rate. Inverting the container in the second melting stage for augmenting the effect of NC and

1  
2  
3  
4  
5  
6  
7  
8  
9  
10  
11  
12  
13  
14  
15  
16  
17  
18  
19  
20  
21  
22  
23  
24  
25  
26  
27  
28  
29  
30  
31  
32  
33  
34  
35  
36  
37  
38  
39  
40  
41  
42  
43  
44  
45  
46  
47  
48  
49

Ghasemi and Molki [25] (1999)	All sides (unfixed solid)	Depending on the $Pr$	C (EPM with CVA based FDM)	increasing the melting rate. Low melting rate, small solid falling velocity and symmetric melting pattern are associated with low values of $Ra$ and Archimedes numbers, whereas, higher values of these numbers result in enhancing melting rate, increasing solid falling velocity and asymmetric melting pattern.
Zivkovic and Fujii [26] (2001)	Vertical side	Calcium chloride hexahydrate	E (TCs, constant-temp. bath, etc.) and C (1-D CVA based FDM)	CON within the PCM in the direction of HTF flow, thermal resistance of the container's wall, and the effects of NC within the melt can be ignored for the study conditions. Rectangular container required nearly 1/2 the melting time compared to the cylindrical one of the same volume and heat transfer area.
Lacroix [27] (2001)	Upper and lower (contact melting) sides	Octadecane	A (neglecting the effect of NC)	Bottom melting fraction was greater by one order of magnitude of that near the top. $Ste$ had a positive significant impact on the melting process, whereas the total melting time increased linearly with the degree of $Sc$ .
Jiji and Gaye [28] (2006)	Vertical side with volumetric heat generation	Ice	A (1-D quasi steady state approximation)	The model simplifies phase change problems and often eliminates the need for numerical solutions.
Yanxia et al. [29] (2007)	Vertical side	Ethanolamine-water binary mixture	E (TCs, constant-temp. tank, etc.)	NC enhanced the melting process compared with the conduction-only cases. Pure CON only occurs at the initial stage of melting stage and CON-NC coupled model is necessary for predicting melting process exactly.
Jellouli et al. [30] (2007)	Hot bottom wall (contact melting) and cold top one	PCM with $Pr=54$	C (CVA)	Initially, buoyancy forces cannot overcome the resistance imposed by viscous forces. As thickness of the melt layer increased with time, NC dominated in the liquid phase and the melting front reached a steady position.
Chen et al. [31] (2008)	Vertical side	Magnesium nitrate hexahydrate, stearic acid, acetamide, acetanilide and erythritol hydrated salt	C (FDM)	Thermal conductivity of the PCM and the container has a significant effect on the melt fraction, while the thickness of the container and $Sc$ has a little effect. $T_w$ has a strong impact on the observed melt fraction.

1  
2  
3  
4  
5  
6  
7  
8  
9  
10  
11  
12  
13  
14  
15  
16  
17  
18  
19  
20  
21  
22  
23  
24  
25  
26  
27  
28  
29  
30  
31  
32  
33  
34  
35  
36  
37  
38  
39  
40  
41  
42  
43  
44  
45  
46  
47  
48  
49

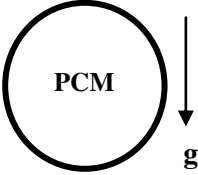
Younsi et al. [32] (2009)	Two vertical sides are at two different $T_w$	Polyethylene glycol 900	C (EPM with FVM)	1-D (pure CON) should not be used even for very low AR. Both numerical methods (2D FVM and FLUENT code) provided excellent correspondence with experimental results.
Wang et al. [33] (2010)	Refer to Fig. 7	Octadecane (low $T_m$ ) and sodium nitrate (high $T_m$ )	C (FVM with new solid vel. correction scheme)	The numerical model eliminated inconsistency associated with the previous methods. Similarity in melting phenomena of two different PCMs can be used as a foundation for conducting room-temperature experiments to investigate the melting/solidification characteristics of high-temperature PCMs.
Joulin et al. [34] (2011)	Two vertical sides are at two different $T_w$	Octadecane	E (TCs, heat flux sensors, etc.) and C (1-D FDM, and 2-D FVM)	Both numerical methods can be used for evaluating melting behavior. The supercooling phenomenon must be taken into account correctly in order to predict the PCM thermal behavior.
Murray and Groulx [35] (2011)	Two vertical sides are at two different $T_w$	Octadecane	C (FEM)	$\Delta T_m$ , thermal conductivity and viscosity affect the amount of molten PCM & interface shape. The importance of accounting for NC during melting in a PCM.

A, C and E stand for analytical, computational and experimental, respectively.

- AR aspect ratio
- CON conduction
- CVA control volume approach
- EPM enthalpy-porosity method
- FDM finite difference method
- FEM finite element method
- FVM finite volume method
- HTF heat transfer fluid
- NC natural convection

1		
2		
3	PCM	phase change material
4		
5	$T_m$	melting temperature
6		
7	$T_w$	wall temperature
8		
9	$\Delta T_m$	melting temperature range for non-pure materials
10		
11	TCs	thermocouples
12		
13		
14		
15		
16		
17		
18		
19		
20		
21		
22		
23		
24		
25		
26		
27		
28		
29		
30		
31		
32		
33		
34		
35		
36		
37		
38		
39		
40		
41		
42		
43		
44		
45		
46		
47		
48		
49		

Table 3. Outline of studies on PCM melting inside spherical containers.

Container Shape	Constrained Melting				
	Authors (Year)	BC	PCM	Type of Study	Highlighted Results
Spherical 	Khodadadi and Zhang [39] (2001)	CWT	Beeswax	C (EPM with FVM) and E (water bath, camera, etc.)	Melting in the top region of the sphere is much faster than in the bottom region. Strength of NC is clearly dependent on the $Ra$ when compared to the $Ste$ . $Pr$ plays an important role in the melting process.
	Tan et al. [42] (2009)	CWT	Octadecane	E (TCs, water bath, camera, etc.) and C (EPM with CVM)	Initially, CON and symmetric melting is shown; later on, melting at top much faster than bottom due to development of NC. Waviness of bottom surface of the PCM, chaotic fluctuations and high discrepancy between experimental and numerical temperatures are observed due to unstable fluid layer, while no waviness, less fluctuations and low discrepancy are recorded in the top stable fluid layer.
	Veerappan et al. [43] (2009)	CWT	65 mol% capric acid and 35 mol% lauric acid, calcium chloride hexahydrate, octadecane, hexadecane and eicosane	A (conduction model combined with an empirical thermal conductivity of the liquid including NC)	The analytical results deviated against the previous experimental results by 15% for solidification and 20% for melting. The pure-conduction model overpredicts the complete melting time. The 65 mol% capric acid with 35 mol% lauric acid and calcium chloride hexahydrate were better options for melting and solidification, respectively.
	Unconstrained Melting				
	Saitoh and Hoshi [36] (1997)	Variable $T_w$	Octadecane	A (neglecting NC in the upper region)	Excellent agreement between the analytical results and numerical solutions for molten mass fraction and melt layer thickness The progress of melting is faster than that of constant $T_w$ case.
Saitoh and Hoshi [37] (1996)	Variable $T_w$	Octadecane	E (TCs, oil bath, camera, etc.)	$Ste$ has a significant effect on the molten mass fraction. $T_w$ varies in a complicated manner, and there is temperature distribution along the peripheral direction that influences the melting time.	
Fomin and Saitoh [38] (1999)	Variable $T_w$	Octadecane	C (boundary fixing method) and A	The approximate analytical solutions were found to be in good agreement with the numerical solutions.	

1  
2  
3  
4  
5  
6  
7  
8  
9  
10  
11  
12  
13  
14  
15  
16  
17  
18  
19  
20  
21  
22  
23  
24  
25  
26  
27  
28  
29  
30  
31  
32  
33  
34  
35  
36  
37  
38  
39  
40  
41  
42  
43  
44  
45  
46  
47  
48  
49

				(neglecting melting at the upper region of the solid core)	Ignoring the effect of streamwise NC in the liquid layer leads to overestimating of melting rate. Assumption of the constant $T_w$ of the capsule can lead to the results which significantly differ from those obtained for the real conditions of melting when the wall of the capsule is non-isothermal.
Assis et al. [40] (2007)	CWT	Paraffin RT27		E (camera, water bath, etc.) and C (EPM with FVM)	The transient phase-change process depended on the thermal and geometrical parameters of the system, including $Ste$ and the diameter of the sphere. Simulated melting time was slightly shorter than experimental one.
Hosseinizadeh et al. [44] (2013)	CWT	Octadecane		E (camera, water bath, etc.) and C (EPM with FVM)	CON with high melting rate is dominant at the beginning through contact melting with the surface of container. Later on, NC becomes dominant at the top half of sphere where the melting rate is lower than the bottom half. The geometrical parameter such as diameter has more influence on the melting rate and heat release compared to the operating condition such as $Ste$ .
Rizan et al. [45] (2012)	CHF	Octadecane		E (TCs, heater, camera, water bath, etc.)	Melting was primarily dependent on the temperature level to which the PCM is subjected to and the contact plane surface area. CON dominates the initial melting condition with increasing liquid boundary layer shifting dominant heat transfer mode to NC. Larger surface area in contact with the liquid front of the same volume will yield a higher melting rate.

**Constrained and Unconstrained Melting**

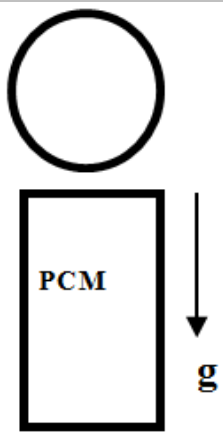
Tan [41] (2008)	CWT	Octadecane		E (TCs, water bath, camera, etc.)	In unconstrained melting, the melting in bottom half is much faster due to CON, while the NC is responsible for melting in upper half. In constrained melting, top melted faster than bottom and CON only exists at the beginning; therefore, melting is mainly through NC in the liquid at the top and bottom halves of the solid PCM.
-----------------	-----	------------	--	-----------------------------------	---

The abbreviations of Table 2 apply to the table above.



Table 4. Summary of studies on PCM melting inside cylindrical containers.

### Vertical Cylindrical Capsules



Authors (Year)	BC	PCM	Type of Study	Highlighted Results
Sparrow and Broadbent [46] (1982)	CWT at side	Eicosane	E (test cell, TCs, water bath, etc.) and A (pure CON model)	Melting process with no $Sc$ displayed heat transfer and melting fraction were about 50% greater than that predicted by pure-CON model. Initial $Sc$ decreases the melting rate and sensible heat storage.
Wenzhen et al. [47] (1993)	CWT at bottom and side	Eicosane	A (melting is dominated by CON in the close-contact layer film at bottom and by CON through the stable liquid at the side)	The effect of CON through the liquid phase on the total melted mass fraction is little. Increasing the $Ste$ and/or reducing the $AR$ were advantageous to increasing the melting rate and lowering the charging time.
Wu and Lacroix [48] (1995)	CWT for all sides	Depending on the $Pr$	C (body-fitted coordinates with FDM)	CON is dominated at the top, while the highest melting rate occurs at the bottom. Benard convection occurred at a much earlier time than that for the case of melting within a cylinder heated from below only.
Jones et al. [49] (2006)	CWT at side and constant-temp. base	Eicosane	E (test cell, TCs, water bath, etc.) and C (EPM based FVM)	Very good agreement was obtained between the predictions and the experiment for $Ste$ up to 0.1807. Melting regimes are: a) pure CON, b) mixed NC/CON, c) NC dominant, and d) shrinking solid.
Shmueli et al. [50] (2010)	CWT at side	Commercial paraffin RT27	C (EPM based FVM)	Initially, heat transfers by CON from the wall to solid PCM. Then NC in the liquid dominates, changing the solid shape to conical and making it shrink from top to bottom.
Wang et al. [51] (2012)	CWT at side (inward melting) or at center (outward melting), insulated top, and constant-temp. base	Eicosane	C (FVM)	Good agreement was obtained between simulated results of inward melting and previous experimental findings. For outward melting, the agreement between the simulated and previous predicted results agree well at low $Ra$ and consistent correlations for the $Nu$ as well as total and latent energy storage, all as functions of $Ste$ , $Fo$ and $Ra$ .

## Horizontal Cylindrical Capsules

### *Unconstrained Melting*

Nicholas and Bayaziloglu [52] (1980)	CHF	Depending on the selected $Ste$	C (FDM)	Small $Ste$ assured closest agreement between analytical and numerical results. Temperature is higher at the top where NC is dominated.
Bareiss and Beer [54] (1984)	CWT	Octadecane and p-xylene	A (Assumptions) and E (test cell, water bath, etc.)	The analytical model agreed very well with the experimental findings. $Nu$ is a maximum at the beginning and decreases monotonically to zero at the end of the melting process.
Prasad and Sengupta [56] (1988)	CWT	Octadecane	A (Assumptions)	$Nu$ increases as the $Ra$ increases. Useful correlations for the melt time and $Nu$ were obtained. Melting rate changes significantly with $Ste$ and $Pr$ , while it varies weakly with $Ra$ .
Maldonado et al. [58] (1990)	External convection	Octadecane	E (test cell, TCs, wind tunnel, etc.)	Half of the tests show the melt rate was approximately identical to that for constant $T_w$ . In most cases, the melt rate during the initial stages of melting was significantly lower than expected.
Saitho and Kato [60] (1993)	CWT and constant-temperature bath	Octadecane	E (test cell, TCs, water bath, etc.) and C (Growth Ring Method)	Small $Ste$ confirms close-contact melting is dominant with 10-15% being the contribution of NC to the melting rate. As $Ste$ increases, NC becomes significant.
Kawanami et al. [63] (1999)	CHF	Slush ice	E (test cell, TCs, heater, etc.)	Local heat transfer coefficient is greatest at the top and tends to decrease along the wall and it is proportional to heat flux and initial solution concentration.

### *Constrained Melting*

Ho and Viskanta [53] (1984)	CWT	Octadecane	E (test cell, TCs, water bath, heating coil, etc.) and C (FDM)	NC was dominant in the melt during inward melting. In addition to NC, a secondary vortex circulation initiated at the bottom part of the melt region and this secondary flow will finally merge with main convective flow.
Hirata and Nishida	CWT	Octadecane	E (test cell, TCs, water bath,	Analytical results showed a good agreement

1  
2  
3  
4  
5  
6  
7  
8  
9  
10  
11  
12  
13  
14  
15  
16  
17  
18  
19  
20  
21  
22  
23  
24  
25  
26  
27  
28  
29  
30  
31  
32  
33  
34  
35  
36  
37  
38  
39  
40  
41  
42  
43  
44  
45  
46  
47  
48  
49

[57] (1989)				camera, etc.) and A ( pure CON model with equivalent $k$ of the liquid phase)	with experimental data for wide range of $Ra$ . The influence of NC is insignificant when $Ra < 10^5$ .
Park et al. [59] (1991)	CWT	PCM of $Pr = 50$		C(pseudo-compressibility method based FVM)	NC flow is unicellular, bi-cellular and tri-cellular depending on $Ra$ . Initial small perturbations of very minor difference can induce different melting patterns.
Costa et al. [61] (1997)	CWT	Octadecane		C (FVM)	At relatively low $Ra$ , the axial flow velocity is low, but for high $Ra$ , distinct 3-D flow is recognized with axial waviness at bottom of solid PCM. The 3-dimensionality has no effect on the melt fraction and the overall $Nu$ . $Nu$ along the axial direction varies significantly according to the flow pattern.
Chung et al. [62] (1997)	CWT	Octadecane		C (EPM with FVM)	At low $Ra$ , the flow in the liquid gap is stable as the viscous force is dominant. The intermediate $Ra$ showed the thermal buoyancy and viscous forces are balanced in a neutrally stable state. At the high $Ra$ , the Benard convection shows an orderly behavior without being affected by the base flow.
Hirose et al. [64] (2003)	CWT	Ice/water		A (boundary fixing method) and E (test cell, TCs, water bath, camera, etc.)	The developed model is applicable to other general melting process in free shaped tube. Good agreement was achieved between analytical and experimental data of melting fraction and melting front progress.
Regin et al. [65] (2006)	CWT	Paraffin wax		C (FDM with merging NC effect in the $k$ of the liquid) and E (test cell, TCs, constant temp. bath, etc.)	The melting process is mainly governed by $Ste$ , $\Delta T_m$ and the capsule radius. Good agreement between numerical and experimental results when considering phase change temperature range and NC instead of considering CON domination only.

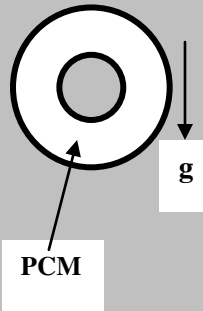
***Unconstrained and Constrained Melting***

1  
2  
3  
4  
5  
6  
7  
8  
9  
10  
11  
12  
13  
14  
15  
16  
17  
18  
19  
20  
21  
22  
23  
24  
25  
26  
27  
28  
29  
30  
31  
32  
33  
34  
35  
36  
37  
38  
39  
40  
41  
42  
43  
44  
45  
46  
47  
48  
49

Sparrow and Geiger [55] (1986)	CWT	Eicosane	E (rig test, TCs, water paths, camera, etc.) and C (FDM)	Melted mass in unconstrained mode exceed that of constrained mode. Majority of melting in wall-adjacent mode occurred at the lower portion. The experiments showed that constrained melting can be treated three-dimensionally; in contrast, unconstrained mode showed 2-D behavior.
--------------------------------	-----	----------	--	--

The abbreviations of Table 2 apply to the table above.

Table 5. Outline of studies on PCM melting inside annular cavities.

Container Shape	Authors (Year)	BC	PCM	Type of Study	Highlighted Results
 <p><b>Annular</b></p> <p><b>PCM</b></p> <p><b>g</b></p>	Khillarkar et al. [66] (2000)	Isothermal tube heating, shell heating and both sides heating	Octadecane	C (EPM based FEM)	Heating both walls suppressed thermal stratification, which occurred in both configurations for heating from the inside wall. High $Ra$ results in an earlier onset of NC, increasing the melting rate for inside and outside heating cases, but higher degree of thermal stratification was shown for inside wall heating.
	Dutta et al. [67] (2008)	Isothermal heating tube with insulated shell	Paraffin wax	E (TCs, water bath, etc.) and C (EPM with FVM)	Eccentricity, inclination angle and inner surface heat flux played an important role for the net circulation of the molten phase. Convective heat transfer is enhanced with the increase in $Ra$ .
	Akgun et al. [68] (2008)	Isothermal heating or cooling tube with insulated shell	P42-44 (P1), P46-48 (P2), P56-58 (P3)	E (TCs, water bath, etc.)	CON is responsible for the heat transfer process inside solid PCM and this region receives heat from the melted part by NC. In order to improve heat transfer during the melting and solidification, the surface of the shell was inclined with an inclination angle of $5^\circ$ .
	Sugawara et al. [69] (2008)	Isothermal heating or cooling tube with insulated shell	Ice/water	C (continuum model)	Melting decreased considerably with increasing the distance from the center of the cylinder to the bottom of the container.
	Wei et al. [70] (2010)	Isothermal heating tube with insulated shell	Commercial paraffin	C (EPM based FVM)	The top portion melted far faster than the bottom suggesting that the heated surface should be placed lower in order to reduce the total melting time. The melt fraction grows with time, while the wall heat flux decreases sharply initially, then increases slowly, and drops sharply after the melt fraction reaches 100%.
	Darzi et al. [71] (2012)	Isothermal heating tube with insulated shell	Eicosane	C (EPM based FVM)	NC becomes dominant in the top half while CON remains dominant in the bottom half. When the inner cylinder tube moves downward, melting rate increases sharply due to the dominance of NC heat transfer in most of PCM.
	Hosseini et al. [72] (2012)	Isothermal heating tube with insulated shell	Commercial paraffin RT50	E (TCs, hot water tank, etc.) and C (EPM based FVM)	The sharp rise in temperatures takes place at the uppermost section of the store. Strong thermal stratification of the melt was shown in the upper half.

1  
2  
3  
4  
5  
6  
7  
8  
9  
10  
11  
12  
13  
14  
15  
16  
17  
18  
19  
20  
21  
22  
23  
24  
25  
26  
27  
28  
29  
30  
31  
32  
33  
34  
35  
36  
37  
38  
39  
40  
41  
42  
43  
44  
45  
46  
47  
48  
49

Increasing the inlet temperature of water leads to expediting of the melting process.

The abbreviations of Table 2 apply to the table above.

## List of Figures

- Fig. 1. Schematic diagram of the generic shape of the container with prescribed boundary conditions and relevant parameters.
- Fig. 2. Schematic diagram of physical configuration of a PCM/air composite cell (Ho and Chu [12]).
- Fig. 3. Experimental cell (all dimensions are in mm) (Pal and Joshi [15]).
- Fig. 4. Schematic diagram of the physical model (Faraji and El Qarnia [17]).
- Fig. 5. Problem geometry and boundary conditions (Samara et al. [19]).
- Fig. 6. Schematic diagram of the physical model and coordinate system (Beckermann and Viskanta [21]).
- Fig. 7. Schematic diagram of the experimental apparatus (Wang et al. [23]).
- Fig. 8. Instantaneous isotherms (a) inside the not-inverted container and (b) within the inverted container (Gong et al. [24]).
- Fig. 9. Comparison of the melting time for rectangular and cylindrical containers of equal volume and heat transfer area (Zivkovic and Fujii [26]).
- Fig. 10. (a) Schematic diagram of the experimental apparatus and (b) Temporal variation of the melt fraction (Yanxia et al. [29]).
- Fig. 11. (a) Configuration geometry and (b) Instantaneous isotherms over the domain (contour level 0.00 represents the positions of the liquid-solid interface) (Jellouli et al. [30]).
- Fig. 12. Location of the fusion front at several time instants: (a) 1000 s, (b) 10,000 s, (c) 20,000 s, (d) 30,000 s and (e) 40,000 s. The dashed vertical line is the corresponding 1-D solution (Younsi et al. [32]).
- Fig. 13. Problem definition for four cases, where  $\theta = \frac{T - T_m}{T_h - T_c}$ ,  $\delta\theta = \frac{\delta T}{T_h - T_c}$  and  $\delta T$  is half width of the mushy zone temperature ranges (Wang et al. [33]).
- Fig. 14. (a) Experimental set-up and (b) Temperature and heat flux variations (Joulin et al. [34]).
- Fig. 15. Experimental setup (Saitoh and Hoshi [37]).
- Fig. 16. (a) Unconstrained and constrained melting inside a sphere and (b) Schematic sketch showing natural convection patterns in constrained melting (Tan [41]).
- Fig. 17. Thermally stable and unstable liquid layer structures along the symmetry axis (Tan et al. [42]).

- 1  
2  
3  
4 Fig. 18. Experimental validation of the position of the liquid-solid interface during melting inside a  
5 spherical container (Veerappan et al. [43]).  
6  
7 Fig. 19. Experimental setup (Rizan et al. [45]).  
8  
9 Fig. 20. Analytical model (Wenzhen et al. [47]).  
10  
11 Fig. 21. (a) Schematic representation of the vertical cylindrical capsule and (b) Timewise variation  
12 of the average Nusselt number on the bottom ( $Nu_B$ ), side ( $Nu_S$ ) and top ( $Nu_T$ ) surfaces (Wu  
13 and Lacroix [48]).  
14  
15 Fig. 22. (a) Schematic diagram of the experimental setup and (b) Photographs during melting of wax  
16 within the vertical cylindrical enclosure for a wall temperature of 45 °C (Jones et al. [49]).  
17  
18 Fig. 23. Instantaneous simulated density distributions and velocity vector maps vs. experimental  
19 images during melting in a vertical cylindrical container for  $D = 3$  cm,  $H = 17$  cm and  $\Delta T =$   
20  $10$  °C (Shmueli et al. [50]).  
21  
22 Fig. 24. Time evolutions of the overall Nusselt number on the surface of a horizontal cylinder in  
23 cases A and B predicted by three- and two-dimensional simulations (Costa et al. [61]).  
24  
25 Fig. 25. Two horizontal annuli configurations with streamlines (right half) and isotherms (left half)  
26 for  $Ra = 2.844 \times 10^6$  with the annuli heated isothermally from the inside, outside or both  
27 walls (Khillarkar et al. [66]).  
28  
29 Fig. 26. Experimental set-up (Dutta et al. [67]).  
30  
31 Fig. 27. Schematic diagram of the inclined shell surrounding a vertically-oriented annular PCM and  
32 the effect of this inclination on the melting time for various inlet water temperatures  
33 (Akgun et al. [68]).  
34  
35 Fig. 28. (a) Physical model and coordinate system and (b) Characteristics of velocity vectors at  
36 different locations of the horizontally-oriented cylinder (Sugawara et al. [69]).  
37  
38 Fig. 29. Detailed phase fields throughout the melting process (Wei et al. [70]).  
39  
40 Fig. 30. (a) Diagram of the experimental set-up and (b) Computed streamlines and isotherms for  
41 different water inlet temperatures (Hosseini et al. [72]).  
42  
43  
44  
45  
46  
47  
48  
49  
50  
51  
52  
53  
54  
55  
56  
57  
58  
59  
60  
61  
62  
63  
64  
65



1  
2  
3  
4  
5  
6  
7  
8  
9  
10  
11  
12  
13  
14  
15  
16  
17  
18  
19  
20  
21  
22  
23  
24  
25  
26  
27  
28  
29  
30  
31  
32  
33  
34  
35  
36  
37  
38  
39  
40  
41  
42  
43  
44  
45  
46  
47  
48  
49  
50  
51  
52  
53  
54  
55  
56  
57  
58  
59  
60  
61  
62  
63  
64  
65

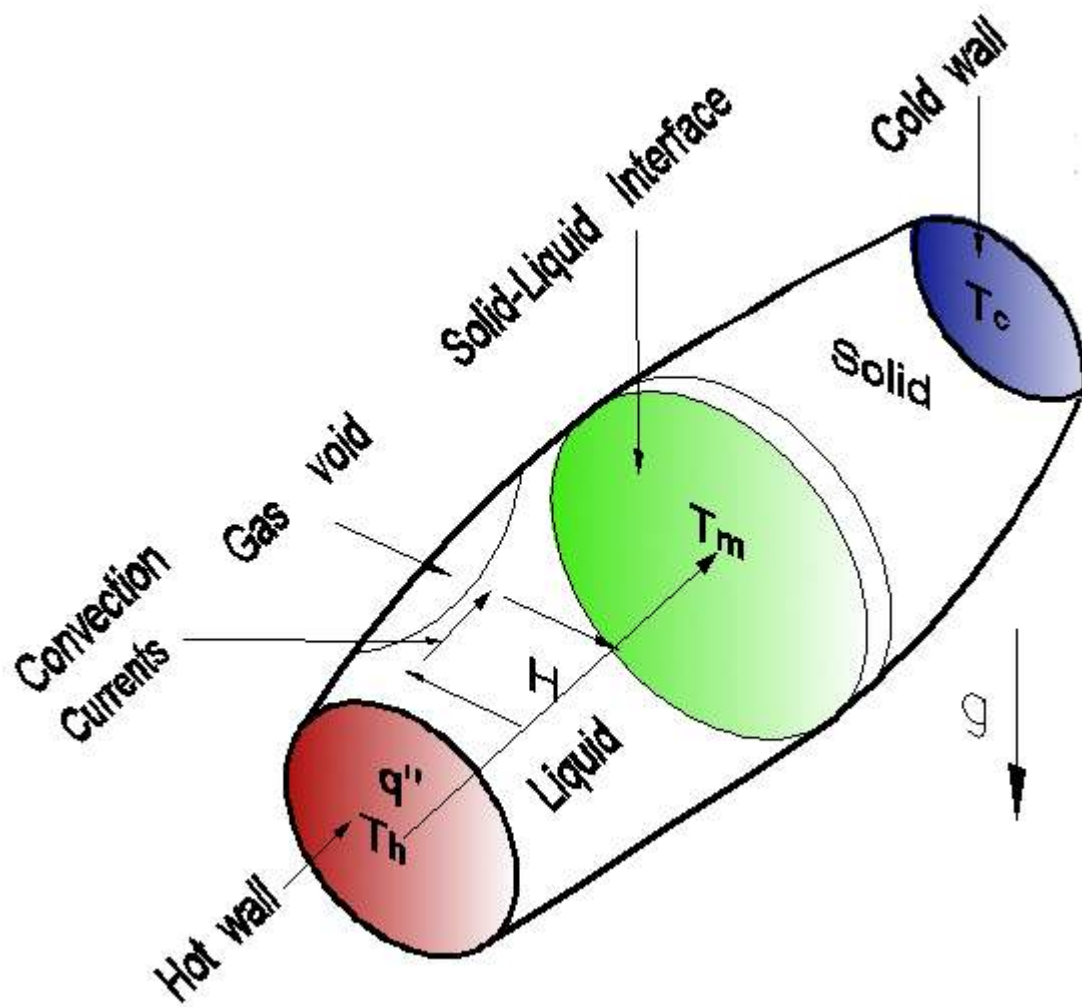


Fig. 1. Schematic diagram of the generic shape of the container with prescribed boundary conditions and relevant parameters.

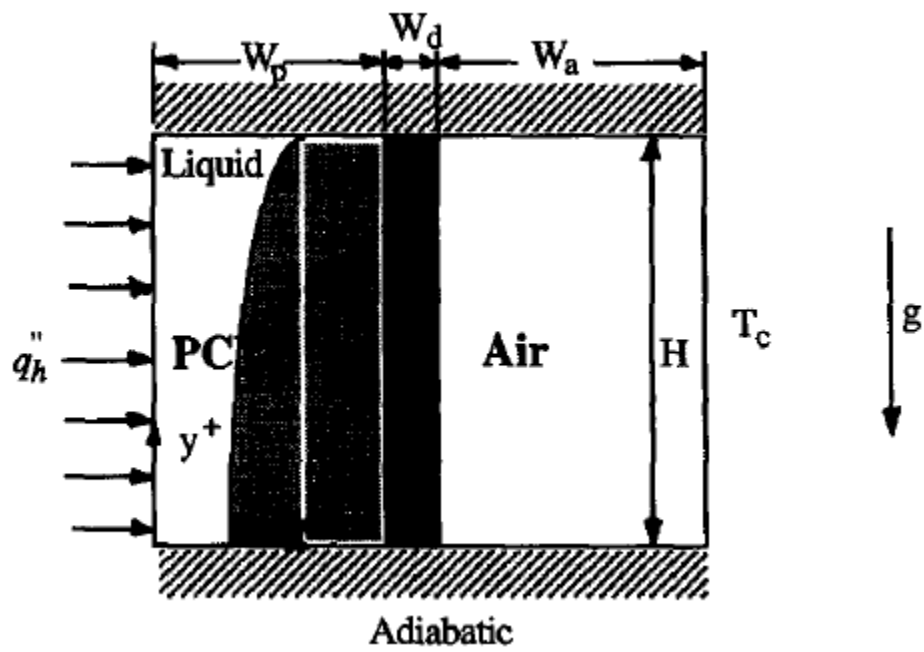


Fig. 2. Schematic diagram of physical configuration of a PCM/air composite cell (Ho and Chu [12]).

1  
2  
3  
4  
5  
6  
7  
8  
9  
10  
11  
12  
13  
14  
15  
16  
17  
18  
19  
20  
21  
22  
23  
24  
25  
26  
27  
28  
29  
30  
31  
32  
33  
34  
35  
36  
37  
38  
39  
40  
41  
42  
43  
44  
45  
46  
47  
48  
49  
50  
51  
52  
53  
54  
55  
56  
57  
58  
59  
60  
61  
62  
63  
64  
65

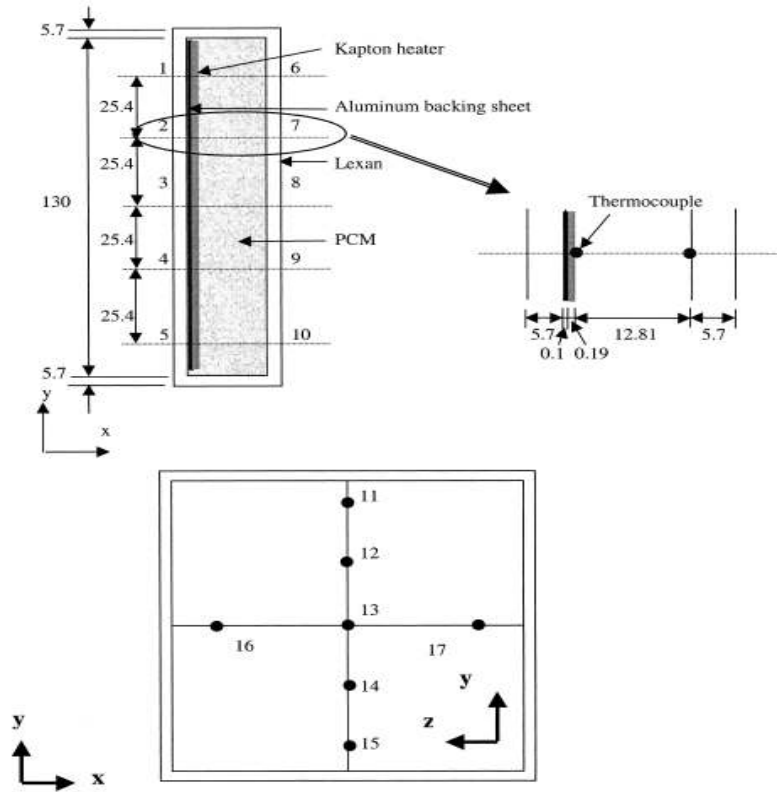


Fig. 3. Experimental cell (all dimensions are in mm) (Pal and Joshi [15]).

1  
2  
3  
4  
5  
6  
7  
8  
9  
10  
11  
12  
13  
14  
15  
16  
17  
18  
19  
20  
21  
22  
23  
24  
25  
26  
27  
28  
29  
30  
31  
32  
33  
34  
35  
36  
37  
38  
39  
40  
41  
42  
43  
44  
45  
46  
47  
48  
49  
50  
51  
52  
53  
54  
55  
56  
57  
58  
59  
60  
61  
62  
63  
64  
65

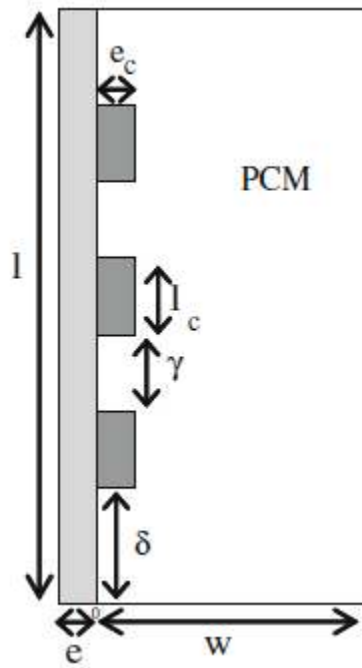


Fig. 4. Schematic diagram of the physical model (Faraji and El Qarnia [17]).

1  
2  
3  
4  
5  
6  
7  
8  
9  
10  
11  
12  
13  
14  
15  
16  
17  
18  
19  
20  
21  
22  
23  
24  
25  
26  
27  
28  
29  
30  
31  
32  
33  
34  
35  
36  
37  
38  
39  
40  
41  
42  
43  
44  
45  
46  
47  
48  
49  
50  
51  
52  
53  
54  
55  
56  
57  
58  
59  
60  
61  
62  
63  
64  
65

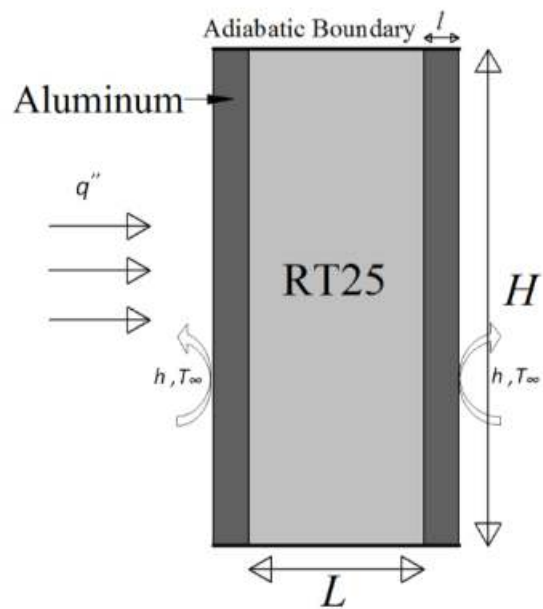
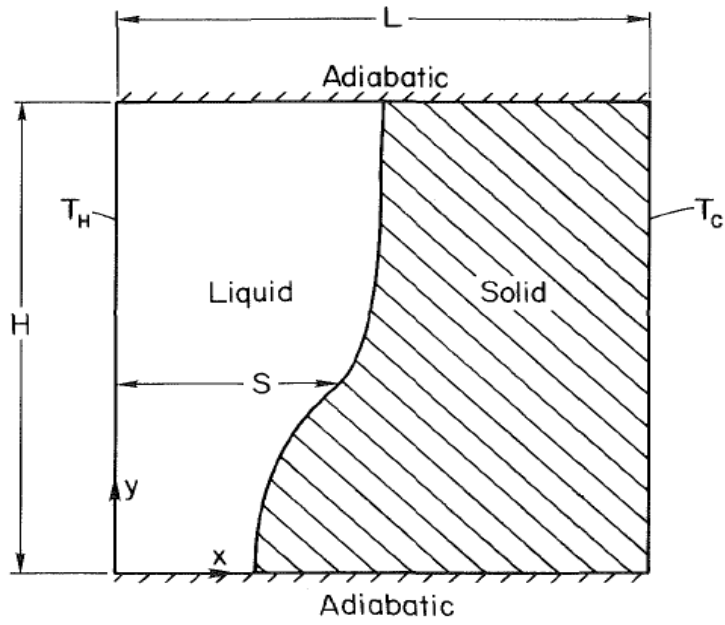


Fig. 5. Problem geometry and boundary conditions (Samara et al. [19]).

1  
2  
3  
4  
5  
6  
7  
8  
9  
10  
11  
12  
13  
14  
15  
16  
17  
18  
19  
20  
21  
22  
23  
24  
25  
26  
27  
28  
29  
30  
31  
32  
33  
34  
35  
36  
37  
38  
39  
40  
41  
42  
43  
44  
45  
46  
47  
48  
49  
50  
51  
52  
53  
54  
55  
56  
57  
58  
59  
60  
61  
62  
63  
64  
65



1  
2  
3  
4  
5  
6  
7  
8  
9  
10  
11  
12  
13  
14  
15  
16  
17  
18  
19  
20  
21  
22  
23  
24  
25  
26  
27  
28  
29  
30  
31  
32  
33  
34  
35  
36  
37  
38  
39  
40  
41  
42  
43  
44  
45  
46  
47  
48  
49  
50  
51  
52  
53  
54  
55  
56  
57  
58  
59  
60  
61  
62  
63  
64  
65

Fig. 6. Schematic diagram of the physical model and coordinate system (Beckermann and Viskanta [21]).

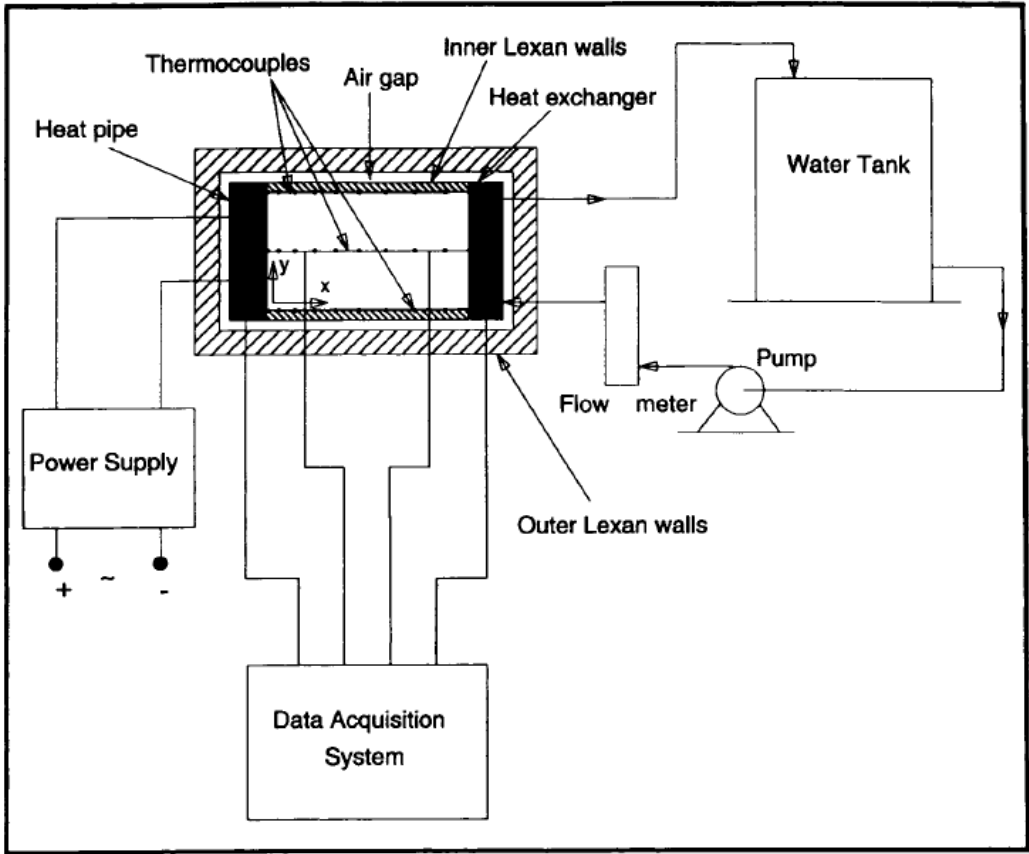


Fig. 7. Schematic diagram of the experimental apparatus (Wang et al. [23]).

1  
2  
3  
4  
5  
6  
7  
8  
9  
10  
11  
12  
13  
14  
15  
16  
17  
18  
19  
20  
21  
22  
23  
24  
25  
26  
27  
28  
29  
30  
31  
32  
33  
34  
35  
36  
37  
38  
39  
40  
41  
42  
43  
44  
45  
46  
47  
48  
49  
50  
51  
52  
53  
54  
55  
56  
57  
58  
59  
60  
61  
62  
63  
64  
65

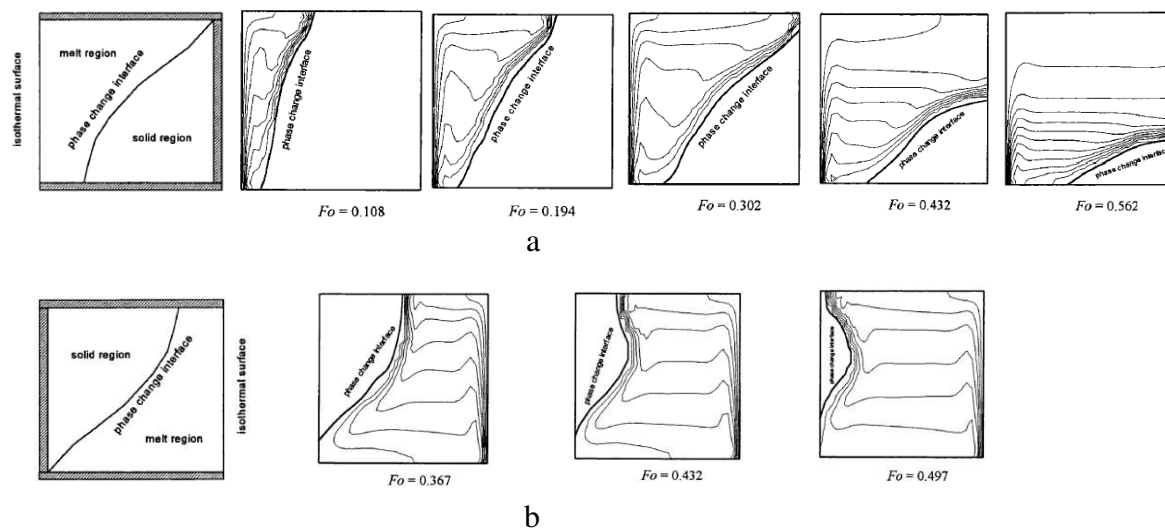


Fig. 8. Instantaneous isotherms (a) inside the not-inverted container and (b) within the inverted container (Gong et al. [24]).



1  
2  
3  
4  
5  
6  
7  
8  
9  
10  
11  
12  
13  
14  
15  
16  
17  
18  
19  
20  
21  
22  
23  
24  
25  
26  
27  
28  
29  
30  
31  
32  
33  
34  
35  
36  
37  
38  
39  
40  
41  
42  
43  
44  
45  
46  
47  
48  
49  
50  
51  
52  
53  
54  
55  
56  
57  
58  
59  
60  
61  
62  
63  
64  
65

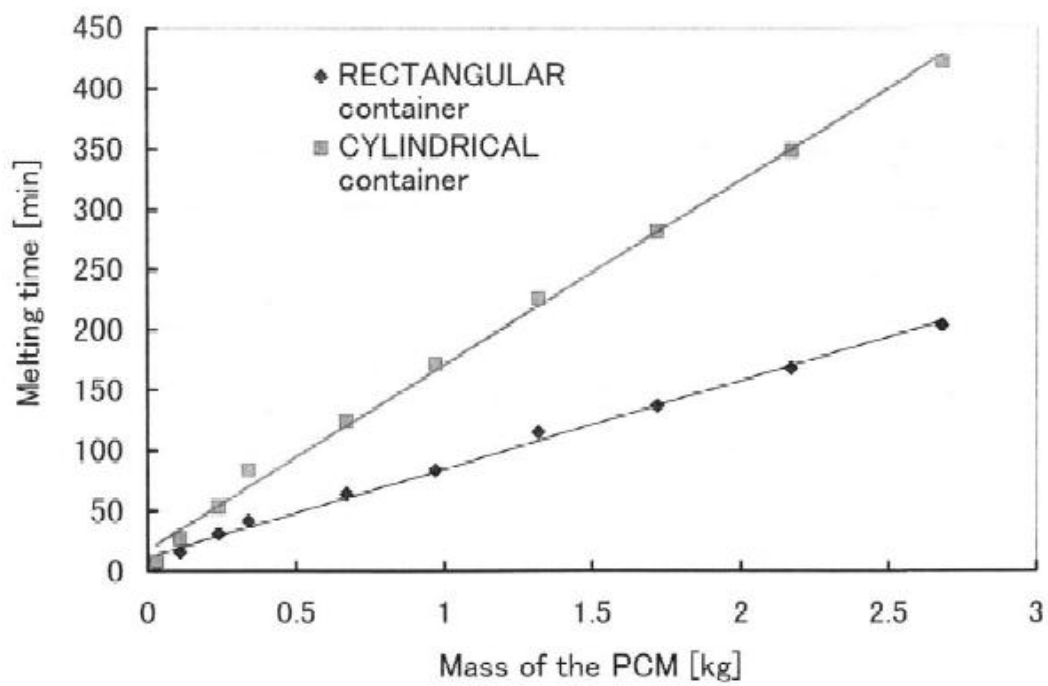
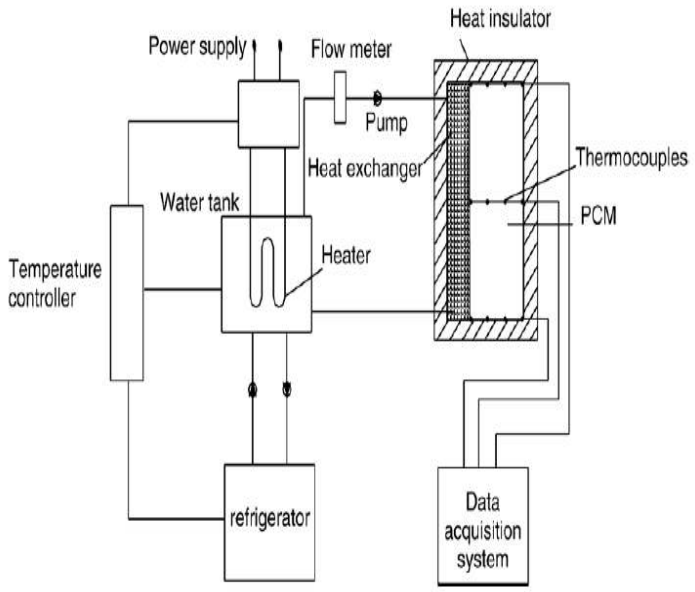
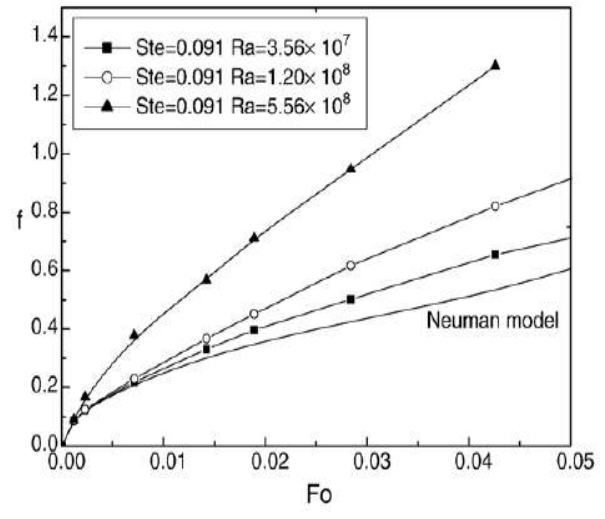


Fig. 9. Comparison of the melting time for rectangular and cylindrical containers of equal volume and heat transfer area (Zivkovic and Fujii [26]).

1  
2  
3  
4  
5  
6  
7  
8  
9  
10  
11  
12  
13  
14  
15  
16  
17  
18  
19  
20  
21  
22  
23  
24  
25  
26  
27  
28  
29  
30  
31  
32  
33  
34  
35  
36  
37  
38  
39  
40  
41  
42  
43  
44  
45  
46  
47  
48  
49  
50  
51  
52  
53  
54  
55  
56  
57  
58  
59  
60  
61  
62  
63  
64  
65



a



b

Fig. 10. (a) Schematic diagram of the experimental apparatus and (b) Temporal variation of melt fraction (Yanxia et al. [29]).

1  
2  
3  
4  
5  
6  
7  
8  
9  
10  
11  
12  
13  
14  
15  
16  
17  
18  
19  
20  
21  
22  
23  
24  
25  
26  
27  
28  
29  
30  
31  
32  
33  
34  
35  
36  
37  
38  
39  
40  
41  
42  
43  
44  
45  
46  
47  
48  
49  
50  
51  
52  
53  
54  
55  
56  
57  
58  
59  
60  
61  
62  
63  
64  
65

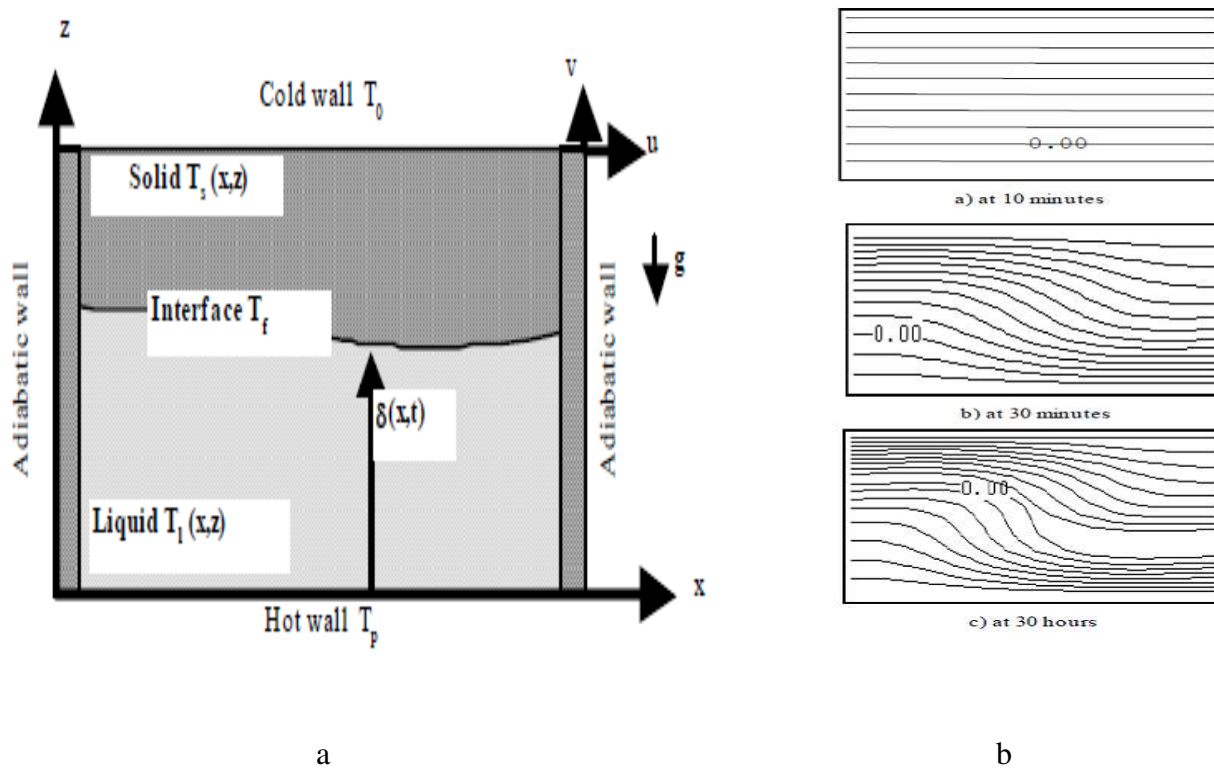


Fig. 11. (a) Configuration geometry and (b) Instantaneous isotherms over the domain (contour level 0.00 represents the position of the liquid-solid interface) (Jellouli et al. [30]).

1  
2  
3  
4  
5  
6  
7  
8  
9  
10  
11  
12  
13  
14  
15  
16  
17  
18  
19  
20  
21  
22  
23  
24  
25  
26  
27  
28  
29  
30  
31  
32  
33  
34  
35  
36  
37  
38  
39  
40  
41  
42  
43  
44  
45  
46  
47  
48  
49  
50  
51  
52  
53  
54  
55  
56  
57  
58  
59  
60  
61  
62  
63  
64  
65

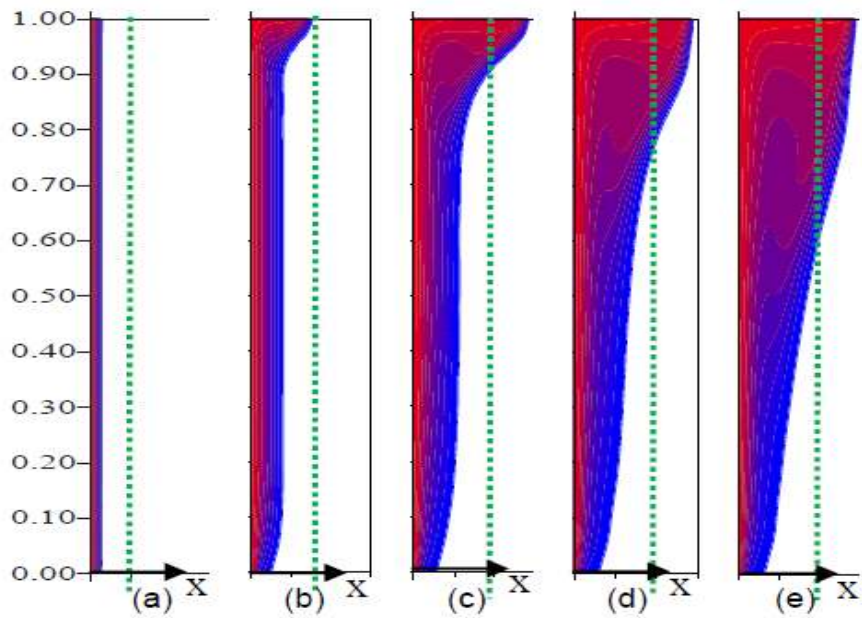


Fig. 12. Location of the fusion front at several time instants: (a) 1000 s, (b) 10,000 s, (c) 20,000 s, (d) 30,000 s and (e) 40,000 s. The dashed vertical line is the corresponding 1-D solution (Younsi et al. [32]).

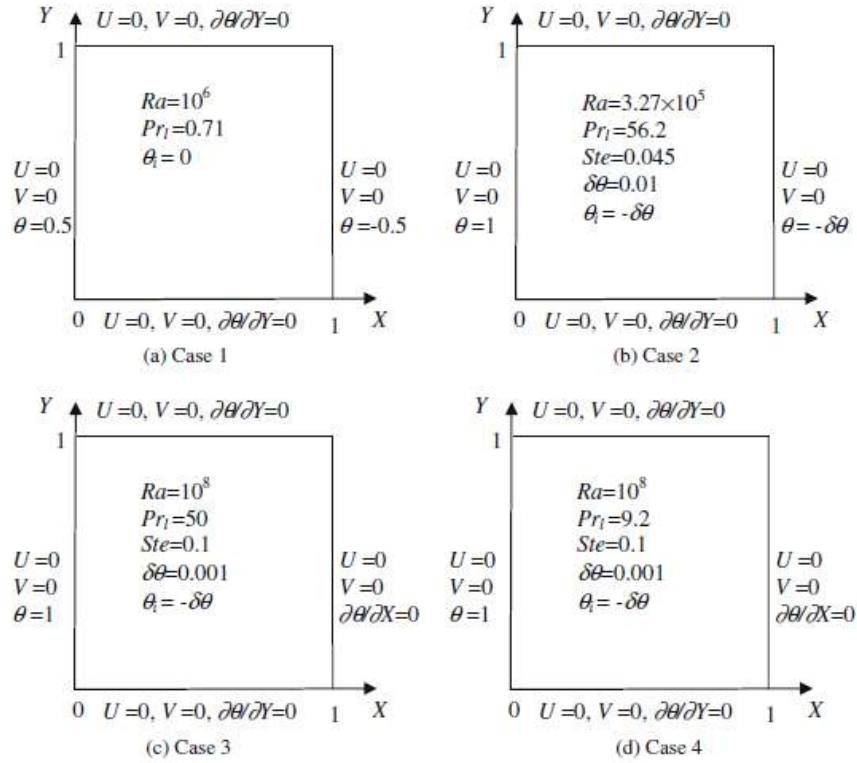


Fig. 13. Problem definition for four cases where  $\theta = \frac{T - T_m}{T_h - T_c}$ ,  $\delta\theta = \frac{\delta T}{T_h - T_c}$  and  $\delta T$  is half of the mushy zone temperature ranges (Wang et al. [33]).

1  
2  
3  
4  
5  
6  
7  
8  
9  
10  
11  
12  
13  
14  
15  
16  
17  
18  
19  
20  
21  
22  
23  
24  
25  
26  
27  
28  
29  
30  
31  
32  
33  
34  
35  
36  
37  
38  
39  
40  
41  
42  
43  
44  
45  
46  
47  
48  
49  
50  
51  
52  
53  
54  
55  
56  
57  
58  
59  
60  
61  
62  
63  
64  
65

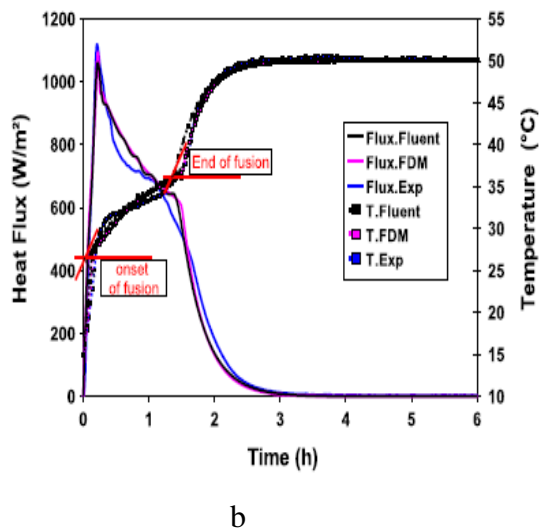
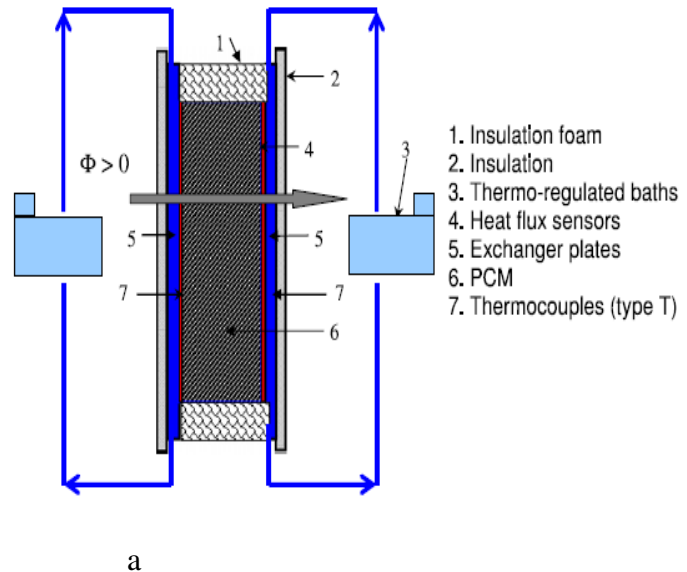


Fig. 14. (a) Experimental set-up and (b) Temperature and heat flux variations (Joulin et al. [34]).

1  
2  
3  
4  
5  
6  
7  
8  
9  
10  
11  
12  
13  
14  
15  
16  
17  
18  
19  
20  
21  
22  
23  
24  
25  
26  
27  
28  
29  
30  
31  
32  
33  
34  
35  
36  
37  
38  
39  
40  
41  
42  
43  
44  
45  
46  
47  
48  
49  
50  
51  
52  
53  
54  
55  
56  
57  
58  
59  
60  
61  
62  
63  
64  
65

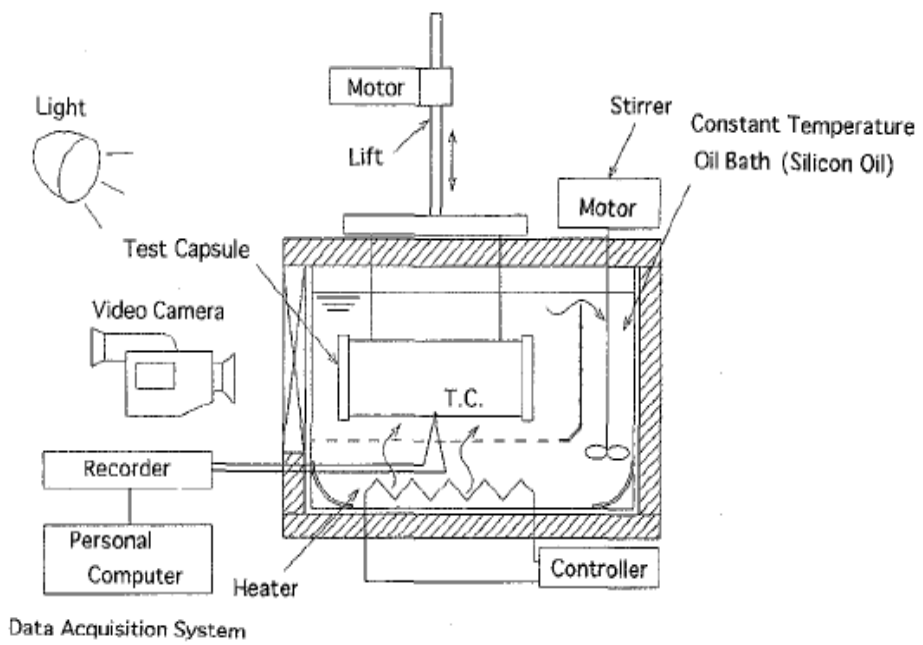


Fig. 15. Experimental setup (Saitoh and Hoshi [37]).

1  
2  
3  
4  
5  
6  
7  
8  
9  
10  
11  
12  
13  
14  
15  
16  
17  
18  
19  
20  
21  
22  
23  
24  
25  
26  
27  
28  
29  
30  
31  
32  
33  
34  
35  
36  
37  
38  
39  
40  
41  
42  
43  
44  
45  
46  
47  
48  
49  
50  
51  
52  
53  
54  
55  
56  
57  
58  
59  
60  
61  
62  
63  
64  
65

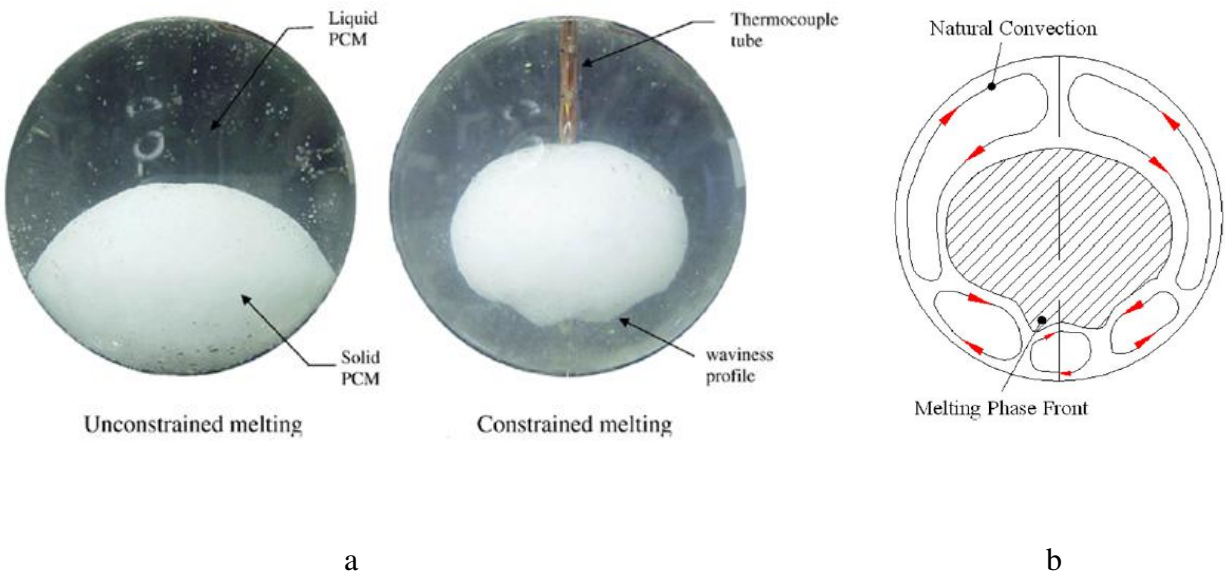


Fig. 16. (a) Unconstrained and constrained melting inside a sphere and (b) Schematic sketch showing natural convection patterns in constrained melting (Tan [41]).



1  
2  
3  
4  
5  
6  
7  
8  
9  
10  
11  
12  
13  
14  
15  
16  
17  
18  
19  
20  
21  
22  
23  
24  
25  
26  
27  
28  
29  
30  
31  
32  
33  
34  
35  
36  
37  
38  
39  
40  
41  
42  
43  
44  
45  
46  
47  
48  
49  
50  
51  
52  
53  
54  
55  
56  
57  
58  
59  
60  
61  
62  
63  
64  
65

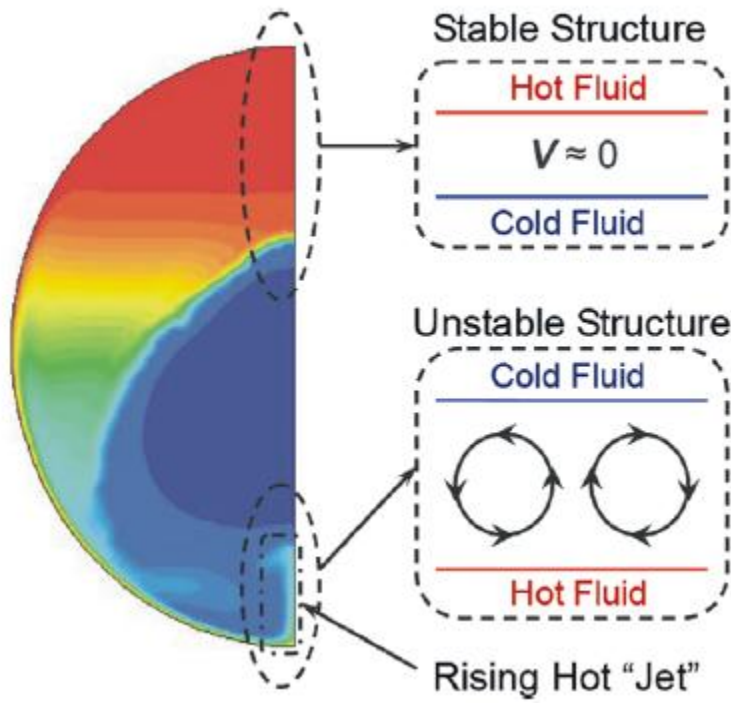


Fig. 17. Thermally stable and unstable liquid layer structures along the symmetry axis (Tan et al. [42]).

1  
2  
3  
4  
5  
6  
7  
8  
9  
10  
11  
12  
13  
14  
15  
16  
17  
18  
19  
20  
21  
22  
23  
24  
25  
26  
27  
28  
29  
30  
31  
32  
33  
34  
35  
36  
37  
38  
39  
40  
41  
42  
43  
44  
45  
46  
47  
48  
49  
50  
51  
52  
53  
54  
55  
56  
57  
58  
59  
60  
61  
62  
63  
64  
65

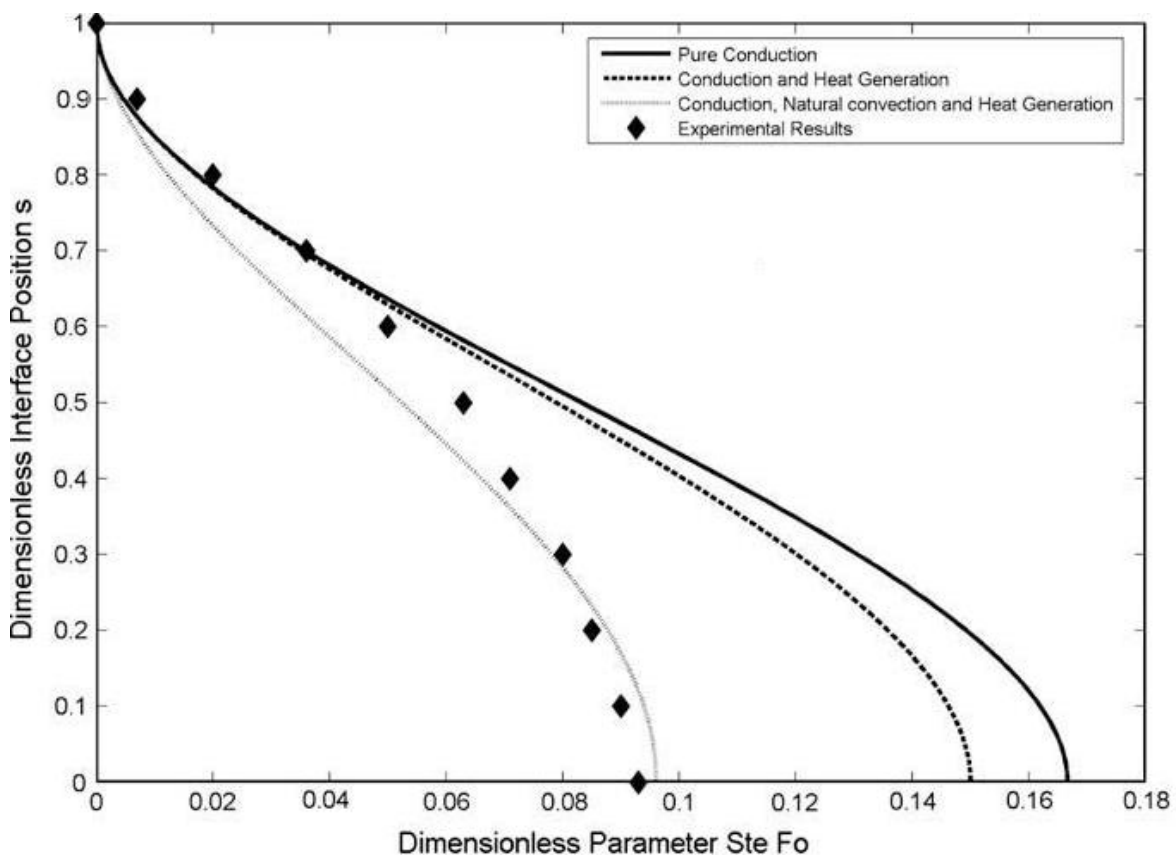


Fig. 18. Experimental validation of the position of the liquid-solid interface during melting inside a spherical container (Veerappan et al. [43]).

1  
2  
3  
4  
5  
6  
7  
8  
9  
10  
11  
12  
13  
14  
15  
16  
17  
18  
19  
20  
21  
22  
23  
24  
25  
26  
27  
28  
29  
30  
31  
32  
33  
34  
35  
36  
37  
38  
39  
40  
41  
42  
43  
44  
45  
46  
47  
48  
49  
50  
51  
52  
53  
54  
55  
56  
57  
58  
59  
60  
61  
62  
63  
64  
65

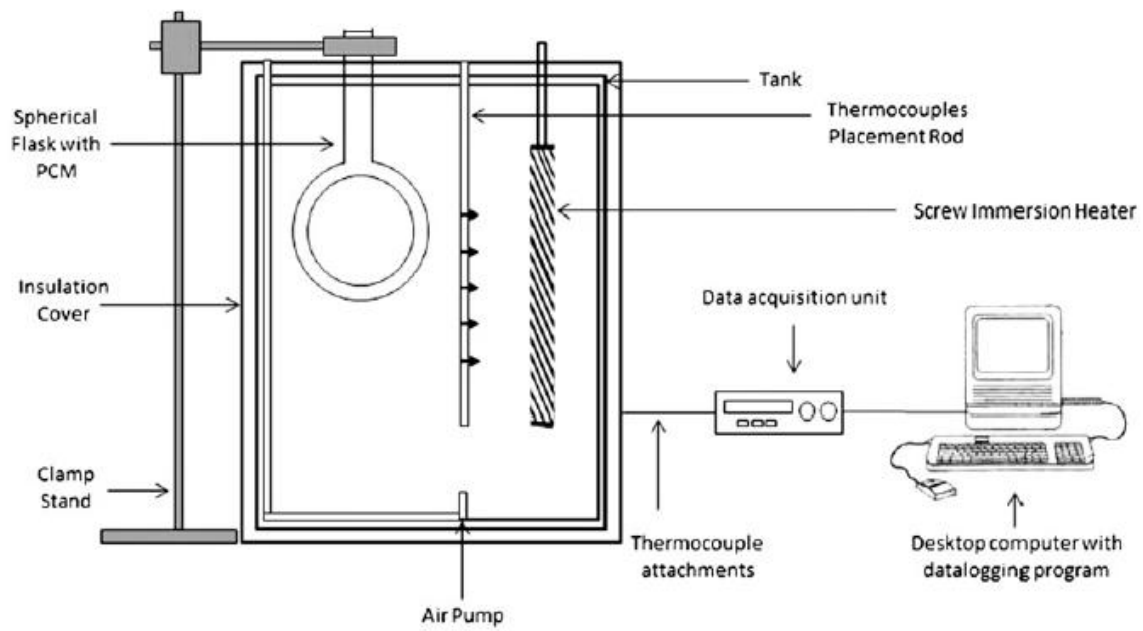


Fig. 19. Experimental setup (Rizan et al. [45]).

1  
2  
3  
4  
5  
6  
7  
8  
9  
10  
11  
12  
13  
14  
15  
16  
17  
18  
19  
20  
21  
22  
23  
24  
25  
26  
27  
28  
29  
30  
31  
32  
33  
34  
35  
36  
37  
38  
39  
40  
41  
42  
43  
44  
45  
46  
47  
48  
49  
50  
51  
52  
53  
54  
55  
56  
57  
58  
59  
60  
61  
62  
63  
64  
65

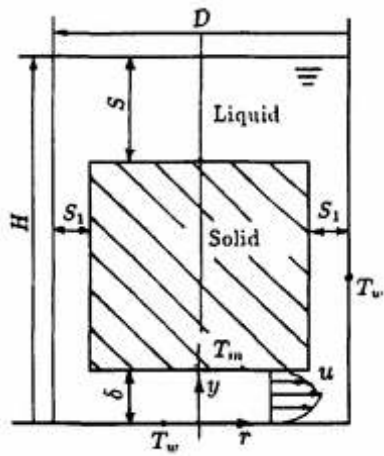


Fig. 20. Analytical model (Wenzhen et al. [47]).

1  
2  
3  
4  
5  
6  
7  
8  
9  
10  
11  
12  
13  
14  
15  
16  
17  
18  
19  
20  
21  
22  
23  
24  
25  
26  
27  
28  
29  
30  
31  
32  
33  
34  
35  
36  
37  
38  
39  
40  
41  
42  
43  
44  
45  
46  
47  
48  
49  
50  
51  
52  
53  
54  
55  
56  
57  
58  
59  
60  
61  
62  
63  
64  
65

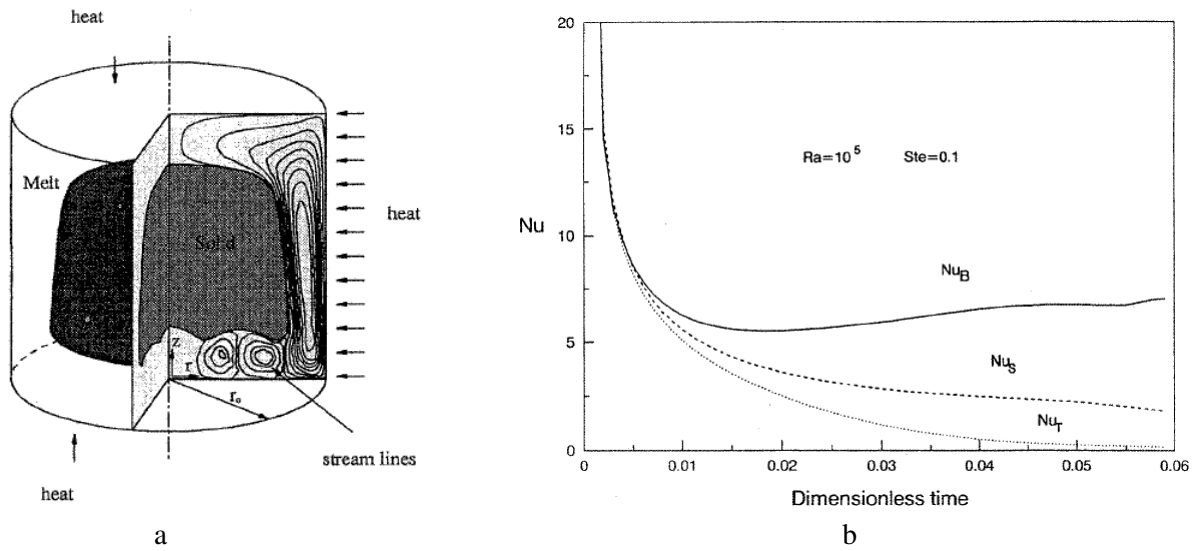


Fig. 21. (a) Schematic representation of the vertical cylindrical capsule and (b) Timewise variation of the average Nusselt number on the bottom ( $Nu_B$ ), side ( $Nu_S$ ) and top ( $Nu_T$ ) surfaces (Wu and Lacroix [48]).

1  
2  
3  
4  
5  
6  
7  
8  
9  
10  
11  
12  
13  
14  
15  
16  
17  
18  
19  
20  
21  
22  
23  
24  
25  
26  
27  
28  
29  
30  
31  
32  
33  
34  
35  
36  
37  
38  
39  
40  
41  
42  
43  
44  
45  
46  
47  
48  
49  
50  
51  
52  
53  
54  
55  
56  
57  
58  
59  
60  
61  
62  
63  
64  
65

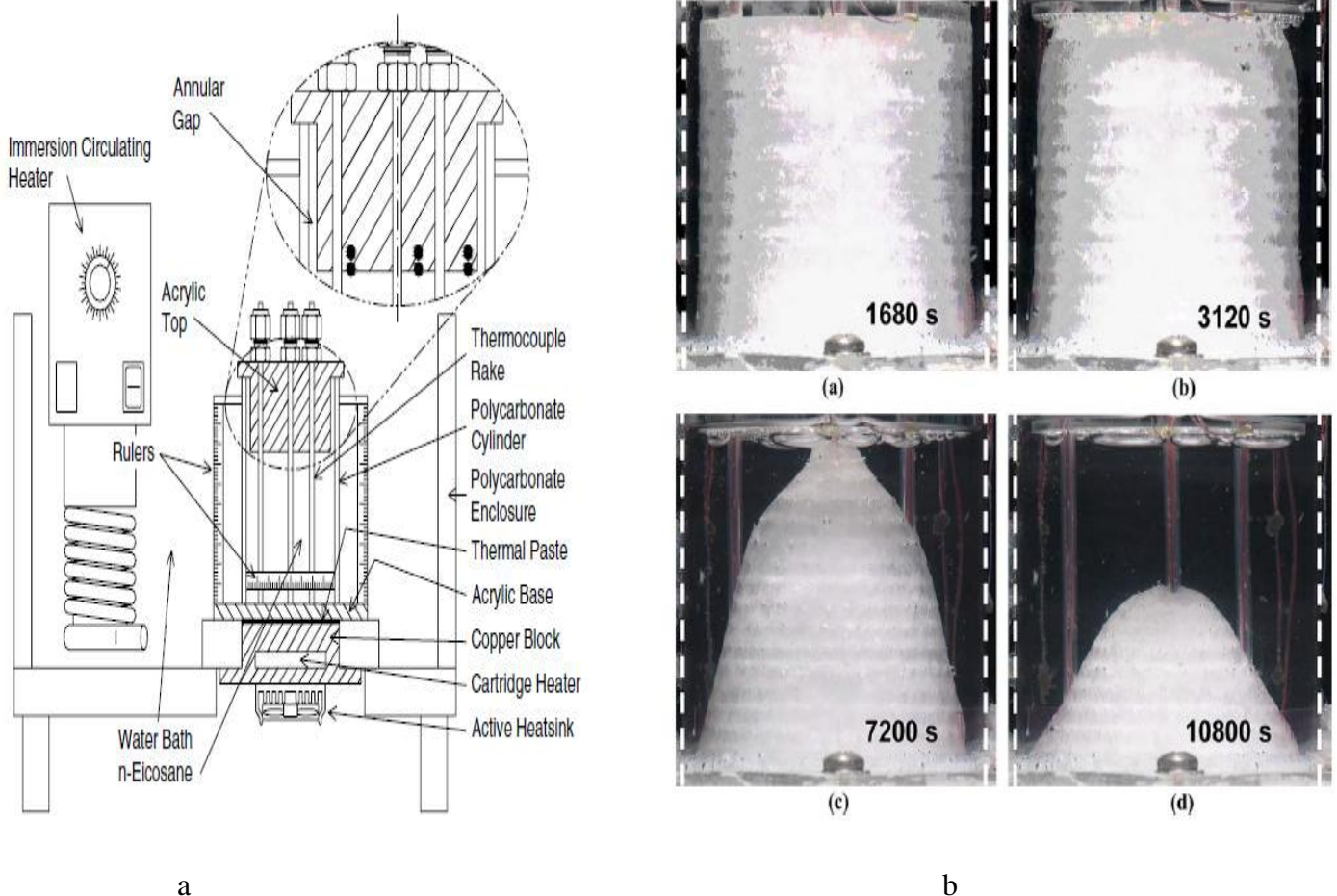


Fig. 22. (a) Schematic diagram of the experimental facility and (b) Photographs during the melting of wax within the cylindrical enclosure for a wall temperature of 45 °C (Jones et al. [49]).

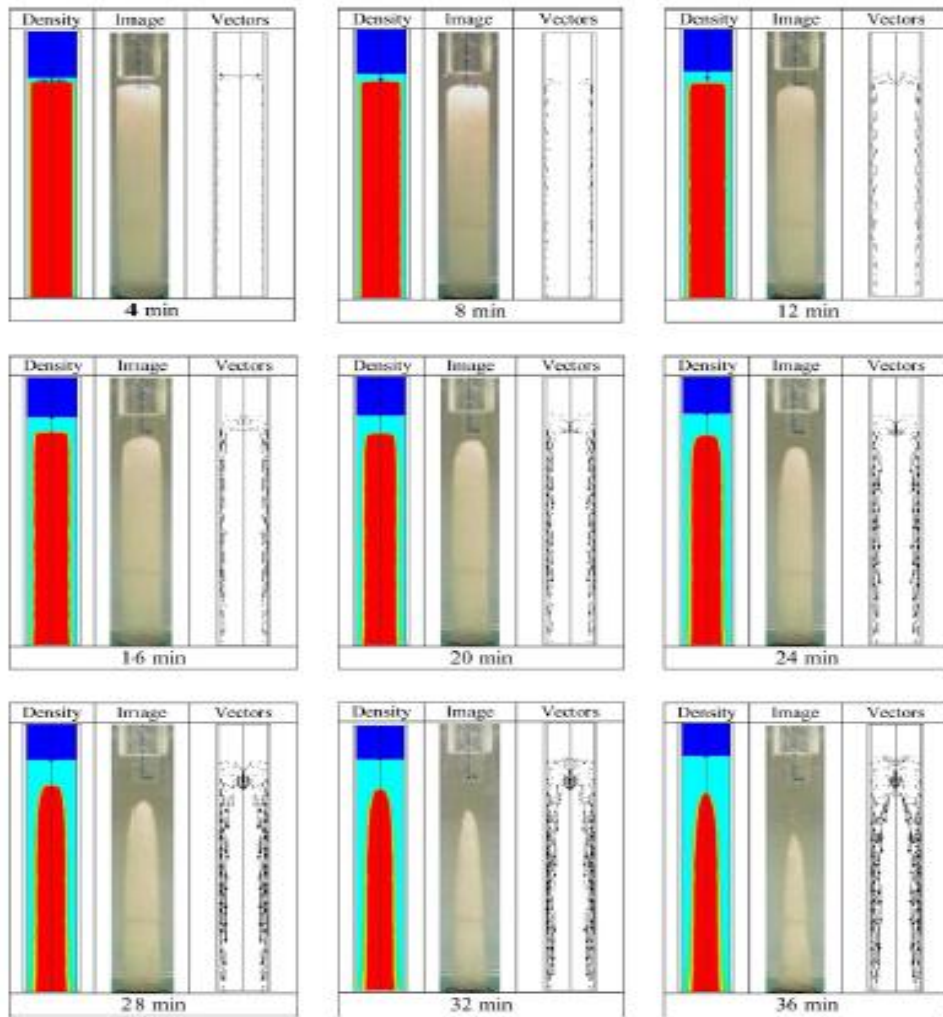


Fig. 23. Instantaneous simulated density distributions and velocity vector maps vs. experimental images during melting in a vertical cylindrical container for  $D = 3$  cm,  $H = 17$  cm and  $\Delta T = 10$  °C (Shmueli et al. [50]) .

1  
2  
3  
4  
5  
6  
7  
8  
9  
10  
11  
12  
13  
14  
15  
16  
17  
18  
19  
20  
21  
22  
23  
24  
25  
26  
27  
28  
29  
30  
31  
32  
33  
34  
35  
36  
37  
38  
39  
40  
41  
42  
43  
44  
45  
46  
47  
48  
49  
50  
51  
52  
53  
54  
55  
56  
57  
58  
59  
60  
61  
62  
63  
64  
65

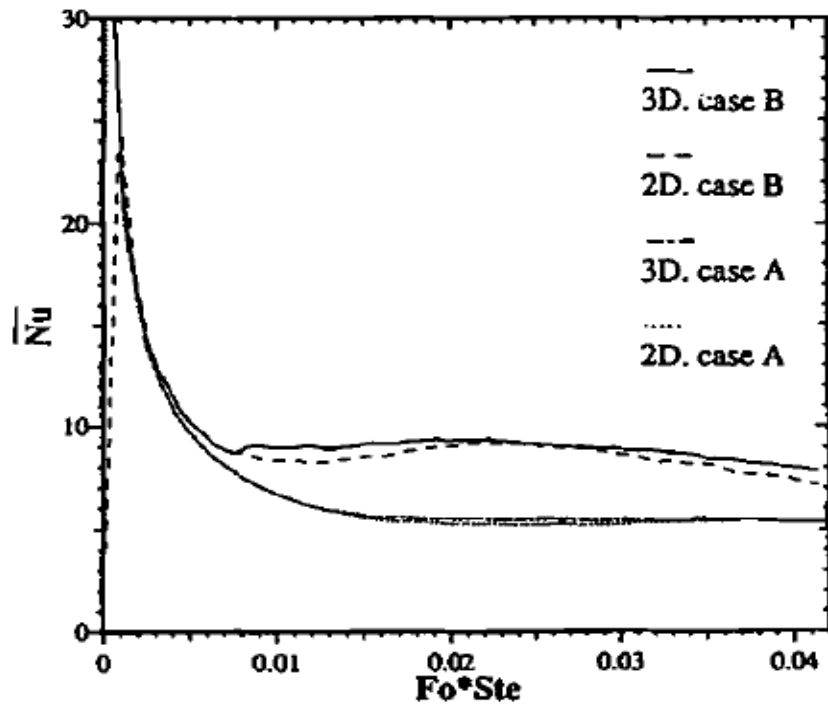


Fig. 24. Time evolutions of the overall Nusselt number on the surface of a horizontal cylinder in cases A and B predicted by three- and two-dimensional simulations (Costa et al. [61]).



1  
2  
3  
4  
5  
6  
7  
8  
9  
10  
11  
12  
13  
14  
15  
16  
17  
18  
19  
20  
21  
22  
23  
24  
25  
26  
27  
28  
29  
30  
31  
32  
33  
34  
35  
36  
37  
38  
39  
40  
41  
42  
43  
44  
45  
46  
47  
48  
49  
50  
51  
52  
53  
54  
55  
56  
57  
58  
59  
60  
61  
62  
63  
64  
65

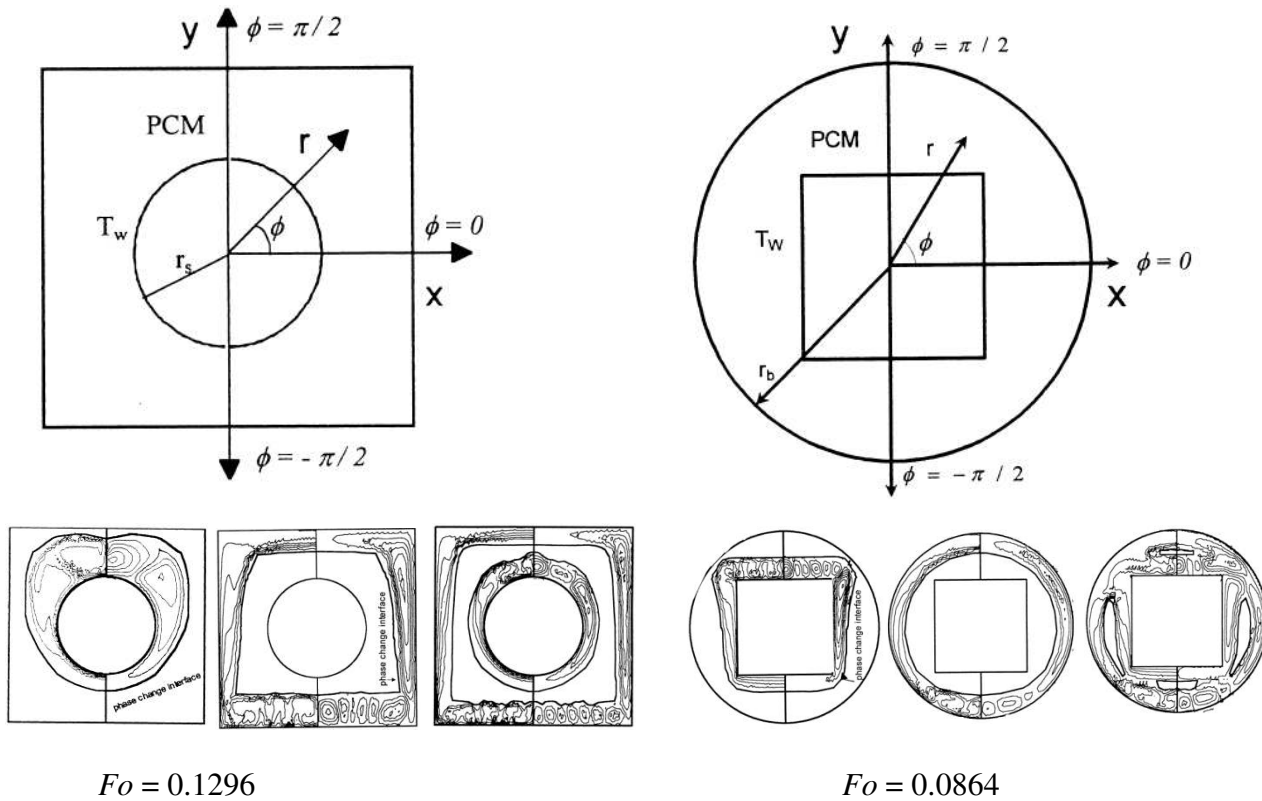


Fig. 25. Two horizontal annuli configurations with streamlines (right half) and isotherms (left half) for  $Ra = 2.844 \times 10^6$  with the annuli heated isothermally from the inside, outside or both walls (Khillarkar et al. [66]).

1  
2  
3  
4  
5  
6  
7  
8  
9  
10  
11  
12  
13  
14  
15  
16  
17  
18  
19  
20  
21  
22  
23  
24  
25  
26  
27  
28  
29  
30  
31  
32  
33  
34  
35  
36  
37  
38  
39  
40  
41  
42  
43  
44  
45  
46  
47  
48  
49  
50  
51  
52  
53  
54  
55  
56  
57  
58  
59  
60  
61  
62  
63  
64  
65

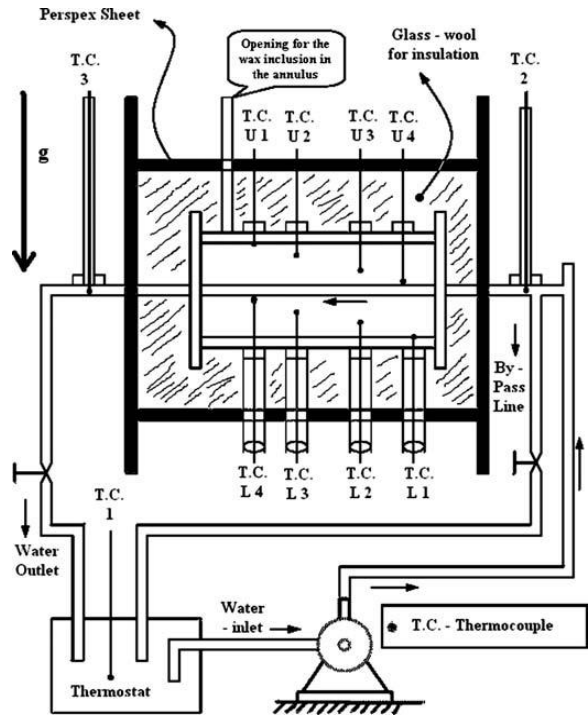


Fig. 26. Experimental set-up (Dutta et al. [67]).

1  
2  
3  
4  
5  
6  
7  
8  
9  
10  
11  
12  
13  
14  
15  
16  
17  
18  
19  
20  
21  
22  
23  
24  
25  
26  
27  
28  
29  
30  
31  
32  
33  
34  
35  
36  
37  
38  
39  
40  
41  
42  
43  
44  
45  
46  
47  
48  
49  
50  
51  
52  
53  
54  
55  
56  
57  
58  
59  
60  
61  
62  
63  
64  
65

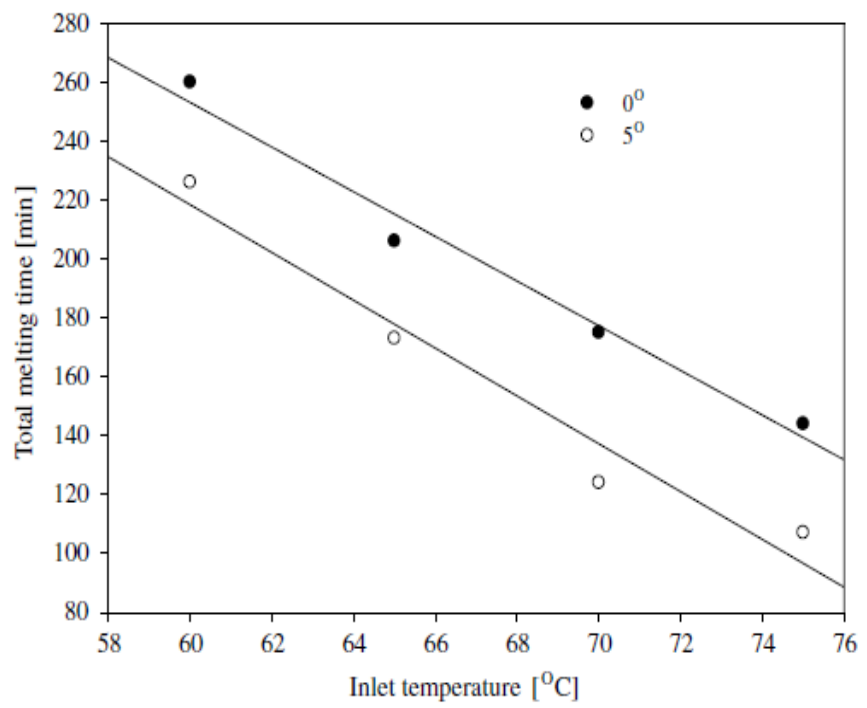
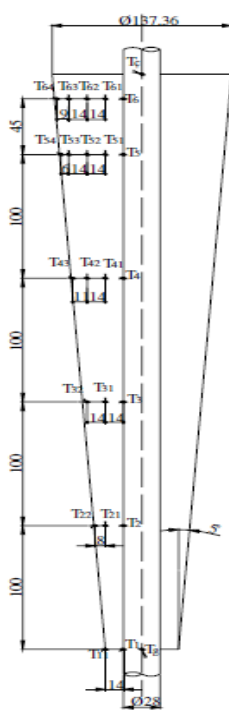


Fig. 27. Schematic diagram of the inclined shell surrounding a vertically-oriented annular PCM and the effect of this inclination on the melting time for various inlet water temperatures (Akgun et al. [68]).

1  
2  
3  
4  
5  
6  
7  
8  
9  
10  
11  
12  
13  
14  
15  
16  
17  
18  
19  
20  
21  
22  
23  
24  
25  
26  
27  
28  
29  
30  
31  
32  
33  
34  
35  
36  
37  
38  
39  
40  
41  
42  
43  
44  
45  
46  
47  
48  
49  
50  
51  
52  
53  
54  
55  
56  
57  
58  
59  
60  
61  
62  
63  
64  
65

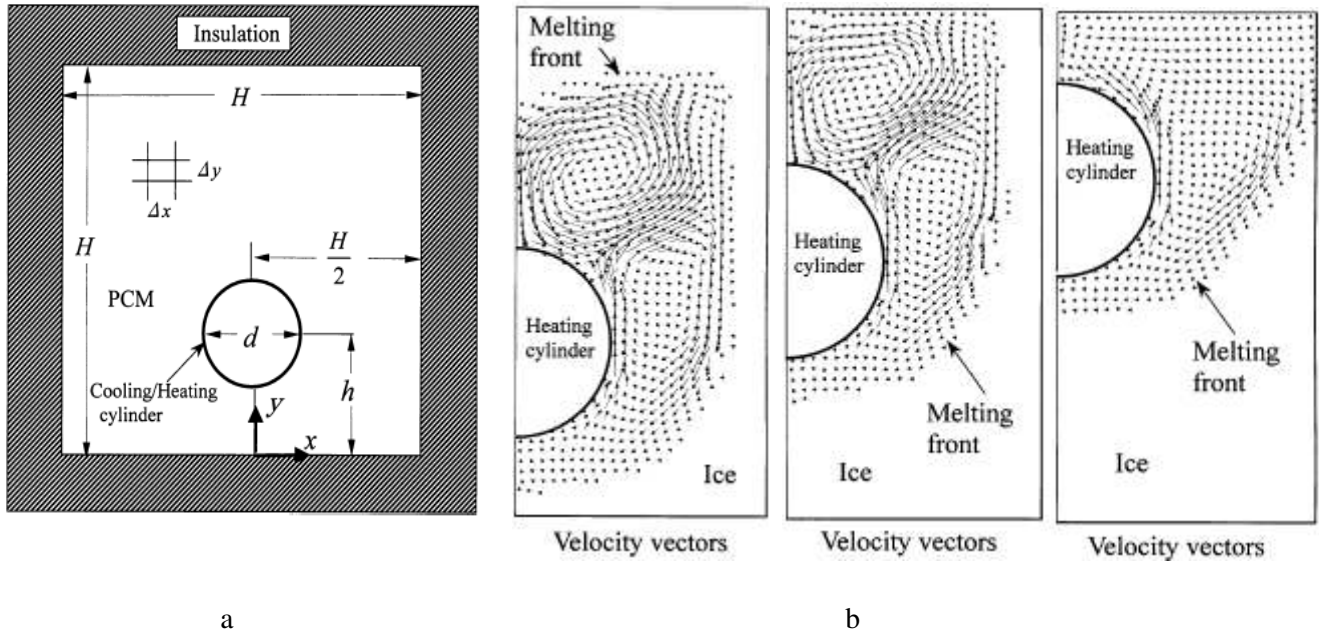


Fig. 28. (a) Physical model and coordinate system and (b) Characteristics of velocity vectors at different locations of the horizontally-oriented cylinder (Sugawara et al. [69]).

1  
2  
3  
4  
5  
6  
7  
8  
9  
10  
11  
12  
13  
14  
15  
16  
17  
18  
19  
20  
21  
22  
23  
24  
25  
26  
27  
28  
29  
30  
31  
32  
33  
34  
35  
36  
37  
38  
39  
40  
41  
42  
43  
44  
45  
46  
47  
48  
49  
50  
51  
52  
53  
54  
55  
56  
57  
58  
59  
60  
61  
62  
63  
64  
65

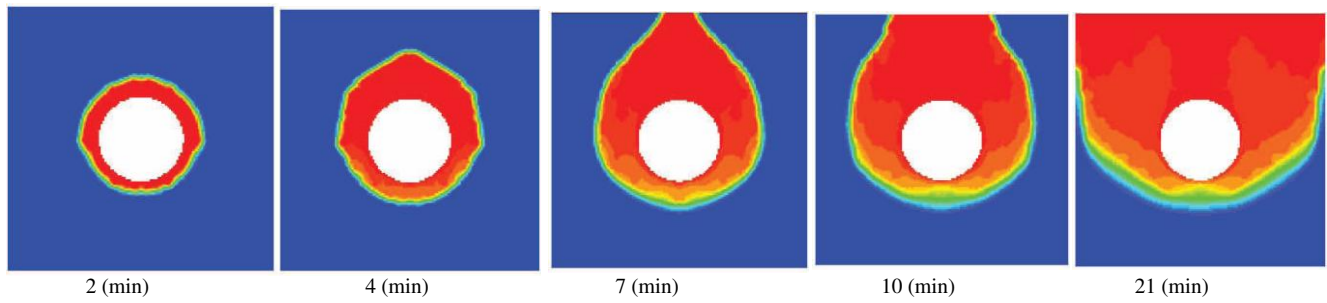


Fig. 29. Detailed phase fields throughout the melting process (Wei et al. [70]).

1  
2  
3  
4  
5  
6  
7  
8  
9  
10  
11  
12  
13  
14  
15  
16  
17  
18  
19  
20  
21  
22  
23  
24  
25  
26  
27  
28  
29  
30  
31  
32  
33  
34  
35  
36  
37  
38  
39  
40  
41  
42  
43  
44  
45  
46  
47  
48  
49  
50  
51  
52  
53  
54  
55  
56  
57  
58  
59  
60  
61  
62  
63  
64  
65

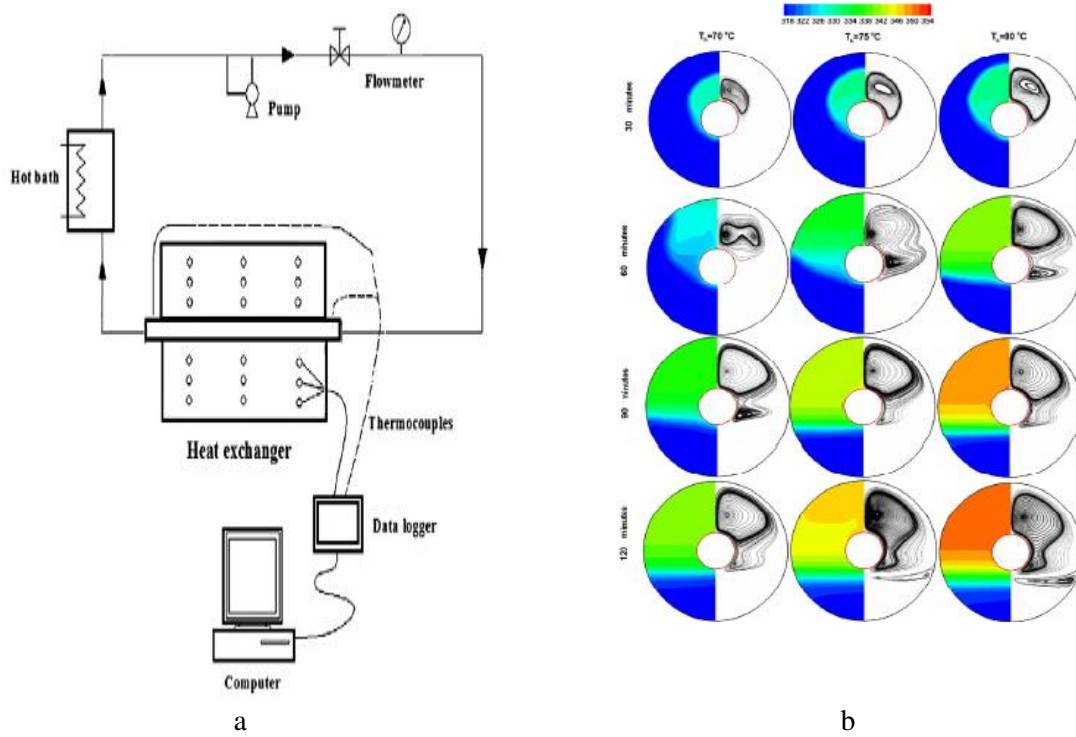


Fig. 30. (a) Diagram of the experimental set-up and (b) Computed streamlines and isotherms for different water inlet temperatures (Hosseini et al. [72]).